Flow Visualization Study of Passive Flow Control Features On a Film-Cooled Turbine Blade Leading Edge

THESIS

Daniel R. Carroll, Captain, USAF

AFIT/GAE/ENY/09-D01

AFIT/GAE/ENY/09-D01

FLOW VISUALIZATION STUDY OF PASSIVE FLOW CONTROL FEATURES
ON A FILM-COOLED TURBINE BLADE LEADING EDGE

THESIS

Presented to the Faculty

Department of Aeronautics and Astronautics

Graduate School of Engineering and Management

Air Force Institute of Technology

Air University

Air Education and Training Command

In Partial Fulfillment of the Requirements for the

Degree of Master of Science in Aeronautical Engineering

Daniel R. Carroll, B.S.
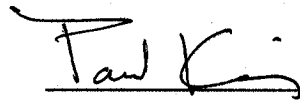
Captain, USAF

December, 2009

AFIT/GAE/ENY/09-D01

FLOW VISUALIZATION STUDY OF PASSIVE FLOW CONTROL FEATURES
ON A FILM-COOLED TURBINE BLADE LEADING EDGE
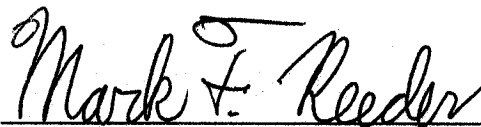
Daniel R. Carroll, B.S.

Captain, USAF

Approved:

_____   ___14 Dec 09___
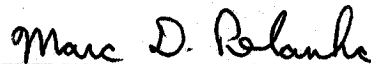Paul King   Date
Thesis Advisor

_____   ___14 Dec 09___
Mark Reeder   Date
Committee Member

_____   ___14 Dec 09___
Marc Polanka   Date
Committee Member

AFIT/GAE/ENY/09-D01

Abstract

A flow visualization study was conducted on a model of a film-cooled turbine blade leading edge in a closed-loop water channel at $Re_D = 30k$. The model consisted of an 8.89 cm diameter half-cylinder with flat afterbody joined at the ninety degree point. A single radial coolant hole ($d_c/D = 0.054$) drilled 21.5° from the stagnation line, angled 20° to the surface and 90° to the flow direction generated a coolant jet transverse to the freestream. Water channel testing assessed the hydrodynamic effects of 16 passive flow control features, to include a variety of dimples upstream and downstream of the coolant hole and transverse trenches milled directly over the coolant hole. Compared to an unmodified coolant hole, a single row of small cylindrical or spherical dimples ($d/d_c = 0.79$, $h/d = 0.2$) upstream of the coolant hole steadies the coolant jet at blowing ratios up to $M = 0.75$. Medium ($d/d_c = 1.59$, $h/d = 0.2$) and large ($d/d_c = 2.38$, $h/d = 0.2$) spherical dimples downstream of the coolant hole also have a calming effect on the coolant jet up to $M = 0.75$. None of the dimple geometries studied affect the coolant jet at $M \geq 0.75$. A single-depth, square-edged transverse trench ($w/d_c = 1$, $h/w = 0.5$) spreads the coolant, increasing spanwise coverage of a single coolant hole more than two times. This trench suffers from coolant blow-out above $M = 0.50$, but a deeper, tapered-depth trench ($w/d_c = 1$, $h/w = 1$ at coolant hole tapered to $h/w = 0.5$ at end) provides very effective film cooling at blowing ratios above $M = 0.50$. It spreads the coolant in the spanwise direction, prevents coolant jet liftoff, and was the only geometry studied that holds the coolant tighter to the surface than an unmodified coolant hole.

Table of Contents

Symbols

A_c	area of coolant hole (m^2)
D	golf ball diameter
D	leading edge diameter (m)
d	dimple diameter (m)
d_c	coolant hole diameter (m)
h	dimple (or trench) depth (m)
k	roughness height (mm)
k_3	confidence factor
M	coolant blowing ratio – Eq. 3, pg. 11
n	number of observations
Q_c	coolant volumetric flow rate (m^3/s) – Eq. 4, pg. 11
Re_D	leading edge Reynolds number – Eq. 1, pg. 4
Re_d	dimple Reynolds number
Re_x	local Reynolds number
r_f	trench fillet radius (m)
s	standard deviation
T	non-dimensional time step – Eq. 8, pg. 14
t	time step (s)
T_c	film coolant temperature (K)
T_s	film temperature at blade surface (K)
T_∞	freestream temperature (K)
V_c	coolant velocity (m/s)
V_∞	freestream velocity (m/s)
w	trench width (m)
$\bar{x}$	sample mean
x_c	leading edge arc length at coolant hole (mm)

Greek

β_{cp}	confidence probability – Eq. 5, pg. 12
δ_c	boundary layer thickness at coolant hole (mm) – Eq. 9, pg. 23
δ^*	displacement thickness (mm) – Eq. 11, pg. 24
μ_∞	freestream dynamic viscosity $(Pa \cdot s)$
μ	mean
ρ_c	coolant density (kg/m^3)
ρ_∞	freestream density (kg/m^3)
η	adiabatic film cooling effectiveness – Eq. 2, pg. 5
$\pm\Delta x$	confidence interval

Abbreviations

AFIT	Air Force Institute of Technology
AFRL	Air Force Research Laboratory
ASTM	American Society for Testing and Materials
PIV	particle image velocimetry
PVC	polyvinyl chloride
CDD	small cylindrical downstream dimples
CUD	small cylindrical upstream dimples
LCD	large cylindrical downstream dimple
LSD	large spherical downstream dimple
MCD	medium cylindrical downstream dimple
LCD	medium spherical downstream dimple
SCUD	staggered small cylindrical upstream dimples
SDT	single-depth trench
SSUD	staggered small spherical upstream dimples
SUD	small spherical upstream dimples
TDT	tapered-depth trench
UNM	unmodified coolant hole

Flow Visualization Study of Passive Flow Control Features On a Film-Cooled Turbine Blade Leading Edge

I. Introduction

According to Wilson and Korakianitis [1], in 1903 Aegidius Elling engineered a constant-pressure cycle gas-turbine that produced 8 kW of power. By 1904 Elling's second design produced 33 kW, which was a result of increased turbine inlet-temperature. Years later the gas turbine has evolved to be the premier powerplant for larger/high-performance aircraft. What Elling discovered in 1904 still holds true today: increasing the turbine inlet temperature also increases the thermal efficiency and specific power output of a gas-turbine engine.

1.1 Motivation for Research

Modern gas turbine engines are far more advanced than those of the 1930s, but they still have limitations. Martini et al. [2] state that temperatures can be as high as 2000 K in the high-pressure turbine, oftentimes higher than the melting temperature of blade materials. Cooling methods are employed to protect the turbine blades and prolong engine life. According to Han and Ekkad [3], blades are cooled internally by convective-heat transfer: relatively cool air is forced through interior passageways within each blade, transferring heat energy from the blade surface and into the coolant. External film cooling involves blowing air through the blade walls and out over the surface of the blade. This creates a layer of film coolant, shielding the blade from the freestream hot gas. Though these methods are effective, they have drawbacks.

As stated previously, it is advantageous to run the engine at the highest allowable temperature, and inducing cool air into the turbine section lowers the overall turbine temperature. Also, cooling requires bleed air from the engine compressor section. Using air for secondary processes decreases overall engine efficiency. It is for these reasons that the film cooling process must be optimized.

1

1.2 Research Approach

This research focused solely on the film cooling process in the leading edge region of a turbine blade. The leading edge is of particular interest because of its proximity to the stagnation zone and its convex shape. Ko et al. [4] conducted a study in 1986 in which they evaluated film cooling effectiveness over concave and convex surfaces. Their convex test specimen consisted of a quarter-cylinder with a single row of cooling holes inclined $30°$ to the surface. They observed a coolant jet that separates from the surface, causing a region of recirculation and decreased film effectiveness. The separation effect worsens with increasing coolant flow rate. A 1988 study conducted by Mick and Mayle [5] made similar conclusions. Their test specimen consisted of a half-cylinder with three spanwise rows of radial coolant holes drilled $\pm15°$ and $44°$ off the stagnation line, all angled $30°$ to the surface. They also concluded that cooling effectiveness in the region suffers from coolant jet liftoff, and that coolant from the downstream row of holes interferes with coolant from the upstream row, pushing it into the freestream. This behavior results in significant variations in film effectiveness in the spanwise direction.

Jet separation is not the only obstacle to effective leading edge film cooling. High acceleration and thin boundary layers are also challenges to effective cooling. Utilizing a geometry nearly identical to that of Mick and Mayle [5], Salcudean et al. [6] conducted a study that focused on film cooling effectiveness in the leading edge region. They concluded that a strong pressure gradient present in the stagnation region causes a significant difference in coolant flow rate between the $15°$ and $44°$ rows of coolant holes. Cooling effectiveness was seen to be extremely sensitive to average flow rate: at low flow rates coolant flow was completely cut off from the upstream row of holes, and the overall cooling effectiveness suffered from liftoff at higher flow rates.

A large amount of research has focused on preventing the above behavior, including placing passive surface modifications, such as dimples and trenches, adjacent to cooling holes. The objective of the current study was to provide flow visualization data for some of these features that have been evaluated previously in wind tunnel testing and to explore new possibilities based on initial findings. This was not an optimization study, but exploratory

research seeking a method that could potentially improve leading edge film cooling and possibly provide a correlation between flow visualization data and film cooling effectiveness.

This research was conducted in the closed-loop water channel at the AFRL Air Vehicles Directorate at Wright Patterson Air Force Base. Flow visualization pictures were acquired for 16 passive flow control geometries near a film cooling hole on a turbine blade leading edge model. Water colored with blue dye was injected through the coolant hole and into the freestream and the results were captured via a high speed camera from two different camera angles. Initial tests were based on recent research and provided a vector for subsequent tests.

1.3   Outline of Thesis

Chapter 2 discusses previous research regarding the effect of passive flow control features on film cooling. Chapter 3 details model design and fabrication as well as the experimental setup. Chapter 4 will provide a discussion of test results. Conclusions and recommendations for future research are presented in Chapter 5, followed by figures for experimental data, model drawings, detailed pictures and dimensions of each geometry, pictures of the experimental setup, and flowmeter calibration data.

II. Background and Theory

A vast amount of research has been conducted to improve film cooling methods. In 1968, Goldstein et al. [7] determined that injecting film coolant at an angle of 35° to the surface provided much better cooling than injection at 90°. In 1977, Luckey et al. [8] conducted a stagnation region film cooling study on a cylinder, concluding that film cooling effectiveness decreases as cooling holes are moved closer to the stagnation point. Research in 2001 by Teng et al. [9] demonstrated that cooling holes with a diffuser-shaped exit deliver better thermal protection downstream of the coolant hole than a standard cylindrical hole. In 2006, Martini et al. [2] conducted a study on the trailing edge region of a film-cooled turbine blade using different types of slots to deliver the coolant to the surface. The current research focused solely on the ability of passive flow control features to condition the behavior of a coolant jet in the leading edge region.

2.1 Applicable Dimple Research

Dimples have been used for decades as a means to prevent flow separation on golf balls. Dimples trip the boundary layer from laminar to turbulent, moving the location of flow separation from the center to the back side of the ball. This decreases pressure drag and allows the ball to travel further. In 2006, Kim et al. [10] conducted a study that used computational fluid dynamics to compare drag forces on two different golf balls, each with and without spinning. One of the golf balls contained smooth-edged (spherical) dimples and a second had dimples with steep edges that were nearly cylindrical in shape. Flow fields around the stationary and spinning golf balls were analyzed at $Re = 1.65 \cdot 10^5$ and $8.48 \cdot 10^4$, with Re based on the ball's diameter and freestream conditions (Eq. 1).

$$Re_D = \frac{\rho_\infty \cdot V_\infty \cdot D}{\mu_\infty} \tag{1}$$

The study concluded that drag coefficients for the steep-dimpled ball are $14\% - 20\%$ higher than the ball with smooth-edged dimples at high Re. At low Re, the difference in drag coefficient between the two balls is less than 4%.

While the geometry of a turbine blade is much different than that of a golf ball, Lake [11] successfully applied dimples to a low-pressure turbine blade as a means of controlling flow separation. His 1999 study considered shallow dimples with $h/d = 0.1$. He concluded that placing a row of dimples just ahead of the point of separation trips the laminar boundary layer to a turbulent state, reattaching the flow to the blade and decreasing pressure losses by up to 51.7% at $Re = 50$k (Re based on the blade axial chord).

Roland [12] took the dimples a step further in 2008. He evaluated the effect of dimples on film coolant adiabatic effectiveness values within the leading edge region. Adiabatic effectiveness is a non-dimensional parameter defined in Eq. 2. An ideal adiabatic effectiveness of unity would require a surface film temperature equal to that of the film coolant.

$$\eta = \frac{T_\infty - T_s}{T_\infty - T_c} \tag{2}$$

Roland [12] demonstrated that a single row of cylindrical dimples placed directly upstream of the coolant hole increases spanwise adiabatic effectiveness by up to 60% compared to a coolant hole without dimples. However, Frisinger [13] conducted a similar study in 2009 that examined the same set of dimples, concluding that dimples increase adiabatic effectiveness by only 7% at $M = 0.25$. Though there is a disparity between the two studies, dimples show a potential for improving film cooling. Adiabatic effectiveness was not measured in this research, but it will be shown that flow visualization data provide a rough correlation to adiabatic effectiveness.

In 2005, Khalatov et al. [14] conducted a water tunnel flow visualization study on shallow ($h/d = 0.1$) cylindrical and hemispherical dimples on a flat plate at various Re_d with very low turbulence. Just downstream of a cylindrical dimple, an in-dimple separation zone and periodic fluctuations become apparent as Re_d increases past 3,220. Further increases in Re_d cause a proportionate growth in the separation zone, and the periodic fluctuations become stronger and draw more fluid into the dimple. Due to a spherical dimple's gently sloping edges, its behavior is quite different. At low Re_d the streamlines observed over a spherical dimple are smooth and parallel. The rounded edges delay the onset of separation and flow fluctuations to $Re_d = 5,125$ and 7,890, respectively.

2.2 Applicable Trench Research

In his 2002 study, Bunker [15] noted that a continuous, uninterrupted slot (as opposed to discrete holes) is an extremely effective film cooling configuration, with η approaching unity near the slot exit. Though this slot film cooling process is ideal, it is not structurally feasible on a high pressure turbine blade. Therefore, Bunker [15] examined three film cooling geometries that involved discrete holes feeding coolant into a continuous surface trench on a flat plate. The first two geometries had different trench widths: narrow ($w = 1.13d_c$) and wide ($w = 1.5d_c$), each with $h = 3d_c$. A row of radial film cooling holes within the trench was oriented in the spanwise direction and inclined 30° to the surface, with a pitch-to-diameter ratio of 3.57. For both geometries, Bunker determined that adiabatic effectiveness is relatively independent of blowing ratio, and that the trench technique prevents film liftoff at higher blowing ratios. Bunker went on to evaluate a third geometry using axial holes in a shallow trench with a width equal to the elliptical shape of the hole exit and $h = 0.43d_c$. This yielded the best results of all three cases, improving film effectiveness 50% – 75% far downstream compared to a similar row of umodified axial holes.

In 2007, Lu et al. [16] explored the effect of trench depth. They investigated heat transfer coefficients and film effectiveness for a variety of flat plate trench configurations, all with axial holes embedded at an angle of 30° to the surface. Six trench geometries were evaluated in total, with varying widths and depths. They studied narrow trenches (width equal to that of the elliptical hole exit) and wide trenches ($w = 3d_c$). Three different depths were investigated: $0.5d_c$, $0.75d_c$, and $1.0d_c$. The study concluded that narrow and wide trenches of depth $0.75d_c$ perform significantly better than the rest. In the case of the narrow trench, the coolant spreads into the trench after exiting the hole and a two dimensional film appears to exit the trench, increasing coverage in the spanwise direction. As the jet enters the trench and flows over the surface, its velocity decreases by 30% compared to an unmodified coolant hole. This lower velocity prevents jet liftoff and keeps the film coolant tightly attached to the surface. The wider trench behaves similarly and demonstrates increased local film effectiveness compared to the narrow trench. However, it only obtains a 20% reduction in jet velocity compared to an unmodified coolant hole. Overall, their conclusions state that trenching the holes reduces the jet momentum at exit and also spreads

the jets in the spanwise direction compared to discrete film cooling holes, with the optimum trench depth being $0.75d_c$.

Waye and Bogard [17] conducted a study in 2007 in which they took high-resolution film cooling data of axial holes embedded in a variety of transverse trench configurations on the suction side of a simulated turbine vane. Their research considered a single trench depth but varied the geometry and location of the upstream and downstream trench edges. In total they investigated 10 geometries, to include narrow and wide trenches with triangular and rectangular edges. Consistent with previous trench research, they determined that the trench suppresses coolant jet separation and that a narrow trench is most effective. They also concluded that a trench with sharp, square edges both upstream and downstream of the coolant hole is most effective, improving adiabatic effectiveness by up to 50%.

2.3   Implications for Current Research

Because Khalatov et al. [14] observed separation zones in their dimple work as well as bulk flow fluctuations beginning at $Re_d \approx 3{,}500$, dimples of various sizes were investigated in the current study but Re_d was limited to 4,000. It was hypothesized that the in-dimple separation and bulk flow fluctuations associated with high Re_d would have an adverse effect on the coolant jet by turbulating it and enhancing mixing with the freestream.

Not only was dimple size varied, but multiple dimples were required in order to affect the coolant jet at all blowing ratios. According to Khalatov [18], it is typical that the effect of a dimple extends only $\pm 0.55d$ from the dimple center. The coolant hole design used in this research was transverse to the freestream, and at high blowing ratios the jet extended beyond the coolant hole exit in the spanwise direction, bypassing the single dimple.

Though Khalatov [14] observed significant differences in behavior between the cylindrical and spherical dimples, Kim et al. [10] concluded that the difference in drag coefficient between a golf ball with smooth dimples and one with steep-edged dimples was minimal at $Re = 8.48 \cdot 10^4$. Therefore it was necessary to investigate both spherical and cylindrical dimples in this research, which was conducted at $Re = 3.0 \cdot 10^4$.

The general consensus of recent trench research is that a narrow trench with rectangular edges yields the best performance, while trenches of depth $0.43d_c - 1.0d_c$ all perform well [15–17]. This study considered only narrow trenches. However, most of the previous research focused on a row of axial holes embedded in a transverse trench on a flat plate, whereas this study investigated the performance of a single radial coolant hole on a leading edge. Due to the difference in coolant hole geometry, initial trench depth was chosen as $0.5d_c$.

III. Experimental Setup

Testing was conducted in a closed-loop water channel at the AFRL Air Vehicles Directorate at Wright Patterson Air Force Base. A picture of the water channel is shown in Fig. 159 on pg. 112. This water channel has a horizontal free-surface and a 46 cm-wide by 61 cm-high test section. Surface skimmer plates upstream and downstream of the test section damp oscillations in the channel. Two honeycomb screens and three wire-mesh screens provide uniform flow throughout the test section. According to Kaplan et al. [19], turbulence intensity as determined from PIV free-stream data is estimated at 0.1% when freestream velocity is equal to 7.62 – 38.1 cm/s.

3.1 Model Design and Fabrication

Several materials were considered for the models used in this research, and PVC was chosen because it is relatively easy to machine and has very low water absorption. The AFIT model used 10.16 cm-square bar-stock of PVC to create leading edge templates. The design for the leading edge models was based on those recently used by Roland, Frisinger, and Rutledge [12, 13, 20]. The initial design called for the models to be completely hollow on the inside, but because PVC is relatively soft, it deformed once a large volume of material was removed. The model was redesigned to remove minimal material from the inside. Up to four coolant holes were tested on each model ($d_c = 0.48$ cm), each having a dedicated plenum for coolant injection. Each plenum consisted of a 0.75"-diameter hole threaded to accept a Swagelock connector that interfaced with a 0.25" coolant feed line. The coolant holes were drilled on a compound angle: 21.5° off the stagnation line in the radial direction and then inclined 20° from the model's surface in the spanwise direction. The coolant holes were drilled to a radial depth of 1.92 cm, which resulted in a coolant hole length of $11.64d_c$. This generated a coolant jet that flowed in the spanwise direction, perpendicular to the freestream. To prevent coolant hole interaction, adjacent holes were spaced at $24d_c$. Detailed model drawings are located in Figs. 145 – 149 starting on pg. 101.

9

3.2   Water Channel Setup

A schematic of the water channel setup is shown in Fig. 160 on pg. 113. A 19 L (five gallon) tank was filled with water syphoned directly from the water channel to serve as the coolant. The coolant water was dyed with 15 mL of blue food coloring and the tank was pressurized to approximately 206 kPa (30 psi). A gate valve controlled the flow rate out of the tank and through the flowmeter (a King 7459-31W, see Figs. 161 and 162 on pg. 114) which was mounted vertically on the side of the water channel. Though the flowmeter came with a chart from the manufacturer matching float height to flow rate, an extensive calibration was performed: a large beaker was filled with water and timed to determine the flow rate at float heights from 10 mm to 250 mm, with a step size of 10 mm. This process was repeated twice and results were nearly identical for each calibration. A graph showing the calibration data is located in Fig. 164 on pg. 117. It was determined that flowmeter performance did not accurately match the manufacturer's data above a float height of 90 mm. Therefore, information obtained during this calibration was used to determine float height during testing.

The environment experienced by a high pressure turbine blade can be simulated with water as the working fluid by matching the Reynolds number. Though the velocity is much lower than in a gas turbine engine, water is much more dense, creating the same effect. Re_D is defined in Eq. 1, where the characteristic length D in this case is equal to the diameter of the leading edge (8.89 cm). Water density and viscosity are dependent on temperature, and were calculated per ASTM standards [21]. Though the room was air-conditioned and the water channel was typically at a temperature of $19°C$, on occasion it reached as high as $21°C$. The temperature of the water channel was measured before and after each test to ensure an accurate Re_D.

Water channel velocity was determined by releasing a bobber and recording the time it took to travel a distance of 144 cm downstream. The bobber was released far upstream of the first mark to ensure its velocity reached equilibrium prior to crossing the starting point. This process was repeated five times and the data were averaged to determine the actual water channel velocity, which was then adjusted until error in Re_D was less than 2%. Once the velocity was set, the model was placed in the forward half of the channel and

10

centered with the aid of a square. The flow visualization tests were conducted at $Re_D = 30$k. Ideally, tests would also have been conducted at $Re_D = 60$k but the maximum water channel velocity limited Re_D to approximately 43k. However, Rutledge [20] showed little variation between film cooling performance at $Re_D = 30$k and 60k.

The following blowing ratios were tested for each geometry: $M = 0.25$, 0.50, 0.75, 1.00, 1.25, 1.50, 1.75, and 2.00. Blowing ratio is defined in Eq. 3. For this experiment, the densities of the coolant and the freestream were identical, and the blowing ratio equation reduced to a velocity ratio. Velocity of the water channel was known based on the time trials described above, so the required flow rate for the coolant jet was calculated by Eq. 4. Once the flow rate was calculated it was correlated to a float height via the calibration data.

$$M = \frac{\rho_c \cdot V_c}{\rho_\infty \cdot V_\infty} = \frac{V_c}{V_\infty} = \frac{\frac{Q_c}{A_c}}{\frac{Re_D \cdot \mu_\infty}{\rho_\infty \cdot D}} = \frac{Q_c \cdot \rho_\infty \cdot D}{A_c \cdot Re_D \cdot \mu_\infty} \tag{3}$$

$$Q_c = A_c \cdot V_c \tag{4}$$

A 28 mm lens and Video Savant software was used to record high-speed photos of each test. Data was taken for a duration of five seconds at a frame rate of 30 frames per second. For each blowing ratio, the float was adjusted to the proper height and the flow was allowed to steady for several seconds prior to recording data.

3.3   Experimental Uncertainty

Because the coolant used in this study consisted of dyed water, a test was conducted to evaluate its diffusion into the water channel freestream. With the water channel set at test-velocity, drops of blue dye concentrated at 100% were injected into the freestream far upstream of the model. The drops traveled around the model and downstream past the end of the test section and into the return plenum. This test was accomplished several times with no diffusion noted throughout the entire length of the test section. This test clearly showed that the flow visualization information gathered throughout this research was solely a result of coolant interaction with the freestream and was not adversely affected by dye

diffusion. Releasing the bobber at the same time as injecting the dye also confirmed that the water channel velocity is uniform in the vertical direction, so that the velocity calculated via the bobber on the surface equals that at the leading edge model.

Uncertainty in flow rate was minimized by performing two extensive calibrations of the King flowmeter. The process involved measuring volumetric flow rate at 25 different float heights. The error in flow rate between the two calibrations was never more than 3% for each float height. In fact, for 12 of the 25 float heights, the flow rate calculated for the two trials was identical. This data generated a float height vs. flow rate curve that was then broken into five different sections to which linear curve fits were applied (shown in Fig. 164, pg. 117). These curve fits were used to build a table correlating float height to volumetric flow rate, and a table lookup function was used in order to determine the correct float height for each blowing ratio.

Using a gate valve to control flow to the flowmeter made it possible to hold the float steady within 1 mm of the desired float height for each blowing ratio. At low blowing ratios, an error of 1 mm in float height has a maximum error in flow rate of 3.5%, and at the upper end of the scale this error decreases to 0.5%.

The largest source of uncertainty came from setting the water channel velocity. In order to mitigate the human error inherent in using a stopwatch, the bobber time-trial was conducted five times and the data were averaged. It was fairly common that the same time was recorded for two or three of the trials, and the maximum difference between measurements was never more than 5%. In their 1999 text, Barlow et al. [22] present confidence probabilities based on the number of observations, n. Assuming a normally-distributed population of measurements, confidence probability is defined per Eq. 5. This is the probability that the actual mean (μ) falls within a confidence interval based on the calculated mean and the standard deviation of the population.

$$\beta_{cp} = \{\bar{x} - \Delta x < \mu < \bar{x} + \Delta x\} \qquad \Delta x = k_3 \cdot s \qquad (5)$$

The confidence factor (k_3) for a sample size of five and confidence probability of 95% is provided in the Barlow text as 1.2417. The standard deviation in stopwatch times for the

bobber time trials was never more than 0.15. Therefore, the error in mean time measurement (Δx) was not more than 0.18 seconds. With a 95% confidence that the actual mean for the bobber time trials was within 0.18 seconds of the calculated mean, the error in Re_D was limited to $\pm 5\%$. Because the water channel velocity was adjusted until error in Re_D was less than 2%, total error in Re_D was $\pm$ 7%.

Calculating the total uncertainty requires inclusion of the uncertainty in flowmeter flow rate and water channel velocity. Calculated error in water channel velocity was constant throughout the testing, while the error in coolant flow rate was maximum at low flow rates and minimum at high flow rates. Therefore, two cases are shown below. Equation 6 represents the error in blowing ratio for low blowing ratios, such as $M = 0.25$ or 0.50. Equation 7 provides the error calculation for the upper end of the scale, above $M = 1.50$. The worst case scenario is presented in both cases, with positive error in Q_c and negative error in Re_D. At $M = 0.25$, the maximum error is 11%, or $0.22 \leq M \leq 0.28$. For $M = 2.00$, the maximum error decreases to 8%, or $1.84 \leq M \leq 2.16$.

$$M = \frac{1.035 \cdot Q_c \cdot \rho_\infty \cdot D}{0.93 \cdot A_c \cdot Re_D \cdot \mu_\infty} \tag{6}$$

$$M = \frac{1.005 \cdot Q_c \cdot \rho_\infty \cdot D}{0.93 \cdot A_c \cdot Re_D \cdot \mu_\infty} \tag{7}$$

Finally, the flow visualization tests were very repeatable. On occasion, scheduling conflicts required that a geometry be tested on different days in order to obtain both camera views. This involved removing the model from the water channel and storing all the equipment. For example, the coolant jet resulting from two staggered rows of small cylindrical dimples upstream of the coolant hole is very distinct. During the initial test run, a high frequency flutter was observed in the coolant jet. Upon returning the following week to obtain the second camera view (and re-accomplishing the setup process), the coolant jet behaved identically. This repeatability was consistently observed throughout the research effort.

IV. Experimental Results and Discussion

The initial tests in this research were based on the dimple geometries studied by Roland [12] in 2008 and Frisinger [13] in 2009, and the results provided a vector for subsequent research. Flow visualization pictures for all tests are presented in the *Figures* section beginning on pg. 28. The reader will see two rows of pictures for each test case. The first row contains photos angled at approximately 45° upstream of an axis perpendicular to the flow direction. Small ink dots downstream of the cooling hole are spaced at $0.66d_c$, with one dot slightly upstream of the coolant hole denoting the stagnation point. The second row of pictures is a bottom view of the model. This view shows the thickness of the coolant film as well as jet protrusion into the freestream. The sequence of photos for each camera angle is shown at a non-dimensional time step of 0.51, where T is defined in Eq. 8.

$$T = \frac{t \cdot V_\infty}{D} \tag{8}$$

The specific geometries pictured in the *Water Channel Flow Visualization Data* section (pg. 28) do not appear the same as those in the *Model Schematics and Pictures* section (pg. 101) since after initial machining the gray models were painted white for better contrast. Each geometry was masked to prevent the white paint from settling in the dimples/trenches and changing the specifications of the geometry. After testing was completed, each geometry was touched-up with white paint in order to provide more distinguishable pictures for the *Model Schematics and Pictures* section. This issue would have been prevented by painting the gray PVC models white prior to machining.

The effectiveness of each flow control feature was evaluated by using batch-cropping software and Windows Movie Maker to assemble animated clips of each geometry. These animations were approximately one quarter of real-time speed. Microsoft Powerpoint was used to compare videos for multiple geometries side-by-side. Animations are interesting and insightful, but for the purposes of this document the author has included representative snapshots for each geometry.

4.1 Unmodified Coolant Hole

The first geometry tested was an unmodified coolant hole, results for which are shown in Figs. 1 – 8 starting on pg. 29. At low blowing ratios, the coolant jet is unsteady, wavering back and forth. Spanwise coverage is equal to the width of the elliptical coolant hole exit. Because the coolant hole was drilled in the spanwise direction, as blowing ratio increases the coolant jet extends above the hole and there is a lack of coverage directly downstream of the coolant hole. Photos taken from beneath the water channel illustrate the jet thickness off the surface (the coolant jet is denoted by the dark line in the pictures). At low blowing ratios the jet hugs the surface tightly. However, above $M = 0.75$ the jet begins to lift from the surface. Separation bubbles appear for blowing ratios at and above $M = 1.25$. At higher blowing ratios, coolant occasionally bursts from the main jet and into the freestream. Rutledge [20] observed similar coolant jet behavior for an unmodified coolant hole.

Not only do the pictures compare well to Rutledge's flow visualization results, they also correlate to his contour plots of adiabatic effectiveness [20]. Though it is not possible to make a direct comparison between a picture and a contour plot of η, the reader will notice a qualitative trend between the two. In Fig. 9 on pg. 33, for $M = 0.25$ the η contours are pointed directly downstream of the coolant hole, and the flow visualization picture agrees with this flow condition. It should be noted that the flow visualization picture has been flipped about both the horizontal and vertical axes in order to align with the adiabatic effectiveness plots. At $M = 0.50$, the contours show the flow is angled slightly below the coolant hole, nearly identical to the flow visualization picture. At these two low blowing ratios, the coolant is held tight to the surface and there is a sizeable region directly downstream of the coolant hole where $\eta \geq 0.7$. Figure 12 shows data for $M = 1.00$, where the coolant jet begins to lift off the surface and the high-η zone directly downstream of the coolant hole decreases sharply in size. This trend continues through the remaining blowing ratios. Figure 14 shows data for $M = 1.50$. The adiabatic effectiveness contours are angled sharply below the coolant hole, clearly illustrated by the water channel data. Here, the coolant jet extends far from the surface, shown quantitatively by Rutledge's plot where the high-η zone is virtually non-existent. These comparisons show that it is imperative to adhere the coolant to the surface to maximize adiabatic effectiveness.

The first two geometries tested were identical to those used by Roland in 2008 [12]: a row of seven small $(d/d_c = 0.79)$ cylindrical dimples placed either upstream or downstream of a single coolant hole. Schematics and pictures of these two dimple geometries are shown in Figs. 150 and 151, pg. 106. Frisinger [13] examined Roland's upstream pattern in greater detail in 2009. Because they observed increases in adiabatic effectiveness, the author hypothesized that the small dimples may somehow condition the boundary layer and hold the coolant jet tighter to the surface.

Data for the small cylindrical dimples upstream are shown in Figs. 15 – 22, pg. 36. A row of small cylindrical dimples placed directly upstream of the coolant hole has a very noticeable effect on the coolant jet at low blowing ratios. The dimples condition the freestream ahead of the coolant jet, energizing the boundary layer and steadying the coolant compared to the baseline case. However, as the blowing ratio increases beyond $M = 0.75$, this effect is no longer apparent. Pictures taken below the model disprove the hypothesis that the dimples would hold the coolant jet tighter to the surface, as the thickness of the jet looks identical to that of the unmodified case at all blowing ratios. The same separation bubbles are visible as in the unmodified case at the higher blowing ratios.

Comparing the water channel data to Frisinger's [13] adiabatic effectiveness contour plots provides some insight into the dimple effect. He noted a 7% increase in area-averaged η at $M = 0.25$. In Fig. 23 on pg. 40, the size of the high-η zone directly downstream of the coolant hole has increased very slightly compared to the no-dimple case shown in Fig. 9. As described above, flow visualization pictures show a very steady coolant jet resulting from the upstream dimples at $M = 0.25$. The increase in η observed by Roland [12] and Frisinger [13] may be due to the steadying effect the small dimples have on the coolant jet at this low blowing ratio. Furthermore, Frisinger observed negligible changes in η at higher blowing ratios. This also agrees with the flow visualization results, as the dimple effect diminished at $M \geq 0.75$ (see Figs. 24 – 28). Though Roland [12] tested the same upstream dimple pattern, flow visualization data will not be compared to his results because Frisinger's results are more accurate.

Contrary to upstream dimples, a row of small cylindrical dimples placed downstream of the coolant hole has no effect (perhaps even an adverse effect) on the coolant at low blowing ratios. Pictures for the small cylindrical dimples downstream of the coolant hole are shown in Figs. 29 – 36, pg. 43. The jet is unsteady, as in the control case, and the same protrusion into the freestream and separation bubbles are seen at higher blowing ratios.

Test results of the initial dimple patterns agree (in part) with the hypothesis. Though neither dimple pattern holds the coolant film tighter to the surface, small upstream dimples condition the boundary layer ahead of the coolant jet which results in a jet that is much more steady than the baseline case at blowing ratios up to $M = 0.75$. In his 2005 work, Khalatov [18] discusses the way that a staggered and tight arrangement of dimples causes the fluctuating vortex structure of each dimple to interact with the two dimples downstream of it. Because a single row of small upstream dimples is effective at low blowing ratios, it was predicted that a second staggered row of small upstream dimples would amplify dimple interaction with the boundary layer and extend the steadying effect to higher blowing ratios. For this reason, a second staggered row of small cylindrical dimples was added upstream of the existing row, as shown in Fig. 150 on pg. 106. A single row of cylindrical dimples downstream of the coolant hole had no effect on the coolant jet, so a second staggered row was not tested.

Two staggered rows of small cylindrical dimples upstream of the coolant hole do not perform as hypothesized. The coolant jet is steady compared to the baseline case but not as steady that which results from a single row of dimples. A high-frequency flutter is very apparent at low blowing ratios. In Fig. 37 on pg. 47, the middle picture in the top row shows a coolant jet that is slightly wider in the spanwise direction than the other two photos, and this represents a single cycle of the high-frequency flutter. The effect is not noticeable above $M = 0.75$, and the coolant jet looks identical to that observed with a single row of dimples. Regarding film attachment to the surface, the camera view below the model shows no difference compared to the single row of dimples.

Because cylindrical dimples upstream of the coolant hole steady the coolant jet at low blowing ratios, similar spherical dimple patterns were tested as well. Water channel data for this geometry are shown in Figs. 45 – 52, pg. 51. Concerning a single row of small spherical

dimples, there is no discernible difference when comparing its performance to that of the cylindrical dimples. Both have the same steadying effect on the jet below $M = 0.75$, and both look very similar to the unmodified coolant hole at higher blowing ratios. This may be a fortuitous finding because, in the case of this research, the cylindrical dimples were easier to machine.

The staggered dimple pattern was intended to be of the exact same size and placement as the cylindrical dimple pattern. In Fig. 152 on pg. 107, the reader may notice that two machining errors were made when fabricating the dimple pattern. The first row of dimples is located correctly, but the staggered row is one degree closer to the stagnation line than intended. This moved the staggered row 0.762 mm further upstream, and the reader should reference Fig. 150 on pg. 106 for a comparison to the cylindrical dimple pattern. Secondly, the bottom dimple was milled even further upstream, and this is evident in the photo. In the interest of time, this dimple pattern was not re-completed. The staggered row was displaced by a very small amount and the bottom dimple likely has no effect on the coolant jet.

Water channel data for the staggered spherical dimples are shown in Figs. 53 – 60 on pg. 55. At low blowing ratios, the second staggered row of spherical dimples steadies the coolant jet in the same way as the single row. But a very interesting phenomena is observed at $M = 0.25$: comparing Figs. 53 and 45, the staggered row causes a sharp upward draft at the bottom of the coolant hole that narrows the coverage of the coolant jet compared to the single row case. At all other blowing ratios, performance is the same compared to the single row of spherical dimples. Finally, it should be noted that the high-frequency flutter observed in the staggered cylindrical dimple case does not occur with the staggered rows of spherical dimples.

Testing larger dimples was necessary to determine the effect increased Re_d has on the coolant jet. Because $Re_d \approx 1300$ for the small dimples, it was hypothesized that they are unable to affect the coolant jet at high blowing ratios where it extends further from the surface. The medium dimples discussed in this section are twice the size of the small dimples, providing $Re_d \approx 2,600$. Dimensions for the medium dimples are shown in Figs. 153 and 154 on pg. 108. Because of the increased size of these dimples, it was not practical to test them upstream of the coolant hole, so medium cylindrical and spherical dimples were tested at a location downstream of the coolant hole.

A medium cylindrical dimple placed downstream of the coolant hole does not have a steadying effect on the coolant jet. In Figs. 61 – 68 beginning on pg. 59, the coolant jet appears identical to the baseline case at all blowing ratios. However, a medium spherical dimple in the same location steadies the coolant jet at low blowing ratios in a manner similar to what occurs with small dimples upstream. Data for the medium spherical dimple are given in Figs. 69 – 76 beginning on pg. 63. Compared to the small upstream dimples, a medium spherical dimple downstream of the coolant hole acts identically and there is no discernible difference between the two coolant jets at any blowing ratio. Similar to all other test cases, pictures from below the model show that the geometry has no effect on the thickness of the film coolant layer.

Because the coolant jet bypasses the single medium dimple at high blowing ratios, a second dimple was added directly above it and the geometry was retested. Data for the two medium spherical dimples are shown in Figs. 77 – 84 on pg. 67. At $M = 0.25$, the second dimple pulls the coolant towards it and, counterintuitively, the bottom dimple no longer pulls coolant upwards as seen in the single dimple case. Comparing Figs. 77 and 69, the two dimple case slightly increases the spanwise coverage compared to the single dimple case. At $M = 1.00$, the coolant jet extends completely over the second dimple. At $M = 1.25$, the coolant jet is roughly centered on the second dimple and bypasses the lower dimple completely. Unfortunately, doubling Re_d has no effect on the thickness of the coolant jet and did not extend the steadying effect seen with small dimples to higher blowing ratios.

4.4 Large Dimples (d/d_c = 2.38, h/d = 0.2)

Testing a third and final dimple size provided information for $Re_d \approx 4{,}000$. Contrary to medium or small dimples, the effects of a large cylindrical dimple are pronounced. In Figs. 85 and 86 on pg. 71, the large dimple draws coolant in at $M \leq 0.50$. Like the previous cylindrical dimples downstream of the coolant hole, the large cylindrical dimple does not have a steadying effect on the coolant. Regarding both steadiness and height from the surface, the coolant jet acts similarly to the baseline case at blowing ratios above $M = 0.75$.

Compared to the cylindrical dimple at low blowing ratios, a large spherical dimple behaves much differently, shown in Figs. 93 – 100 beginning on pg. 75. For $M \leq 0.75$, the coolant is steady compared to the baseline case. Yet, there is a subtle amount of wavering that is not apparent when analyzing the small and medium dimples. This is likely due to the fact that Re_d is approaching the laminar-turbulent transition range and the dimple is entraining more coolant than the small and medium dimples. The side-view shows the dimple pulling coolant upwards but photos from below the model show that it does not entrain nearly as much coolant as a large cylindrical dimple (compare Figs. 93 and 85). The thickness of the coolant jet is no different than in the baseline case, and though Re_d is approaching the transitional range, it is still not high enough to affect the coolant jet at higher blowing ratios where the film thickness increases.

Finally, adding a second large spherical dimple performed similarly to a single-dimple. Data for the two large spherical dimples are located at Figs. 101 – 108, pg. 79. As in the case of the two medium spherical dimples, the second dimple pulls some coolant upwards at $M = 0.25$, which slightly increases the spanwise coverage of the jet. The jet steadiness is comparable to that of the single-dimple case. At $M = 2.00$, the second dimple is centered in the coolant flow but it appears to have no effect on the coolant jet at high blowing ratios.

4.5 Single-depth Transverse Trench (h/d$_c$ = 0.50, w = d$_c$)

A single-depth transverse trench was investigated based on its performance reported in previous research. The trench geometry is shown in Fig. 157 on pg. 110. A depth of $0.50d_c$ and width of d_c were chosen as a starting point.

Data for the single depth trench are shown in Figs. 109 – 116, pg. 83. This trench is most effective at $M \leq 0.50$, where it entrains the coolant throughout its length and the coolant is slowly pulled out by the freestream. As compared to the baseline coolant hole this effect increases the breadth of coverage by 225% in the spanwise direction. The film coolant is extremely steady at $M \leq 0.50$, more steady than any other case observed thus far. Because the coolant hole is inclined 20° to the surface, at blowing ratios above $M = 0.50$ the coolant jet begins to blow out of the trench, and a gap in coverage appears directly downstream of the coolant hole. The coverage gap widens with increasing blowing ratio. Pictures taken below the model show a similar coolant thickness at all blowing ratios compared to the baseline case, but no separation bubbles were visible. This is not to say that separation bubbles don't exist: they may be masked by the fact that the jet extends so far in the spanwise direction.

In Figs. 109 and 110, the reader will notice some streaking of the coolant, leading to inconsistent coverage in the spanwise direction. It was hypothesized that this streaking may be due to the square downstream edge of the trench and that adding a small fillet to the edge may prevent the effect. In their 2007 work, Dorrington et al. [23] state that adding a 45° notch along the upper half of a trench wall significantly reduces trench performance. However, their research investigated axial coolant holes whereas the current study involves a radial coolant hole. The trench was modified by placing a small fillet along the length of its downstream edge ($r_f = 0.25w$), and flow visualization pictures for the filleted trench are shown in Figs. 117 – 124, pg. 87. Unfortunately, the hypothesis proved to be incorrect, as the fillet did not resolve the coolant streaking. Furthermore, the fillet adversely affected the ability of the trench to entrain the coolant, decreasing jet steadiness at $M = 0.25$ and magnifying the blow-out seen above $M = 0.50$.

4.6 Tapered-depth Trench ($h/d_c = 1.0 \implies 0.50$, $w = d_c$)

Because the single-depth trench suffered from coolant blow-out, a tapered-depth trench was designed to prevent this issue. A schematic detailing the dimensions of the tapered depth trench is presented in Fig. 158 on pg. 111. It was hypothesized that a trench of increased depth at the coolant hole would entrain the coolant at high blowing ratios and that tapering the trench depth would result in very even and increased spanwise coverage.

Data for the tapered-depth are shown in Figs. 125 – 132 beginning on pg. 91. The tapered-depth trench performs much differently than the single-depth trench. Whereas the single-depth trench is most effective at $M \leq 0.50$, the tapered-depth trench is most effective above $M = 0.50$. Because of its increased depth at the coolant hole, at low blowing ratios the coolant settles in the bottom of the trench and is pulled out in a sporadic and uneven manner. Coverage in the spanwise direction is streaky, uneven, and unsteady (see Figs. 125 and 126 on pg. 91). Beginning at $M = 0.75$, the coolant flows out of trench evenly, resulting in excellent spanwise coverage. The above hypothesis proves true for higher blowing ratios: the deeper trench prevents coolant jet blow-out and provides even coverage at all spanwise locations at and above the coolant hole exit. Comparing the two trenches at $M = 2.00$, there is a large gap in coverage downstream of the coolant hole in the single-depth trench, but the tapered-depth trench prevents this problem (compare Figs. 116 and 132).

The tapered-depth trench is the only geometry tested that affects the thickness of the coolant jet. As blowing ratio increases, the thickness of the coolant jet in the baseline case continues to increase, protruding further into the freestream. The thickness of the jet for the tapered-depth trench increases with blowing ratio as well, but at a much slower rate. The first noticeable difference in jet thickness is at $M = 1.00$, as the film coolant layer is held much tighter to the surface with the trench than the baseline hole (compare Fig. 128 on pg. 92 to Fig. 4 on pg. 30). This trend continues through the remaining blowing ratios. The tapered-depth trench also delays the onset of coolant bursting into the freestream. In the baseline case, this begins to occur at $M = 1.25$, and it is not observed until $M = 1.75$ for the tapered-depth trench.

Because the tapered-depth trench holds the coolant jet tight to the surface at high blowing ratios, it was hypothesized that a dimple geometry that is effective at steadying the coolant jet at low blowing ratios may do the same in this case. Therefore, a row of small cylindrical dimples ($d/d_c = 0.79$) was added upstream of the tapered-depth trench (see Fig. 158, pg. 111). Unfortunately, the resulting coolant flow is no more steady than observed in the original tapered-depth trench (reference Figs. 133 – 140, pg. 95). The trench likely has a severe effect on the boundary layer, which overwhelms any conditioning provided by the upstream dimples. Downstream dimples were not tested in conjunction with the tapered-depth trench because their effect on the coolant was very similar to that of the upstream dimples, and it was not thought that they would provide any benefit.

4.7   Boundary Layer and Coolant Jet Thickness

Calculating an approximate boundary layer thickness at the coolant jet provides some insight into the effect dimples have on the coolant jet. White [24] defines boundary layer thickness for a flat plate per Eq. 9. Using the arc-length distance from stagnation to the coolant hole ($x_c = 16.68$ mm) as well as $Re_x = Re_D = 30$k, boundary layer thickness at the coolant hole is approximated as 0.48 mm.

$$\delta_c = \frac{5.0 \cdot x_c}{\sqrt{Re_x}} \tag{9}$$

Because it disturbs the boundary layer, a dimple can be thought of as a roughness element. All dimples studied in this research had $h/d = 0.2$, and for the small dimples this equated to a roughness height (k) of 0.762 mm. Similarly, roughness height equalled 1.524 mm and 2.286 mm for the medium and large dimples, respectively. Figures 141 – 144 on pg. 99 compare coolant jet thickness to roughness height for several geometries at different blowing ratios. At $M = 0.25$, coolant jet height is approximately equal to or less than the height of all the roughness elements: Fig. 141 shows that the jet extends approximately

1 mm from the surface. Because at $M = 0.25$ the coolant jet height is nearly equal to that of the boundary layer, it is intuitive that the dimples have an affect on the coolant jet at this low blowing ratio.

White [24] states that the laminar-turbulent boundary layer transition occurs earlier according to Eq. 10. Displacement thickness (δ^*) is defined in Eq. 11. It is the distance the freestream inviscid flow is pushed away from the surface by the viscous layer at the surface, and is equal to 0.17 mm in this case. With a minimum roughness height of 0.762 mm, the ratio defined in Eq. 10 is equal to 4.2. Therefore, it is apparent that the dimples have a steadying effect on the coolant jet at $M = 0.25$ because they are tripping the laminar boundary layer to a turbulent state. Turbulent boundary layers have higher energy and more momentum, characteristics that likely contributed the steadying effect of the dimples at low blowing ratios.

$$0.3 = \frac{k}{\delta^*} \tag{10}$$

$$\delta^* = \frac{1.721 \cdot x_c}{\sqrt{Re_x}} \tag{11}$$

Figure 142 shows why the dimple effect starts to break down at $M = 0.75$. Here, the coolant jet extends 4-5 mm above the surface, which is far greater than the boundary layer thickness as well as the roughness height of even the largest dimples studied. Though the dimples are still affecting the boundary layer, the coolant jet extends far beyond the boundary layer and is generally unaffected by what occurs close to the surface. Furthermore, the coolant jet at the higher blowing ratios has much higher momentum than at low blowing ratios, and therefore is less affected by the dimples. Figures 143 and 144 illustrate the effect of the tapered-depth trench, as the coolant jet height is 3-5 mm less than other cases at $M = 1.25$ and 2.00.

V. Conclusions and Recommendations

In total, 16 geometries were tested, each at eight different blowing ratios for a total of 128 test cases. High-speed photos were taken from both a side angle and from beneath the water channel, the latter illustrating jet protrusion into the freestream. Of these geometries, several have a positive impact on the behavior of a coolant jet: a single row of small cylindrical or spherical dimples upstream of the coolant hole, medium or large spherical dimples downstream of the coolant hole, a constant-depth transverse trench, and a tapered-depth transverse trench.

5.1 Conclusions

A great deal of leading-edge film cooling flow visualization information was acquired during this research. As a result, several flow control methods can be eliminated from future leading edge film cooling research due to their inability to condition a film coolant jet in a positive manner. Cylindrical dimples downstream of the coolant hole, regardless of size, have no positive impact on the relative steadiness or attachment to the blade surface compared to a baseline cooling hole. Also, adding a second staggered row of dimples upstream of the coolant hole does not extend the steadying effect to higher blowing ratios. Finally, placing a fillet on the downstream edge of a transverse trench allows coolant to exit the trench more easily, aiding in jet liftoff and adversely affecting performance.

Several geometries had positive impacts on the coolant jet at low blowing ratios. A single row of small cylindrical or spherical dimples placed directly upstream of the coolant hole significantly reduces coolant jet unsteadiness at $M \leq 0.75$. The increases in adiabatic effectiveness observed by Roland in 2008 [12] and Frisinger in 2009 [13] may be due, in part, to this steading effect. It is also apparent that medium and large spherical dimples placed downstream of the coolant jet have a similar effect at $M \leq 0.75$: coolant is drawn into the dimple and this results in an extremely steady, unwavering coolant jet. However, no dimples evaluated in this study have an impact on the coolant jet at high blowing ratios where the thickness of the coolant jet increases well beyond the boundary layer. Furthermore, dimples are known to affect a laminar boundary layer, and it is likely that the coolant-freestream

interaction causes a turbulent state at high blowing ratios, diminishing the dimple effect. Finally, a single-depth transverse trench not only steadies the coolant jet, but increases the coverage of a single coolant hole more than two times in the spanwise direction. The coolant blows out of the trench at blowing ratios above $M = 0.50$, resulting in a gap in coverage directly downstream of the trench.

At blowing ratios above $M = 0.75$, the only geometry found to be effective is a tapered-depth trench. While dimples and a single-depth trench are effective at blowing ratios up to $M = 0.75$, a deeper, tapered-depth trench is more effective when $M \geq 0.75$. Because of its increased depth at the coolant hole exit, a tapered-depth trench entrains the coolant at high blowing ratios, preventing coolant jet liftoff and creating very evenly distributed coverage from the centerline of the coolant hole to the end of the trench. A tapered-depth trench was the only geometry studied that has a noticeable impact on the thickness of the coolant jet. At $M \geq 1.00$, a tapered-depth trench holds the film coolant much closer to the surface than an unmodified coolant hole. The general ability of a trench to increase the spanwise coverage of a single coolant hole and prevent jet liftoff is consistent with previous research [15-17].

Though the above geometries were not optimized and need further investiagtion, the potential impact of this research is clear. Depending on the blowing ratio used in a specific film cooling application, geometries evaluated in this research could significantly increase performance. Dimples have a steadying effect and a single-depth trench increases the coverage of a single coolant hole at low blowing ratios. For high blowing ratios, a tapered depth trench also increases the spanwise coverage of a single coolant hole. It is the only geometry that holds the coolant tight to the surface and prevents jet liftoff, a significant problem consistently seen in previous leading edge film cooling research. These observations have the potential to improve the leading edge film cooling process by decreasing the number of film cooling holes and amount of bleed air required for cooling.

5.2 Recommendations and Suggestions for Future Research

The dimple patterns evaluated in this study have yet to be optimized. Parameters to consider include tighter dimple spacing, distance from the coolant hole exit, and Re_d. Also, staggered rows of medium and large spherical dimples downstream of the coolant hole may yield additional results.

It is highly recommended that the tapered-depth trench be investigated further. Knowledge of fluid dynamics within the trench would aid in the optimization process. Parameters for optimization research should include trench depth (both initial and terminal); trench length; taper ratio; and length of the initial constant depth portion at the coolant hole exit. Beginning with additional flow visualization studies, an attempt should be made to optimize the trench's coverage and ability to hold the coolant tight to the surface. In theory, if the trench is optimized such that the coolant jet is held even tighter to the surface, a row of medium or large spherical dimples directly downstream could steady the coolant as seen in this research.

Ultimately, heat transfer testing in the wind tunnel should be used to compare film cooling effectiveness levels of both the single-depth and optimized tapered-depth trench to that of an unmodified coolant hole. Testing must include higher Re and turbulence to simulate realistic engine conditions. Should wind tunnel testing demonstrate a significant increase in film cooling performance, additional testing would be required to determine the impact on the turbine blade as a whole. Milling a trench on the leading edge of a turbine blade may have adverse aerodynamic effects, and this would have to be investigated prior to employing it as a film cooling technique in engine cycles.

Finally, the coolant-to-freestream density ratio was equal to one in this study. In a real engine, this ratio is closer to 2.0 because of the significant temperature difference between the coolant and the freestream. Ekkad et al. [25] observed that higher density coolant prevents turbulent mixing because it is heavier than the freestream fluid and reduces interaction with the freestream. Once a dimple or trench configuration has been optimized in the water channel, it will be necessary to evaluate the geometry's performance subject to the increased density ratio, as it may behave differently.

Figures

Figures are divided into three sections. The first section contains water channel flow visualization pictures for each geometry. The second section (pg. 101) consists of model schematics and pictures. The third section (pg. 112) provides experimental setup and flowmeter calibration information.

Water Channel Flow Visualization Data

In general, the reader will see two rows of pictures for each test case. The first row contains photos angled at approximately 45° upstream of an axis perpendicular to the flow direction. Small ink dots downstream of the cooling hole are spaced at $0.66d_c$, with one dot slightly upstream of the coolant hole denoting the stagnation point. The second row of pictures is a bottom view of the model. This view shows the thickness of the coolant film as well as jet protrusion into the freestream. The sequence of photos for each camera angle is shown at a non-dimensional time step of 0.51, where T is defined in Eq. 8 on pg. 14. Flow direction is from the right.

There are also comparisons of flow visualization pictures to adiabatic effectiveness contour plots (i.e. pg. 33). In these figures, the flow visualization picture has been flipped about the horizontal and vertical axes to match the adiabatic effectiveness plot. Therefore, flow direction is from the left.
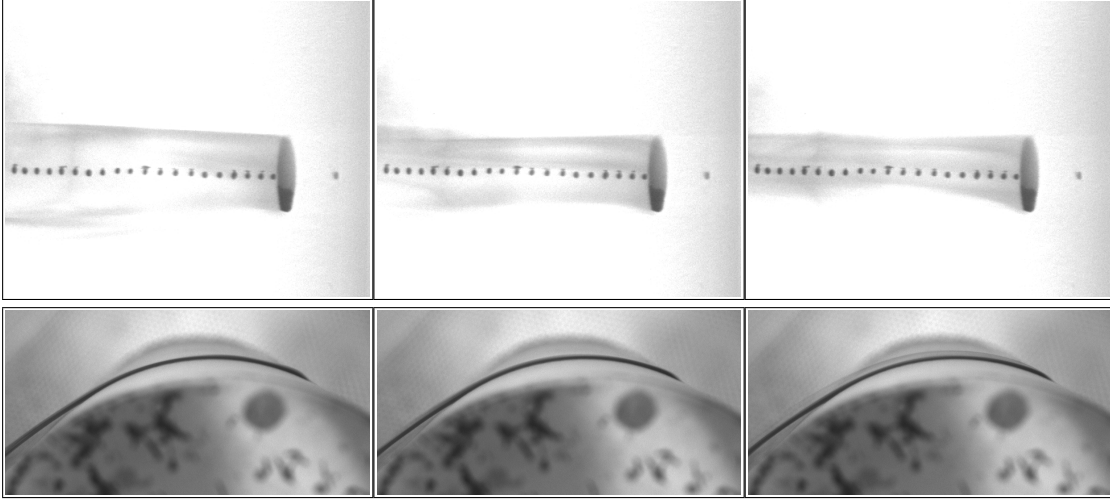
Figure 1   Unmodified coolant hole - $M = 0.25$
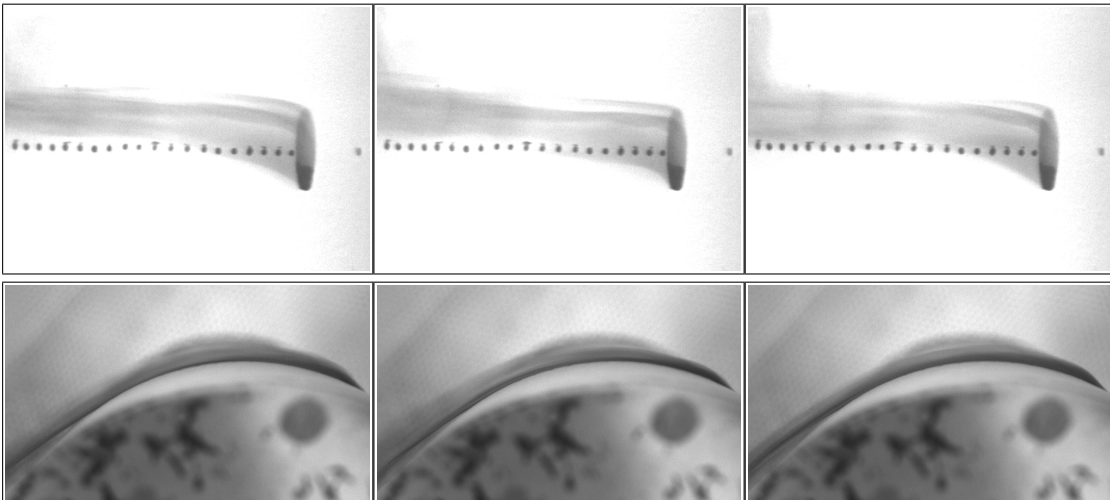
Figure 2   Unmodified coolant hole - $M = 0.50$
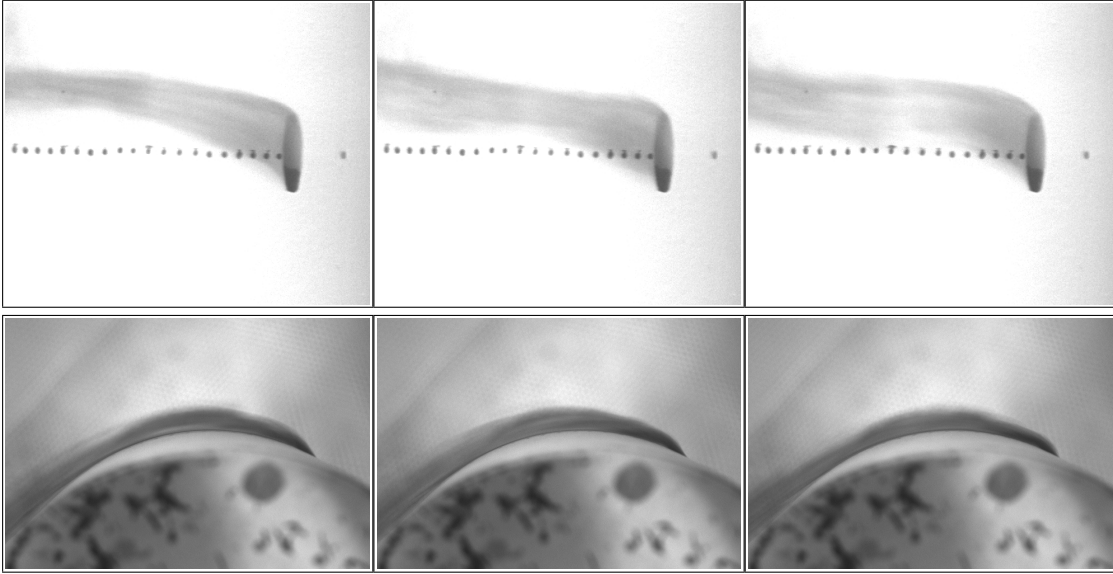
Figure 3   Unmodified coolant hole - $M = 0.75$
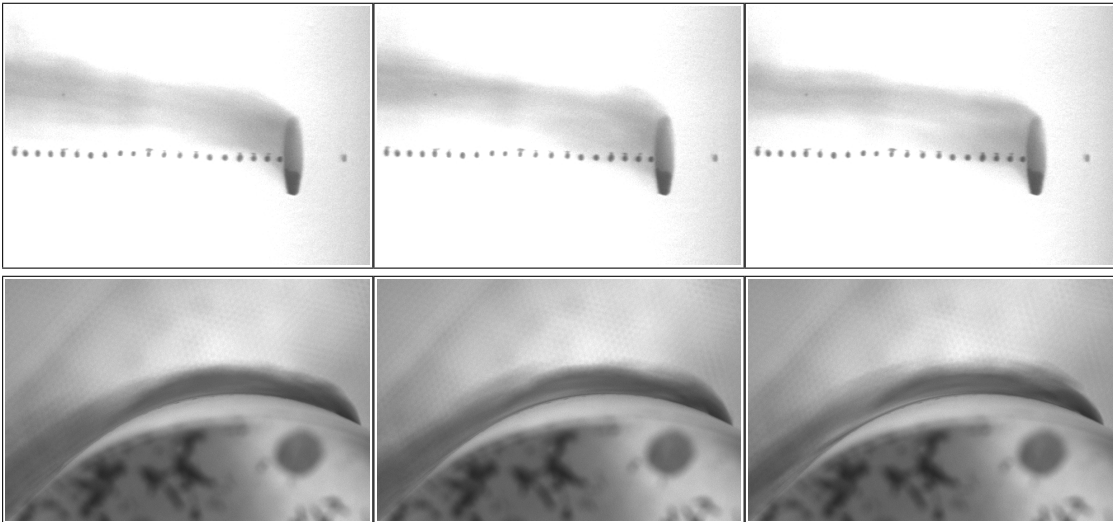
Figure 4   Unmodified coolant hole - $M = 1.00$
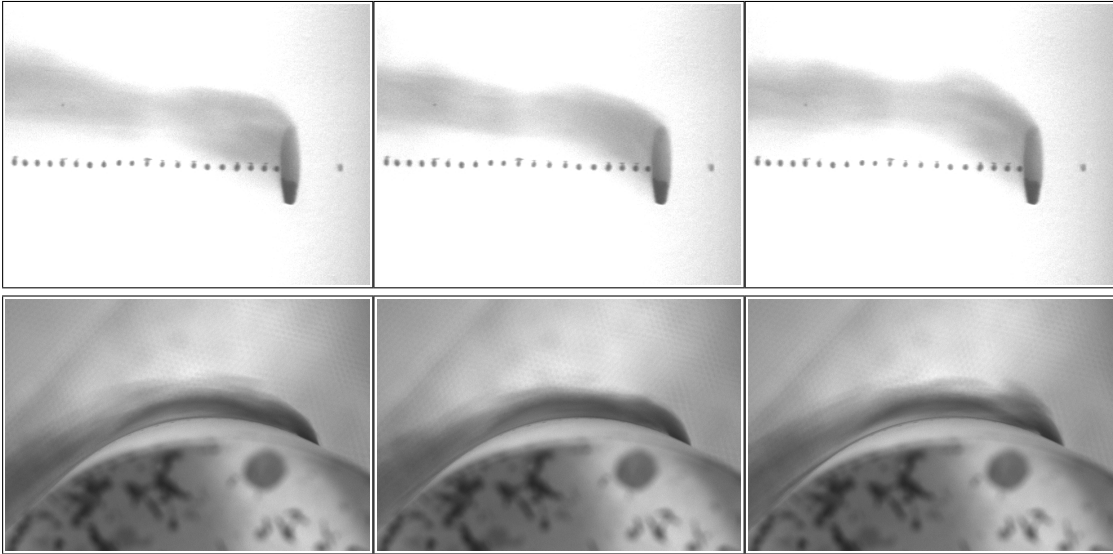
Figure 5   Unmodified coolant hole - $M = 1.25$
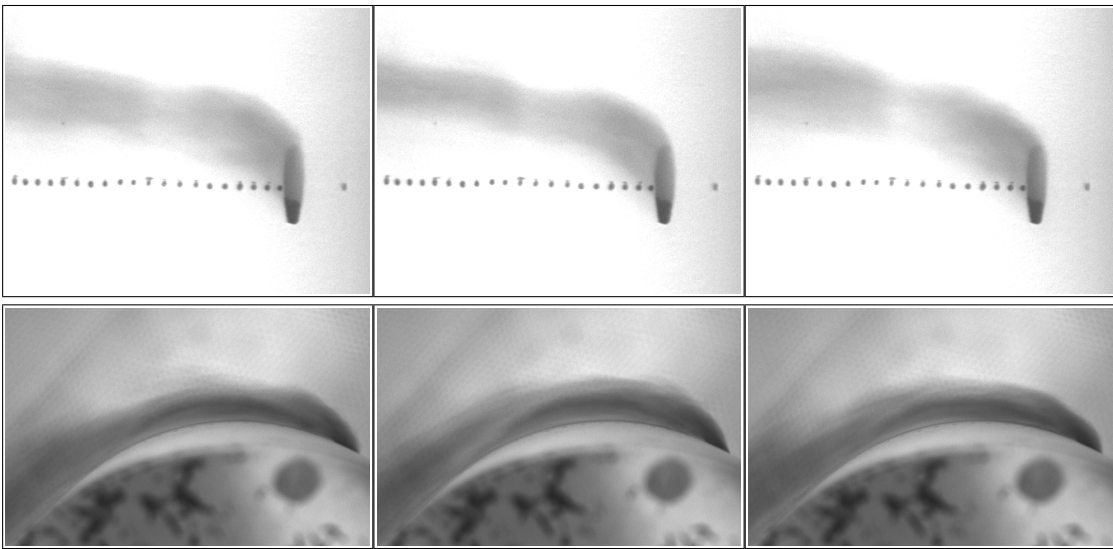
Figure 6   Unmodified coolant hole - $M = 1.50$
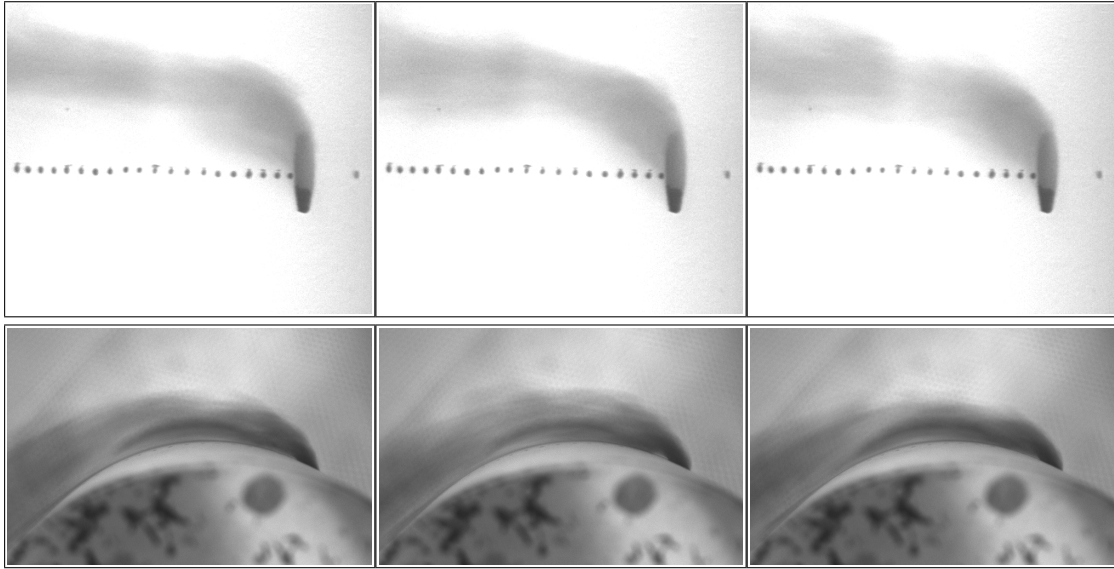
Figure 7   Unmodified coolant hole - $M = 1.75$
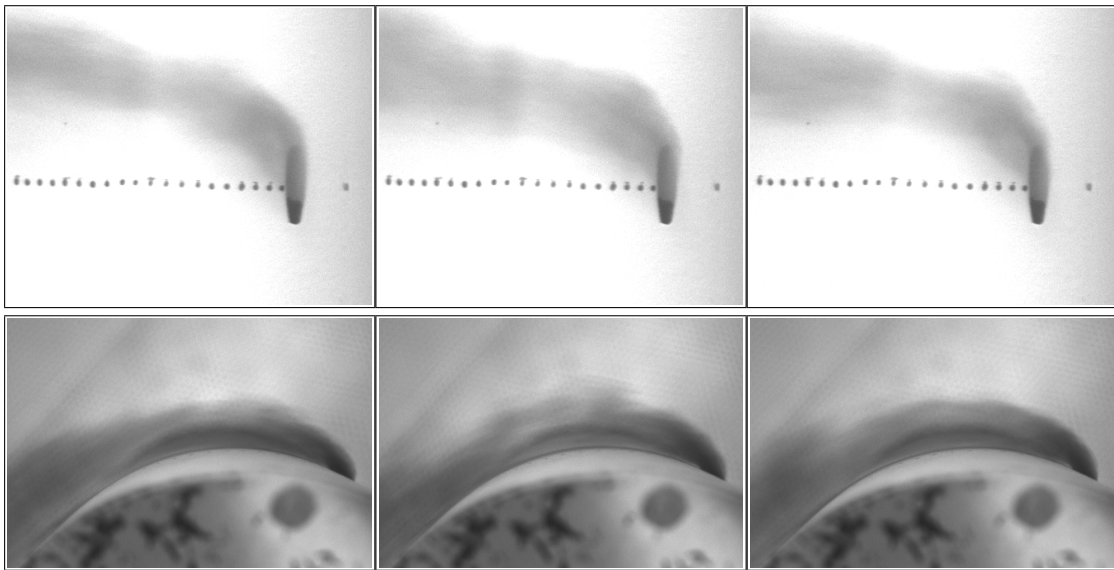
Figure 8   Unmodified coolant hole - $M = 2.00$
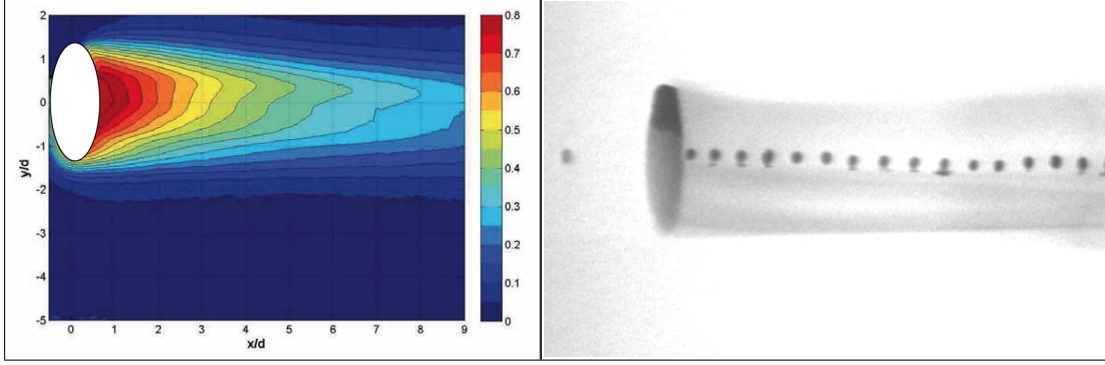
Figure 9   Comparison of adiabatic effectiveness plot from Rutledge [20] to flow visualization data for $M = 0.25$. Adiabatic effectiveness plot was generated at $Re_D = 30$k with low turbulence nearly identical to that of the water channel flow visualization study ($< 1\%$). Flow visualization picture has been flipped on its horizontal and vertical axes to match the adiabatic effectiveness data.
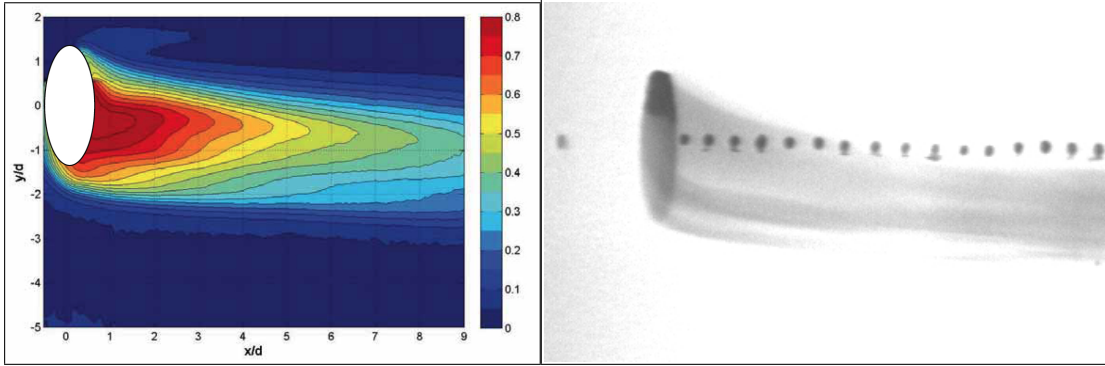
Figure 10   Comparison of adiabatic effectiveness plot from Rutledge [20] to flow visualization data for $M = 0.50$. Adiabatic effectiveness plot was generated at $Re_D = 30$k with low turbulence nearly identical to that of the water channel flow visualization study ($< 1\%$). Flow visualization picture has been flipped on its horizontal and vertical axes to match the adiabatic effectiveness data.
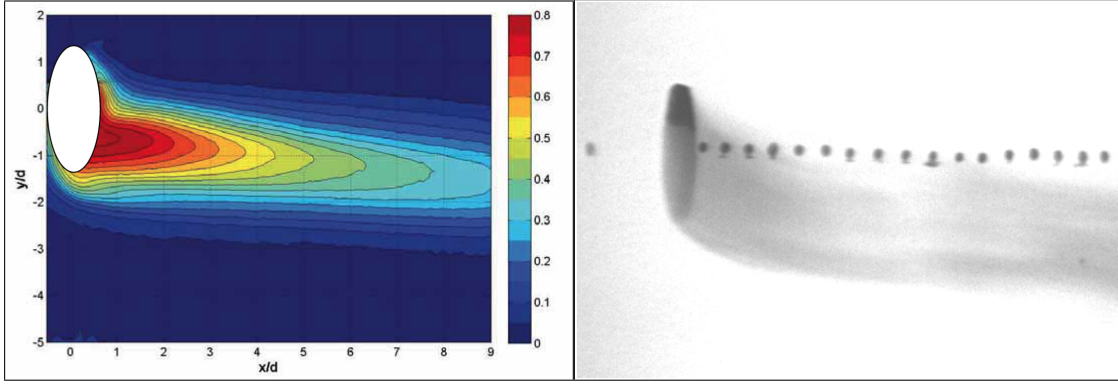
Figure 11   Comparison of adiabatic effectiveness plot from Rutledge [20] to flow visualization data for $M = 0.75$. Adiabatic effectiveness plot was generated at $Re_D = 30k$ with low turbulence nearly identical to that of the water channel flow visualization study ($< 1\%$). Flow visualization picture has been flipped on its horizontal and vertical axes to match the adiabatic effectiveness data.
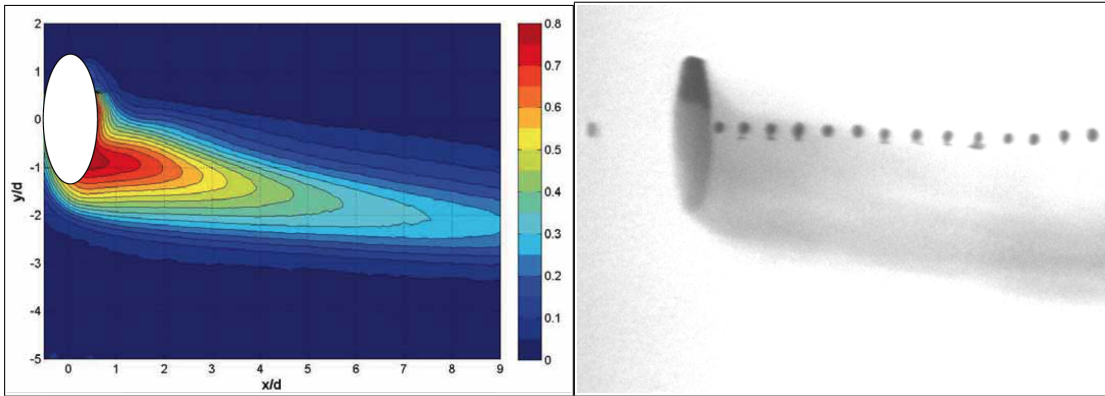
Figure 12   Comparison of adiabatic effectiveness plot from Rutledge [20] to flow visualization data for $M = 1.00$. Adiabatic effectiveness plot was generated at $Re_D = 30k$ with low turbulence nearly identical to that of the water channel flow visualization study ($< 1\%$). Flow visualization picture has been flipped on its horizontal and vertical axes to match the adiabatic effectiveness data.
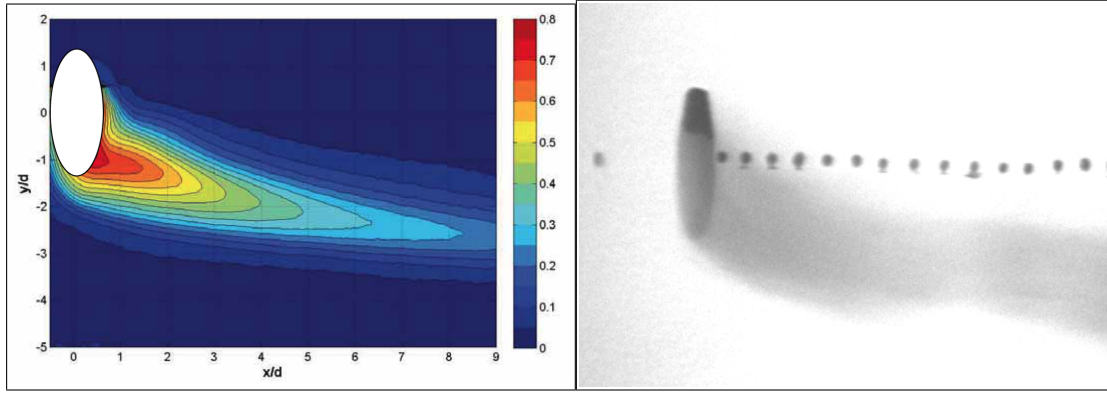
Figure 13   Comparison of adiabatic effectiveness plot from Rutledge [20] to flow visualization data for $M = 1.25$. Adiabatic effectiveness plot was generated at $Re_D = 30$k with low turbulence nearly identical to that of the water channel flow visualization study ($< 1\%$). Flow visualization picture has been flipped on its horizontal and vertical axes to match the adiabatic effectiveness data.
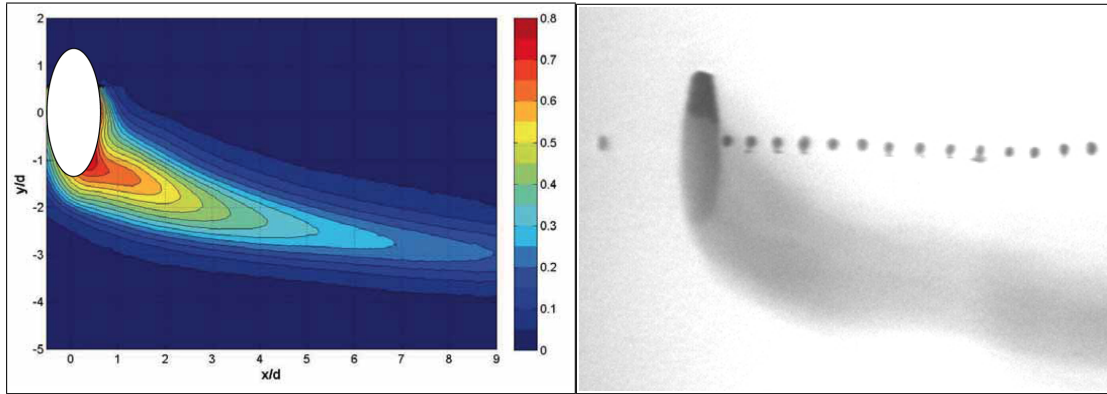
Figure 14   Comparison of adiabatic effectiveness plot from Rutledge [20] to flow visualization data for $M = 1.50$. Adiabatic effectiveness plot was generated at $Re_D = 30$k with low turbulence nearly identical to that of the water channel flow visualization study ($< 1\%$). Flow visualization picture has been flipped on its horizontal and vertical axes to match the adiabatic effectiveness data.
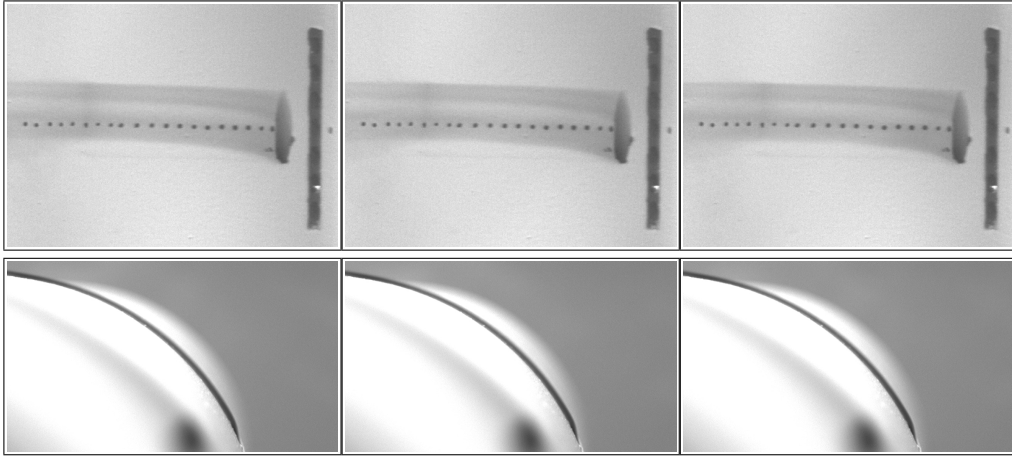
Figure 15   Small cylindrical dimples upstream of coolant hole - $M = 0.25$
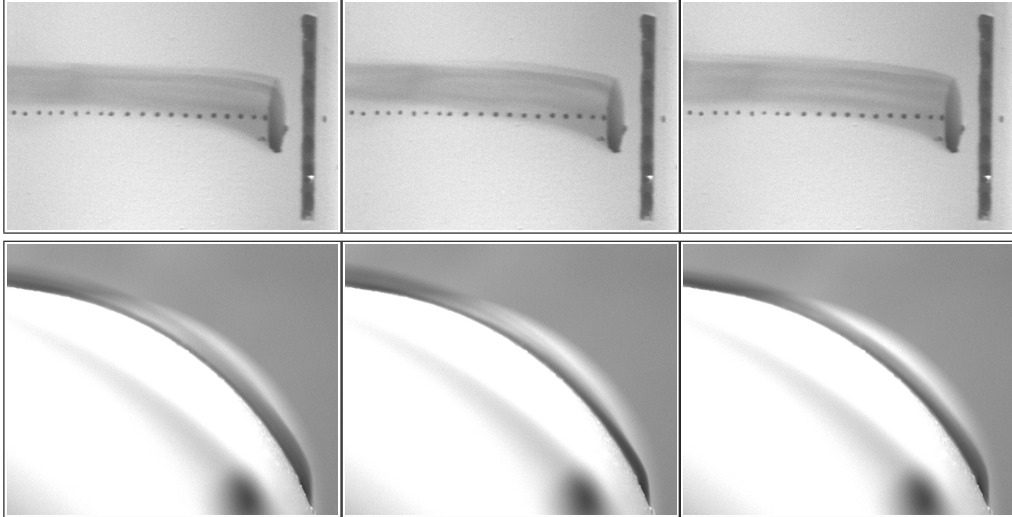
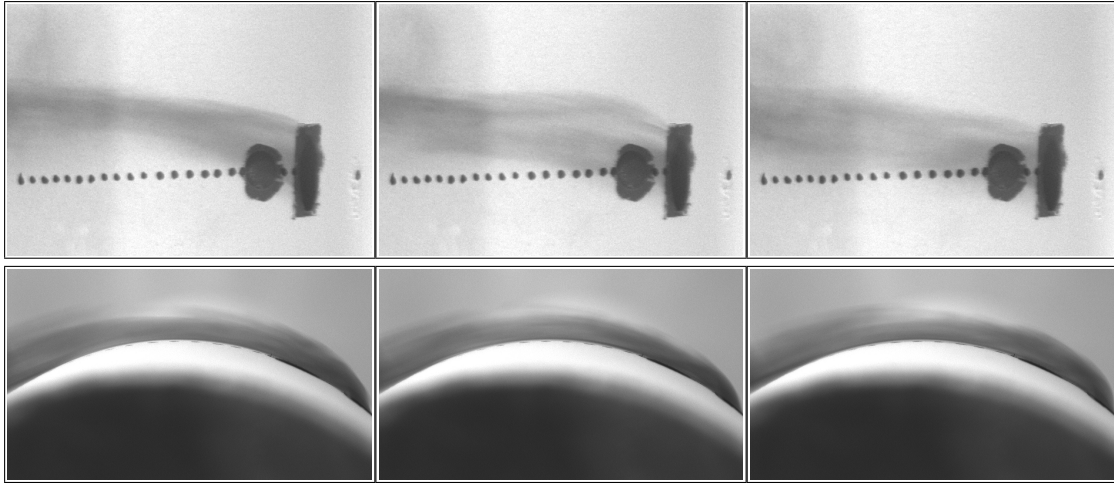Figure 16   Small cylindrical dimples upstream of coolant hole - $M = 0.50$
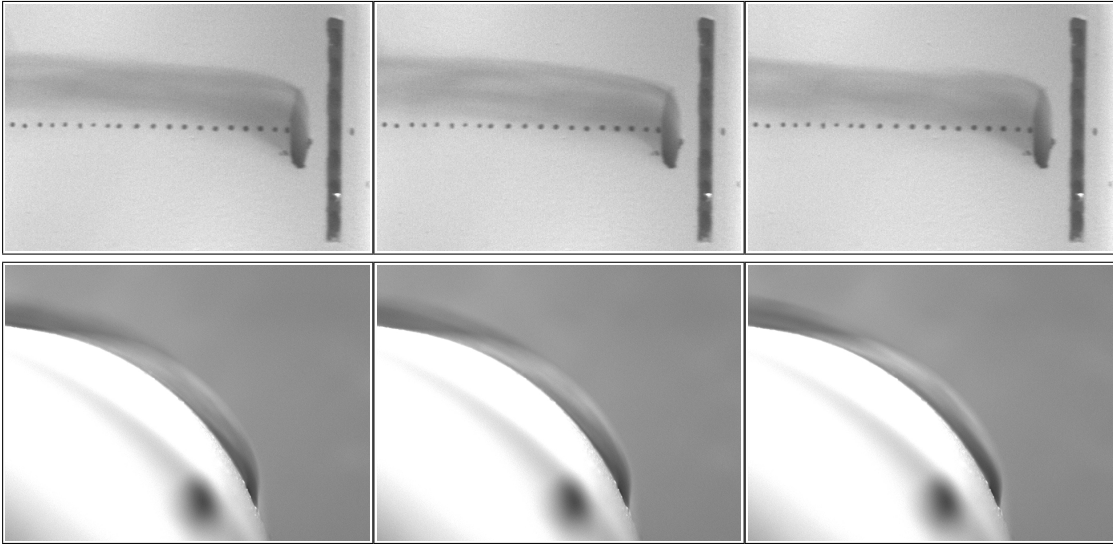
Figure 17   Small cylindrical dimples upstream of coolant hole - $M = 0.75$
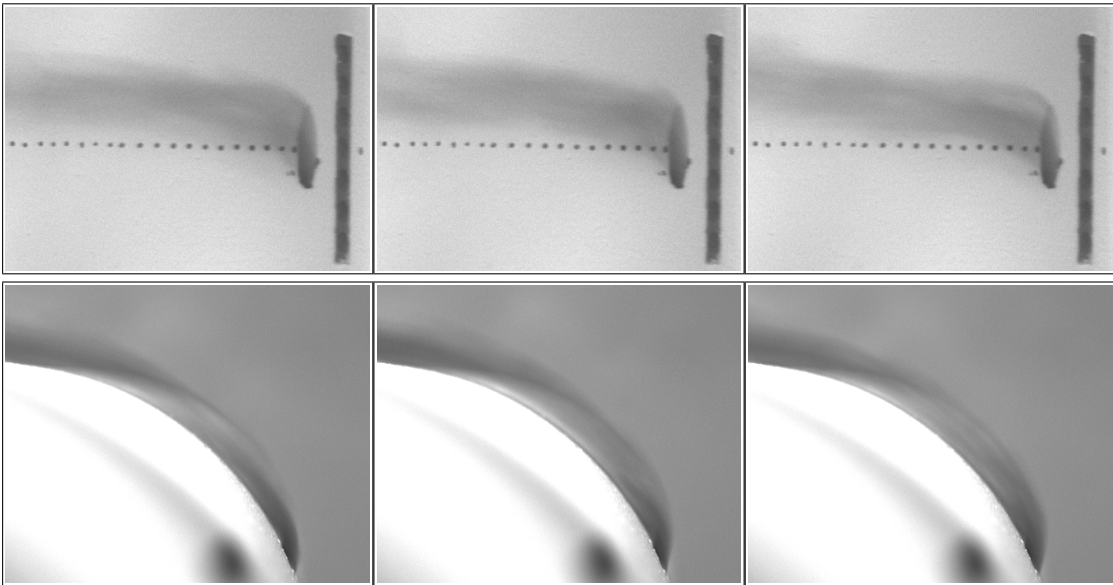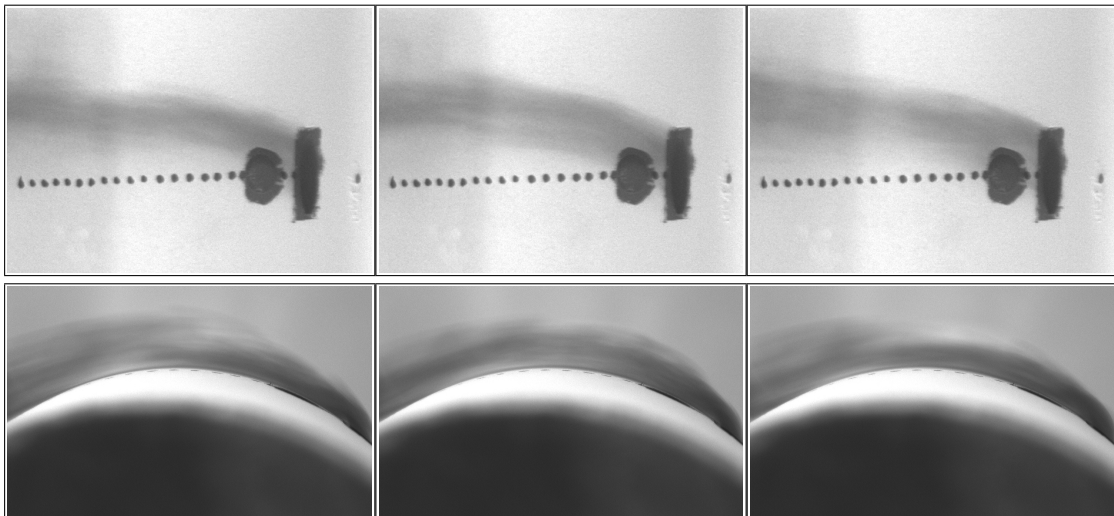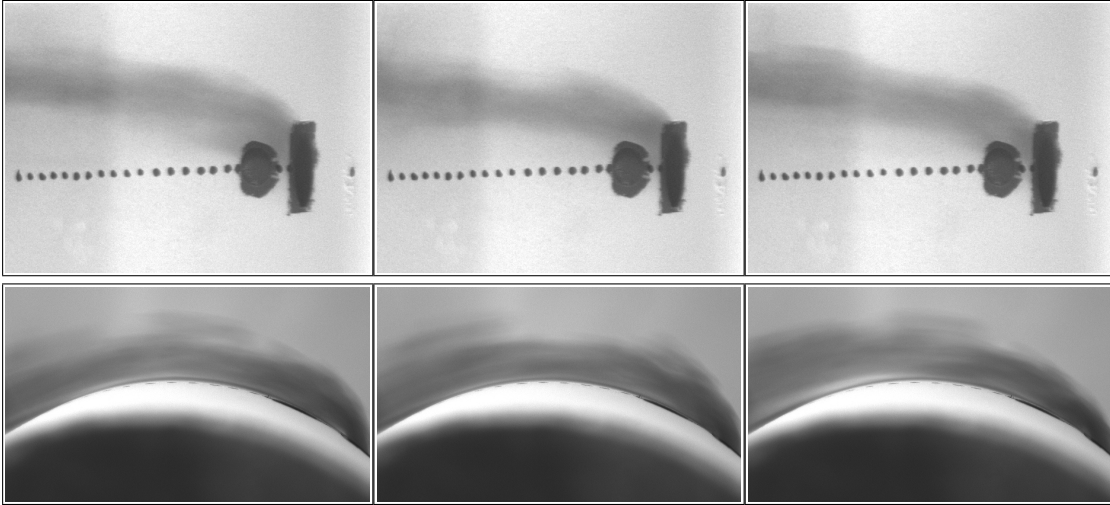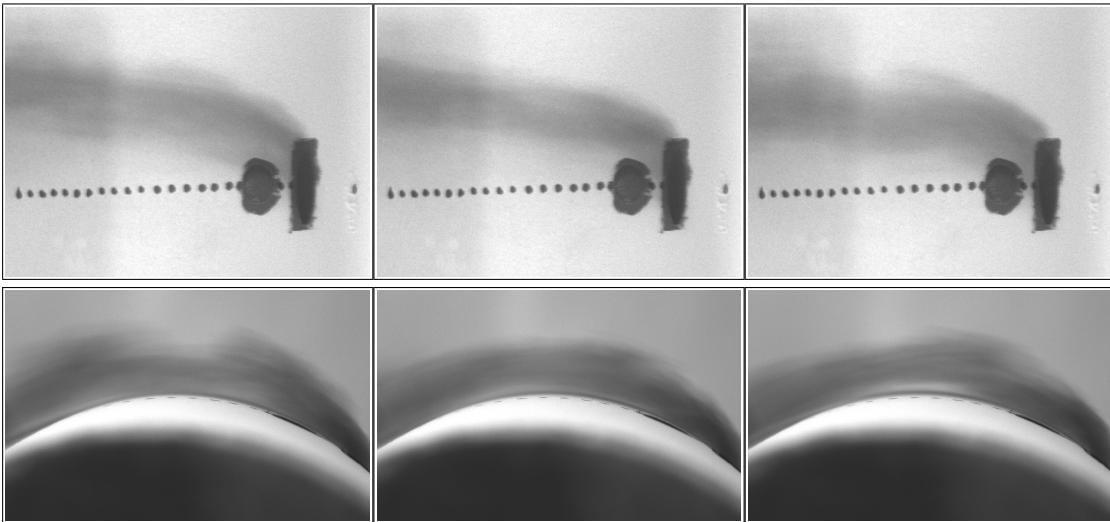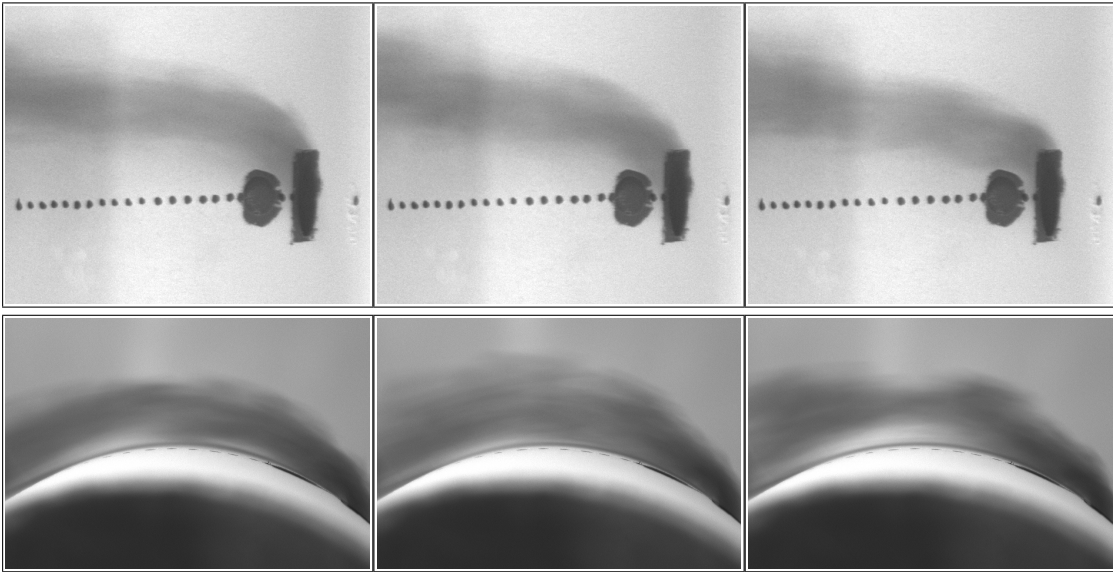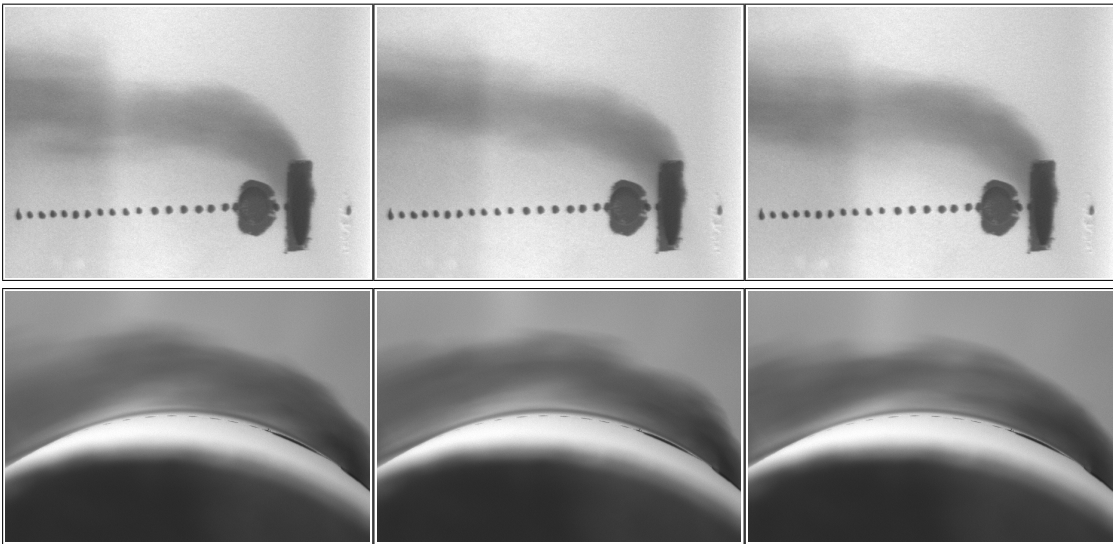

Figure 18   Small cylindrical dimples upstream of coolant hole - $M = 1.00$
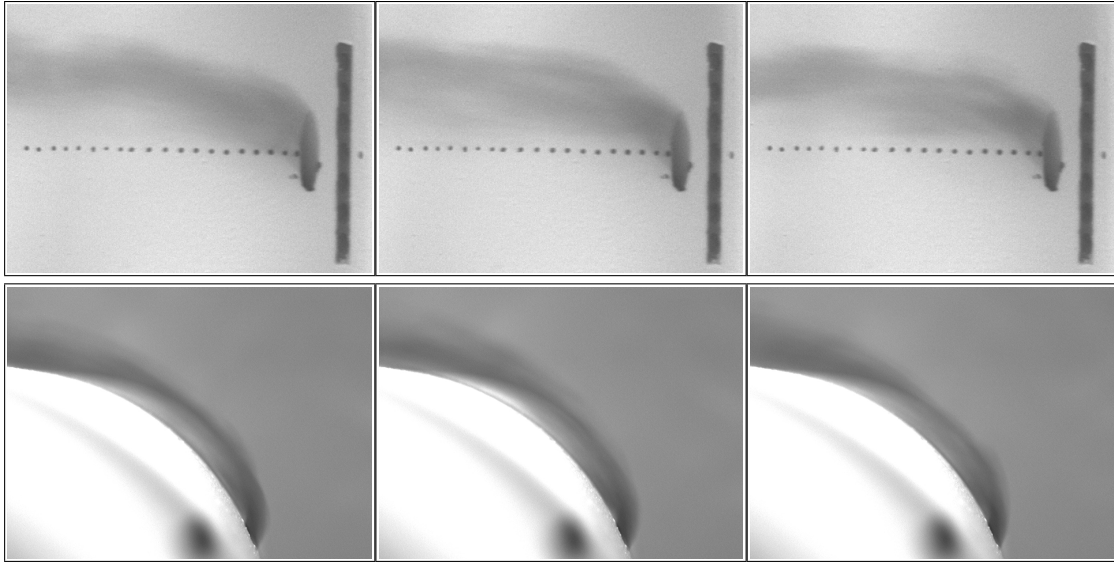
Figure 19   Small cylindrical dimples upstream of coolant hole - $M = 1.25$
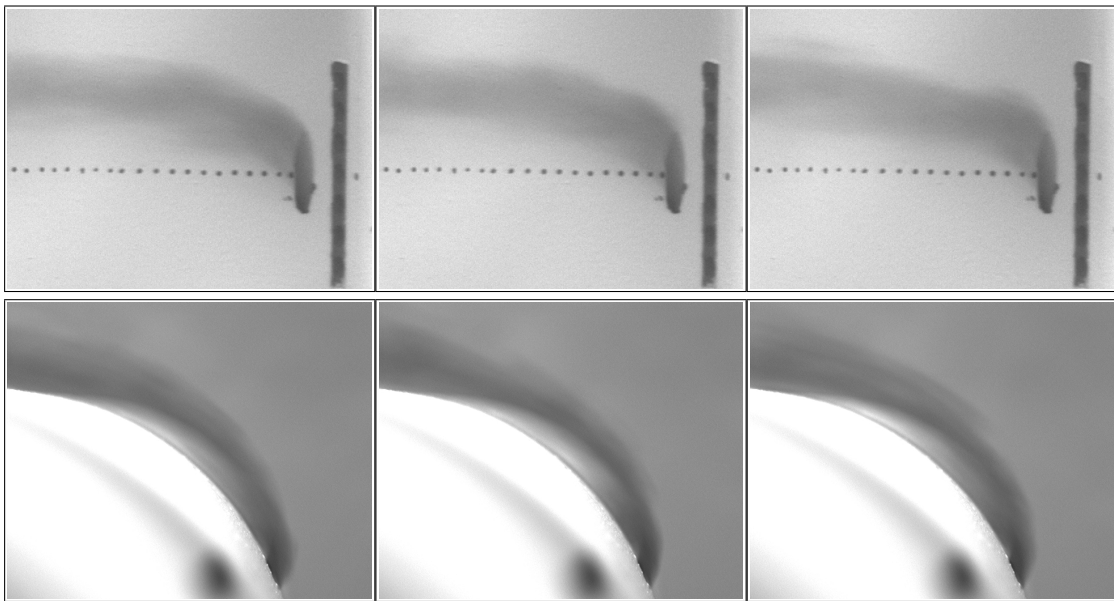
Figure 20   Small cylindrical dimples upstream of coolant hole - $M = 1.50$
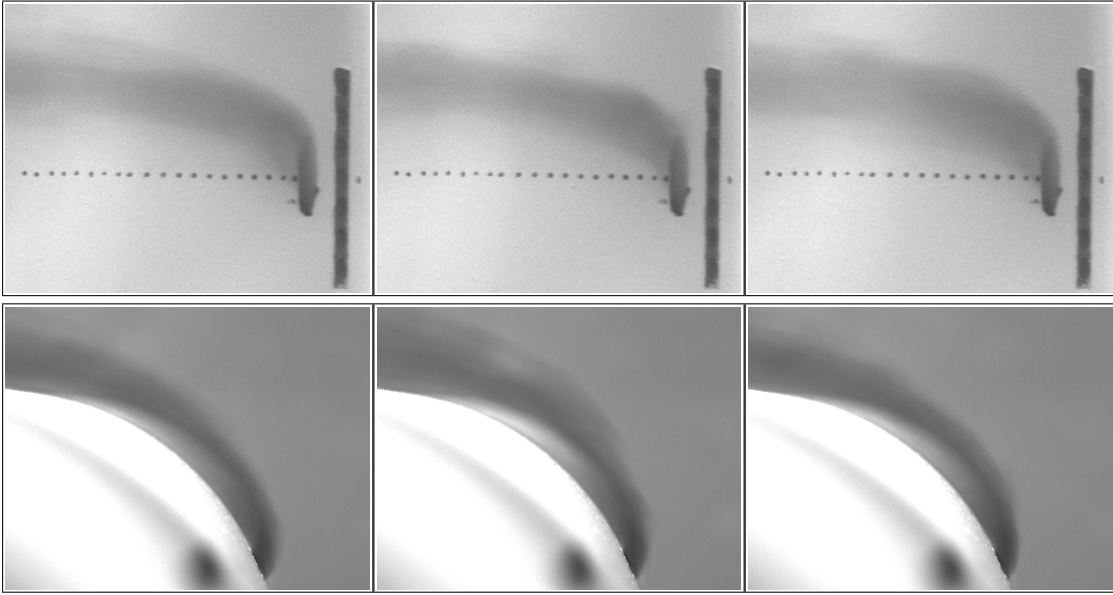
Figure 21   Small cylindrical dimples upstream of coolant hole - $M = 1.75$
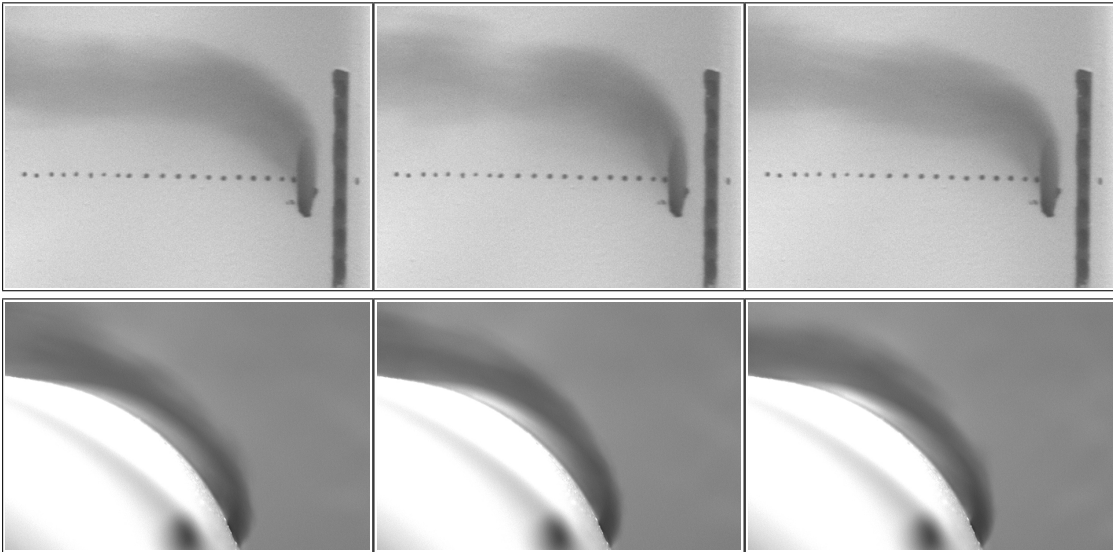
Figure 22   Small cylindrical dimples upstream of coolant hole - $M = 2.00$
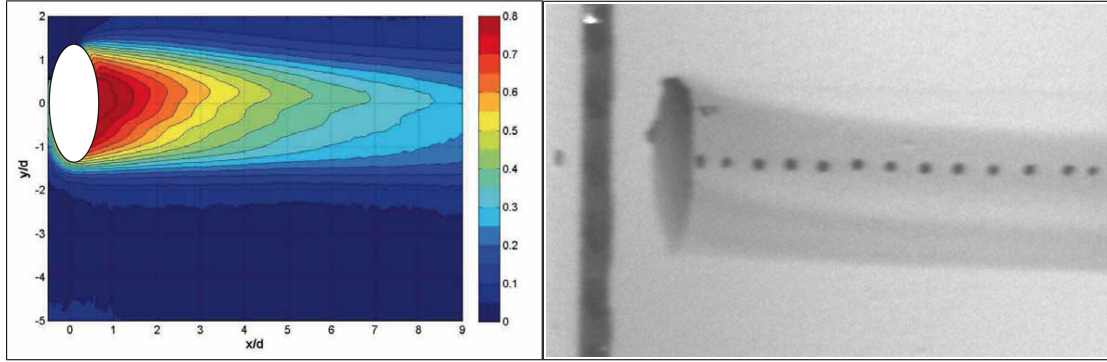
Figure 23   Comparison of adiabatic effectiveness plot from Frisinger [13] to flow visualization data for for small upstream dimples at $M = 0.25$. Adiabatic effectiveness plot was generated at $Re_D = 30k$ with low turbulence nearly identical to that of the water channel flow visualization study ($< 1\%$). Flow visualization picture has been flipped on its horizontal and vertical axes to match the adiabatic effectiveness data.
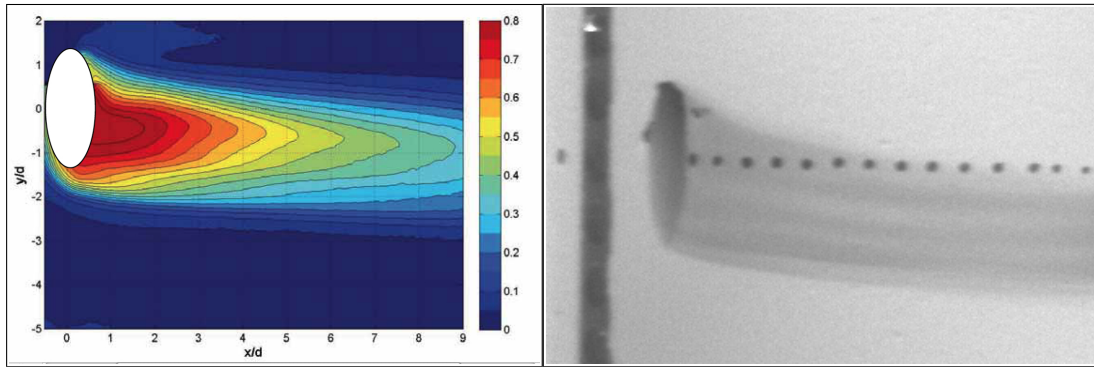
Figure 24   Comparison of adiabatic effectiveness plot from Frisinger [13] to flow visualization data for for small upstream dimples at $M = 0.50$. Adiabatic effectiveness plot was generated at $Re_D = 30k$ with low turbulence nearly identical to that of the water channel flow visualization study ($< 1\%$). Flow visualization picture has been flipped on its horizontal and vertical axes to match the adiabatic effectiveness data.
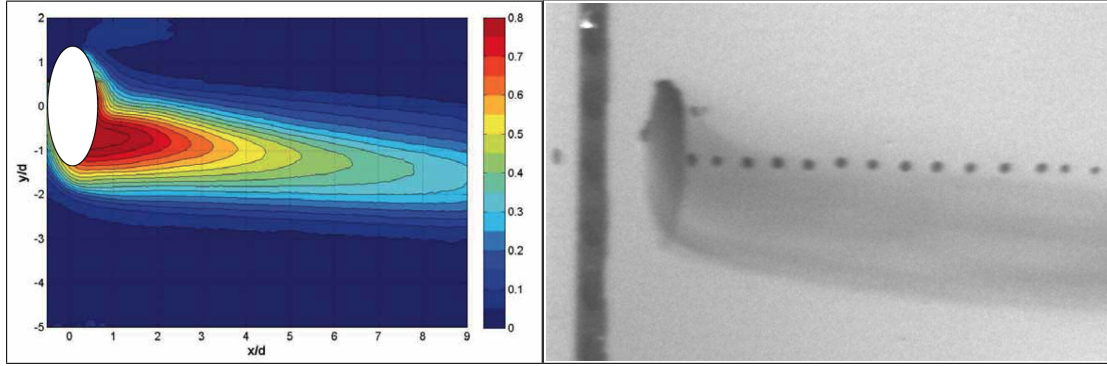
Figure 25 Comparison of adiabatic effectiveness plot from Frisinger [13] to flow visualization data for for small upstream dimples at $M = 0.75$. Adiabatic effectiveness plot was generated at $Re_D = 30$k with low turbulence nearly identical to that of the water channel flow visualization study ($< 1\%$). Flow visualization picture has been flipped on its horizontal and vertical axes to match the adiabatic effectiveness data.
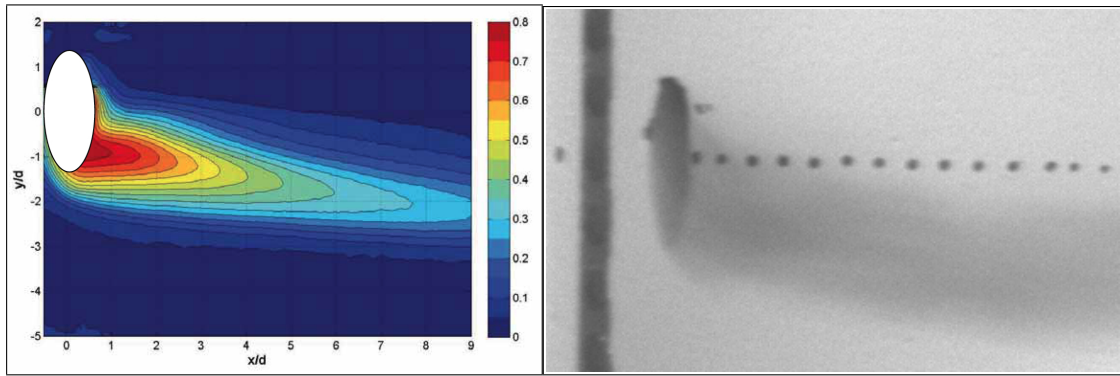
Figure 26 Comparison of adiabatic effectiveness plot from Frisinger [13] to flow visualization data for for small upstream dimples at $M = 1.00$. Adiabatic effectiveness plot was generated at $Re_D = 30$k with low turbulence nearly identical to that of the water channel flow visualization study ($< 1\%$). Flow visualization picture has been flipped on its horizontal and vertical axes to match the adiabatic effectiveness data.
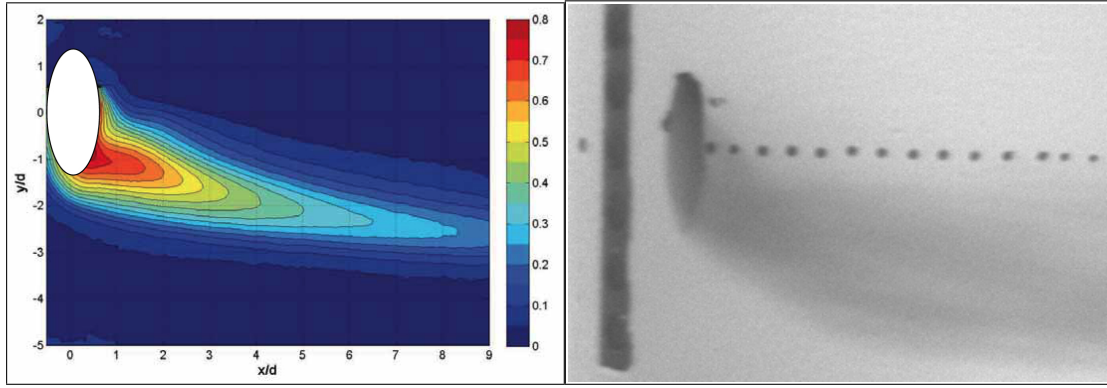
Figure 27   Comparison of adiabatic effectiveness plot from Frisinger [13] to flow visualization data for for small upstream dimples at $M = 1.25$. Adiabatic effectiveness plot was generated at $Re_D = 30$k with low turbulence nearly identical to that of the water channel flow visualization study ($< 1\%$). Flow visualization picture has been flipped on its horizontal and vertical axes to match the adiabatic effectiveness data.
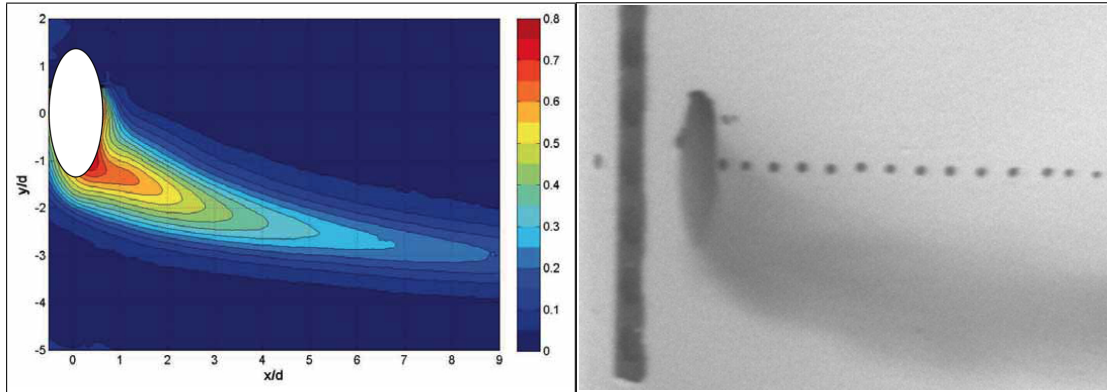
Figure 28   Comparison of adiabatic effectiveness plot from Frisinger [13] to flow visualization data for for small upstream dimples at $M = 1.50$. Adiabatic effectiveness plot was generated at $Re_D = 30$k with low turbulence nearly identical to that of the water channel flow visualization study ($< 1\%$). Flow visualization picture has been flipped on its horizontal and vertical axes to match the adiabatic effectiveness data.
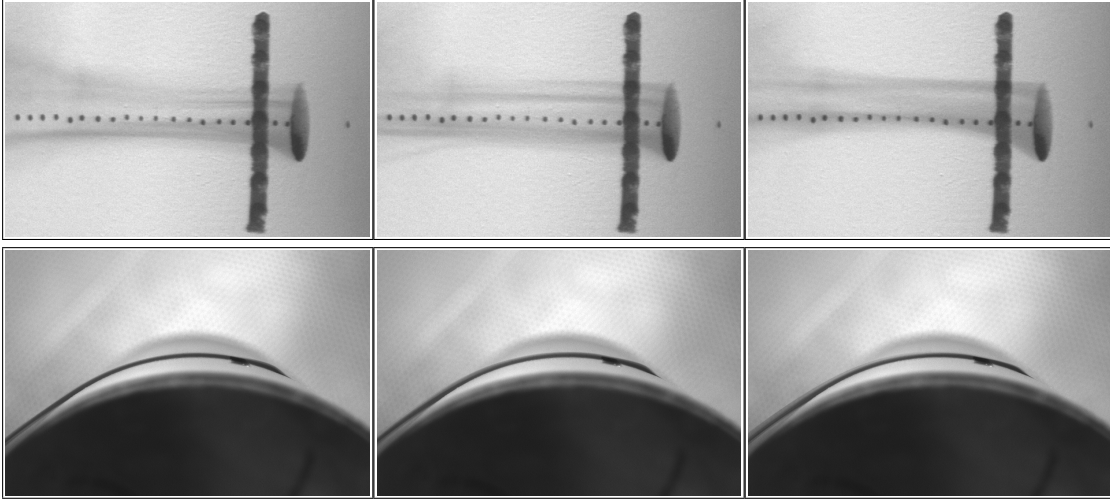
Figure 29   Small cylindrical dimples downstream of coolant hole - $M = 0.25$
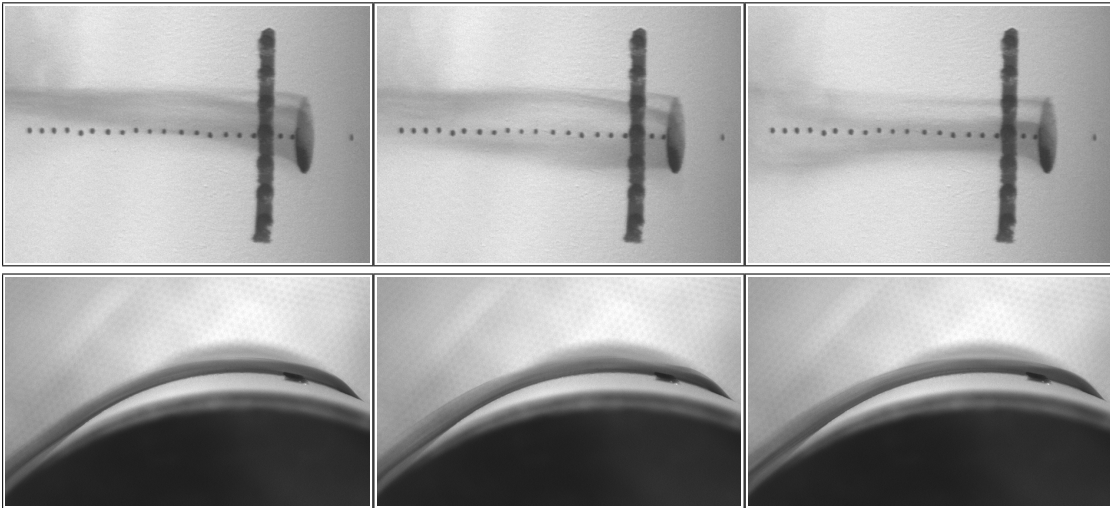
Figure 30   Small cylindrical dimples downstream of coolant hole - $M = 0.50$
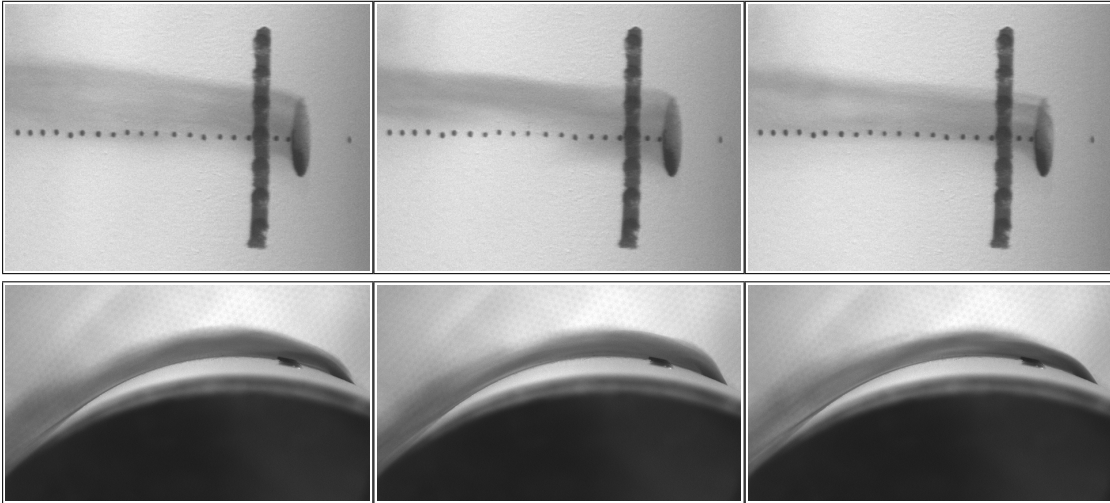
Figure 31   Small cylindrical dimples downstream of coolant hole - $M = 0.75$
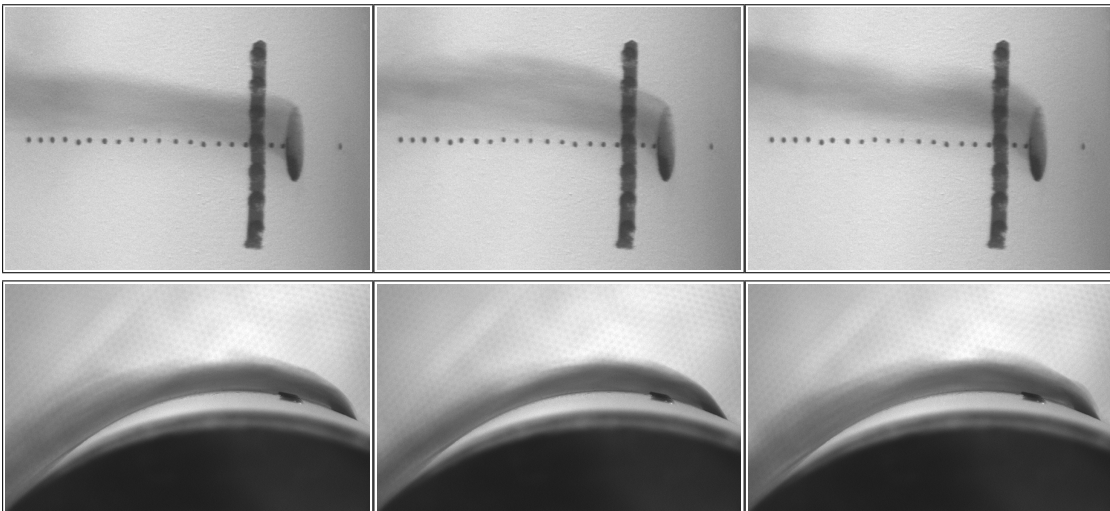
Figure 32   Small cylindrical dimples downstream of coolant hole - $M = 1.00$
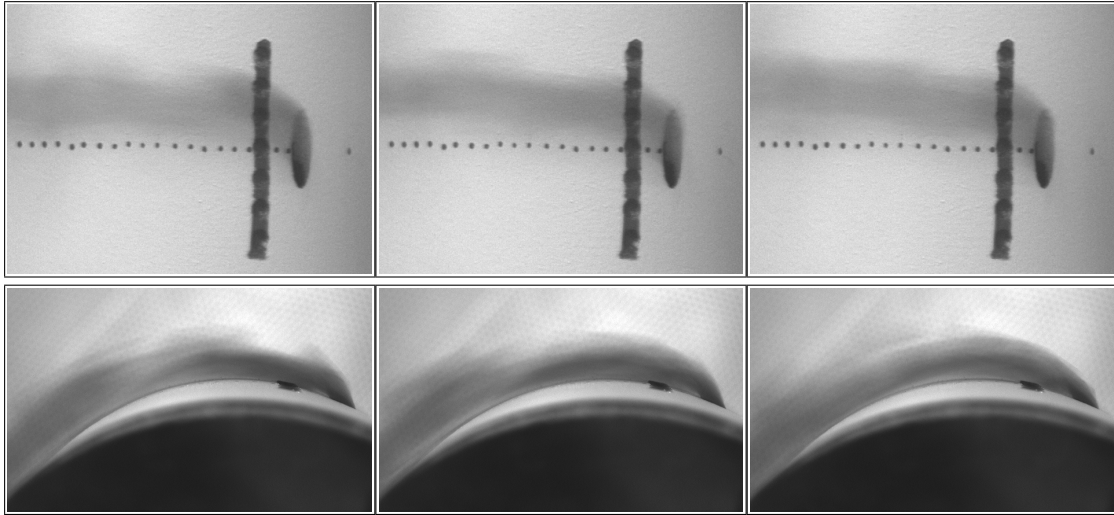
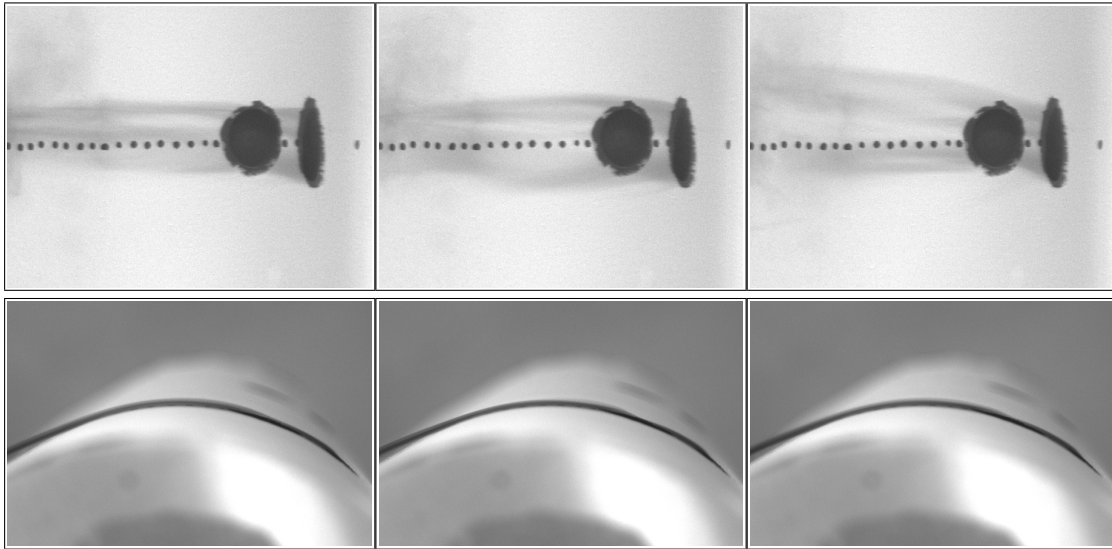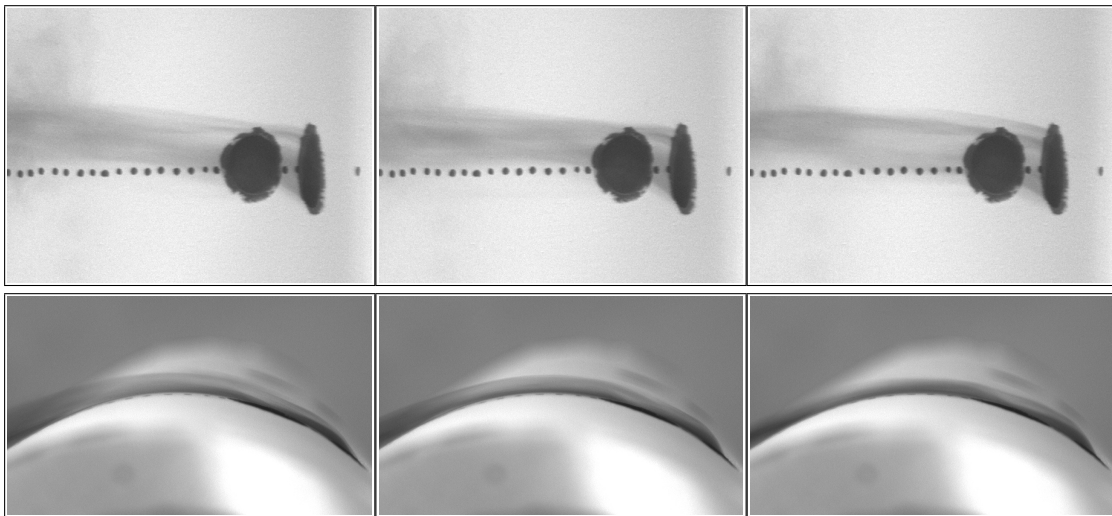Figure 33   Small cylindrical dimples downstream of coolant hole - $M = 1.25$
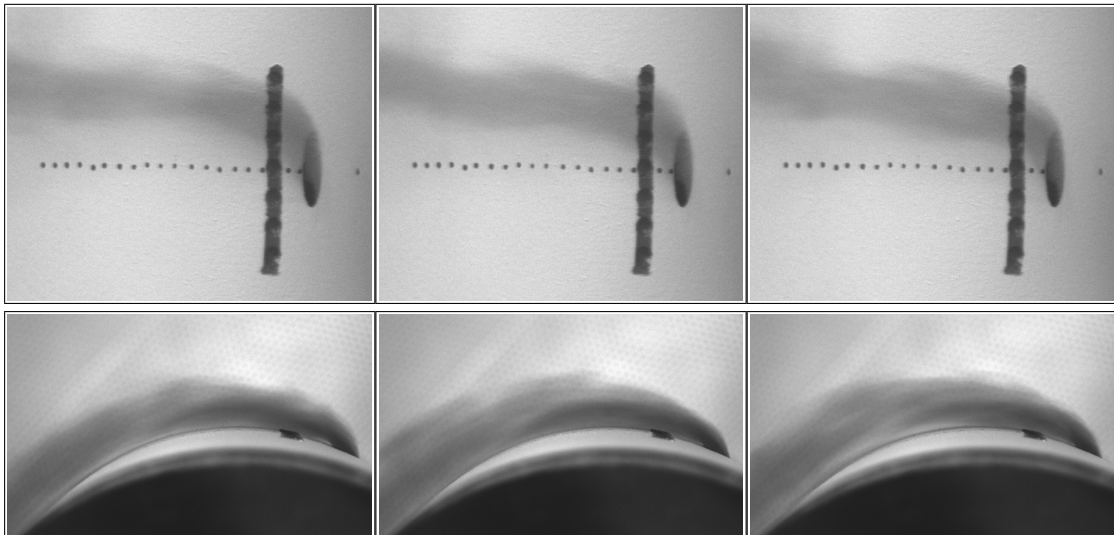
Figure 34   Small cylindrical dimples downstream of coolant hole - $M = 1.50$
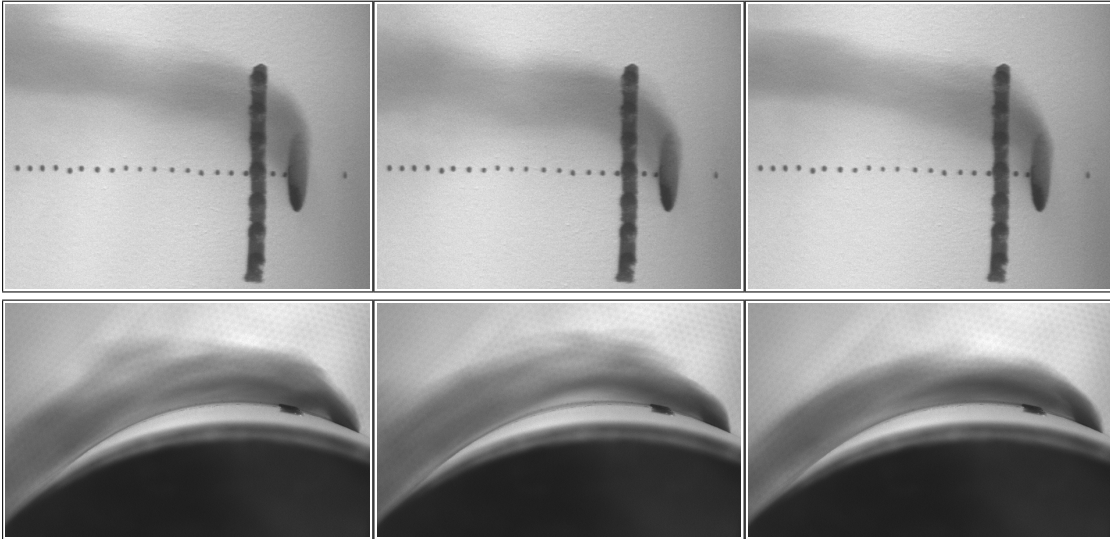
Figure 35   Small cylindrical dimples downstream of coolant hole - $M = 1.75$
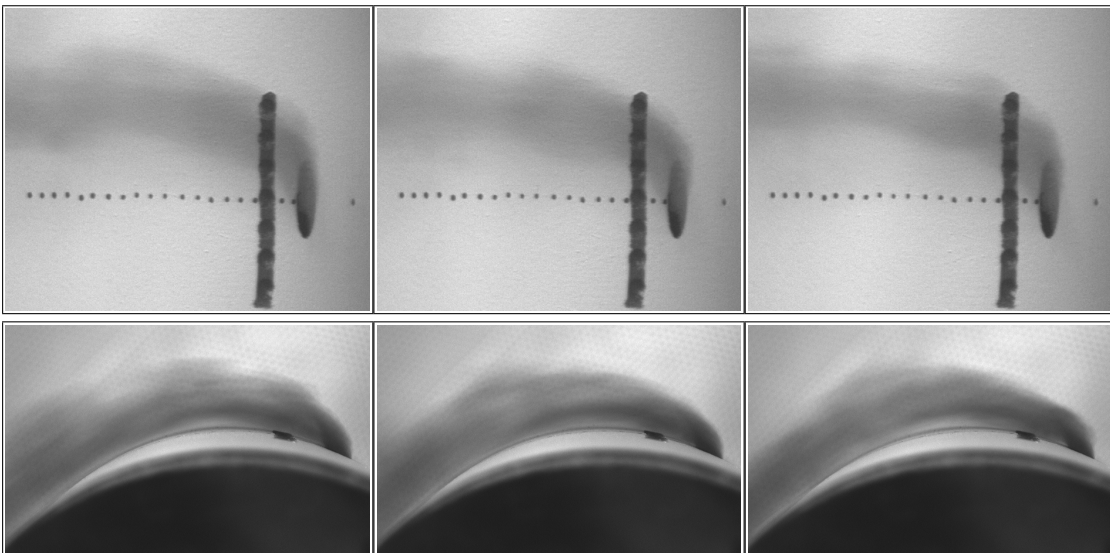
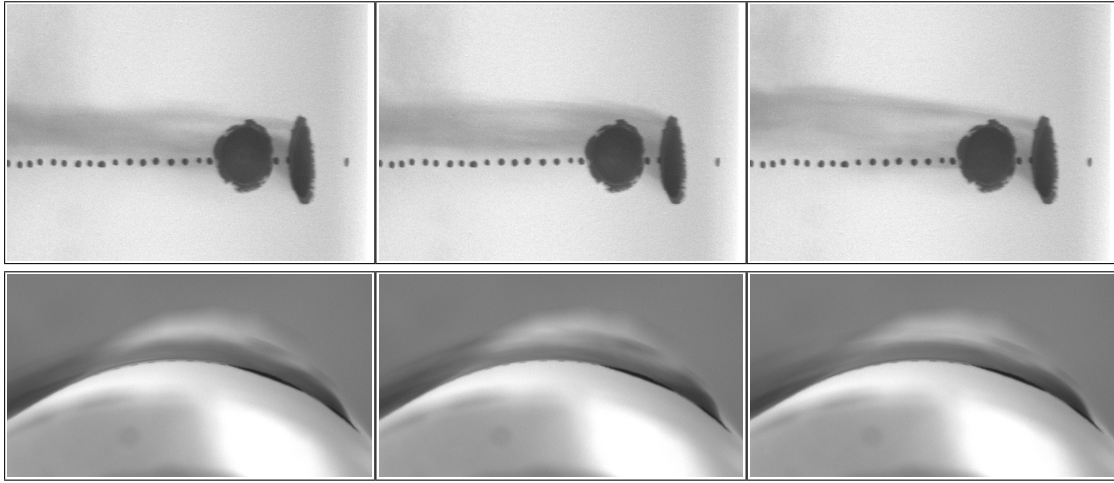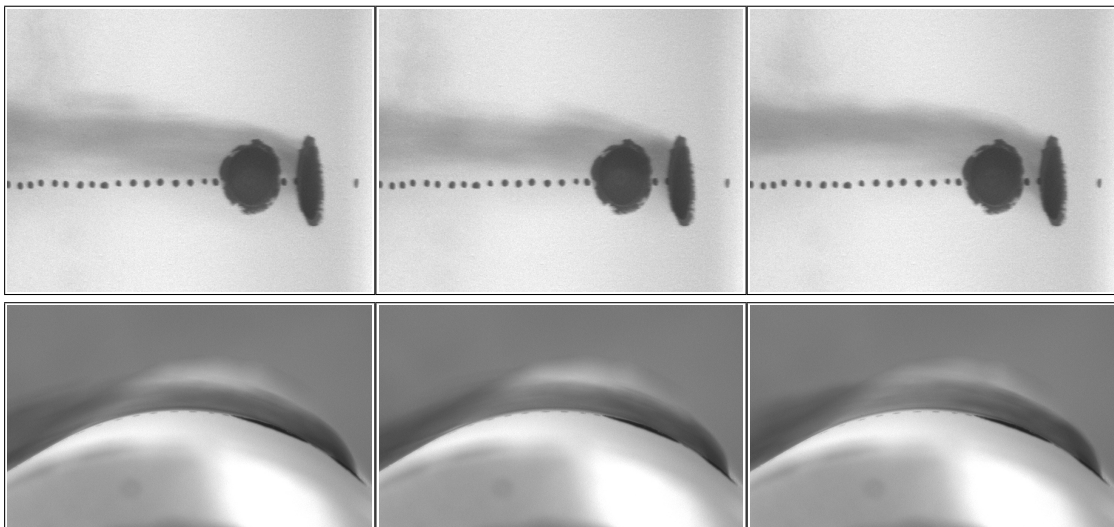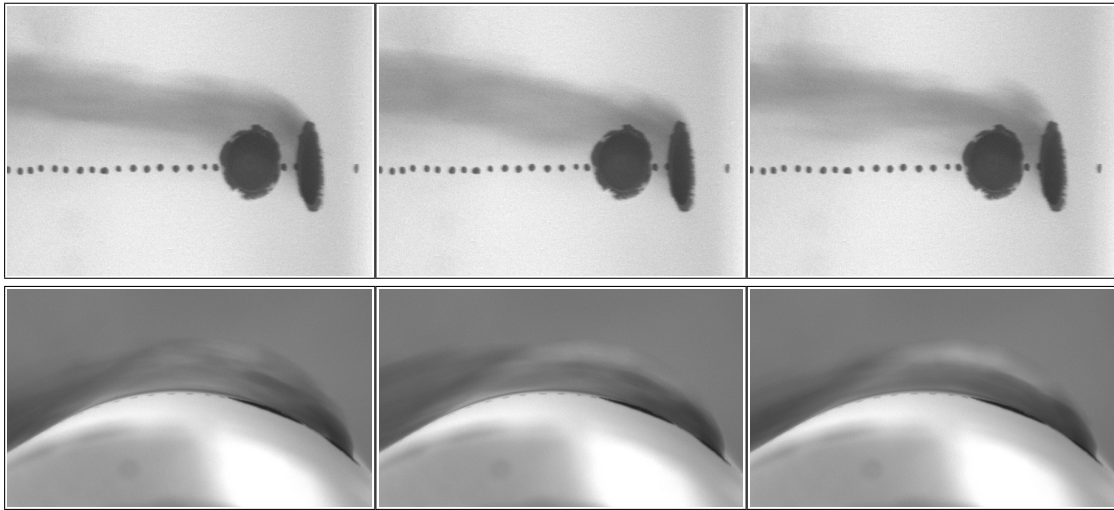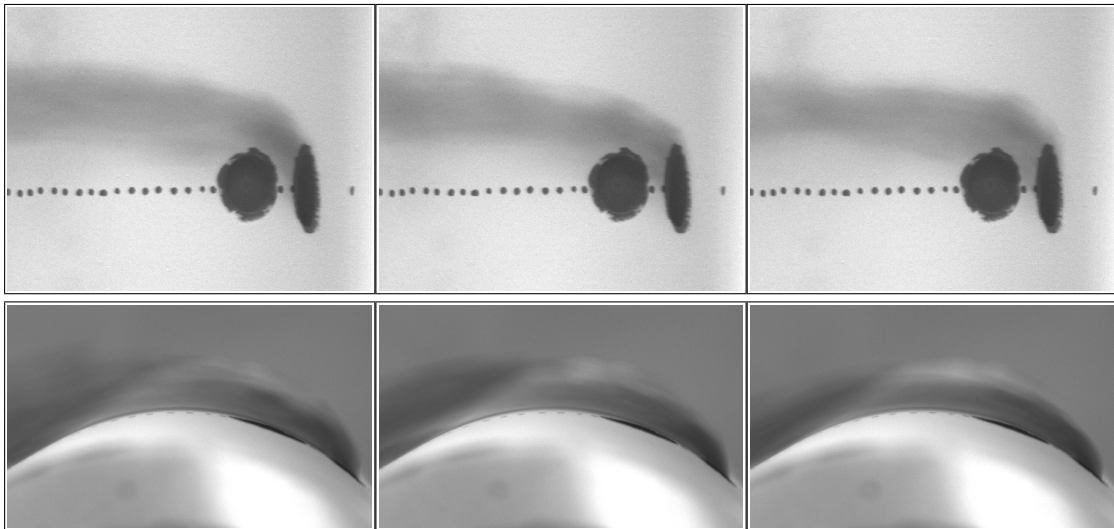Figure 36   Small cylindrical dimples downstream of coolant hole - $M = 2.00$
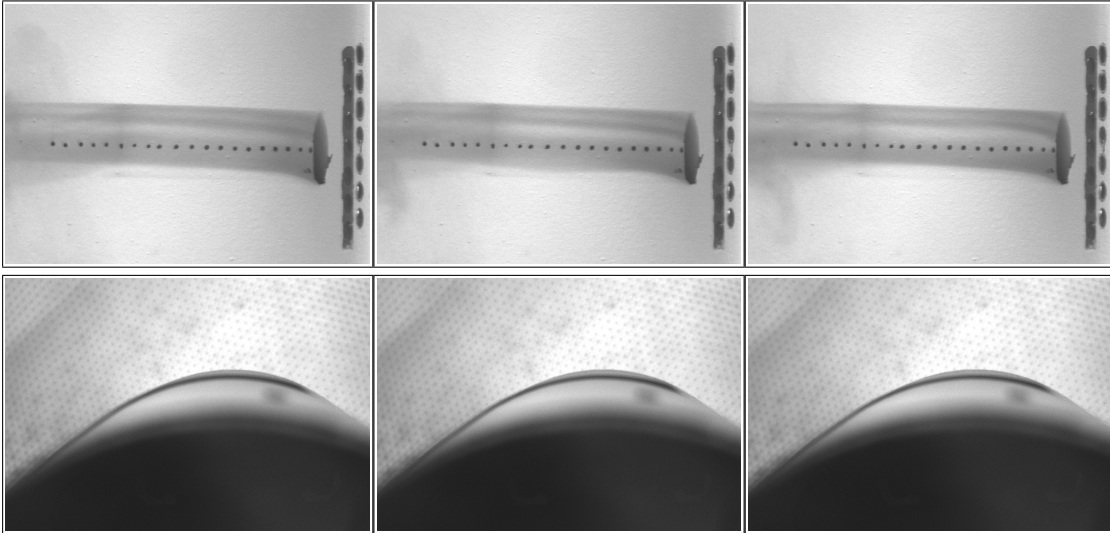
Figure 37   Two staggered rows of small cylindrical dimples - $M = 0.25$
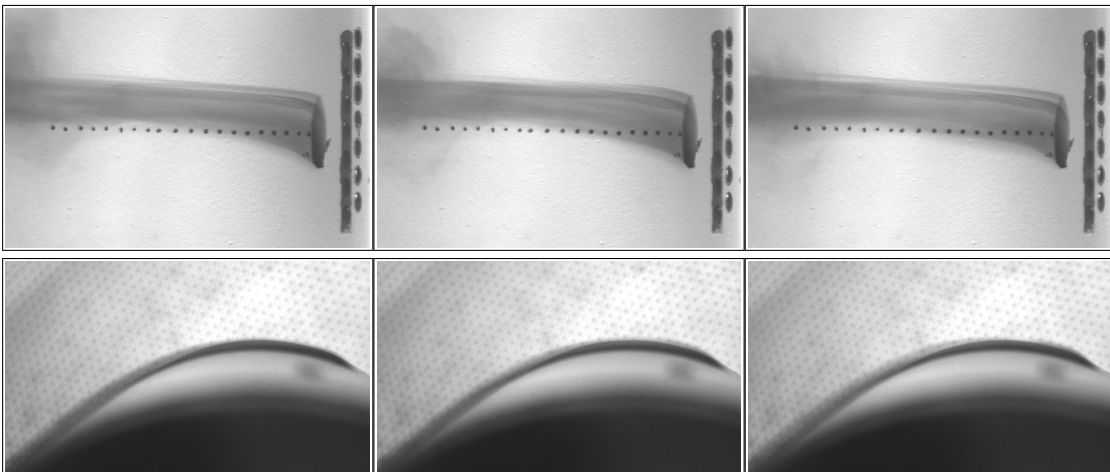
Figure 38   Two staggered rows of small cylindrical dimples - $M = 0.50$
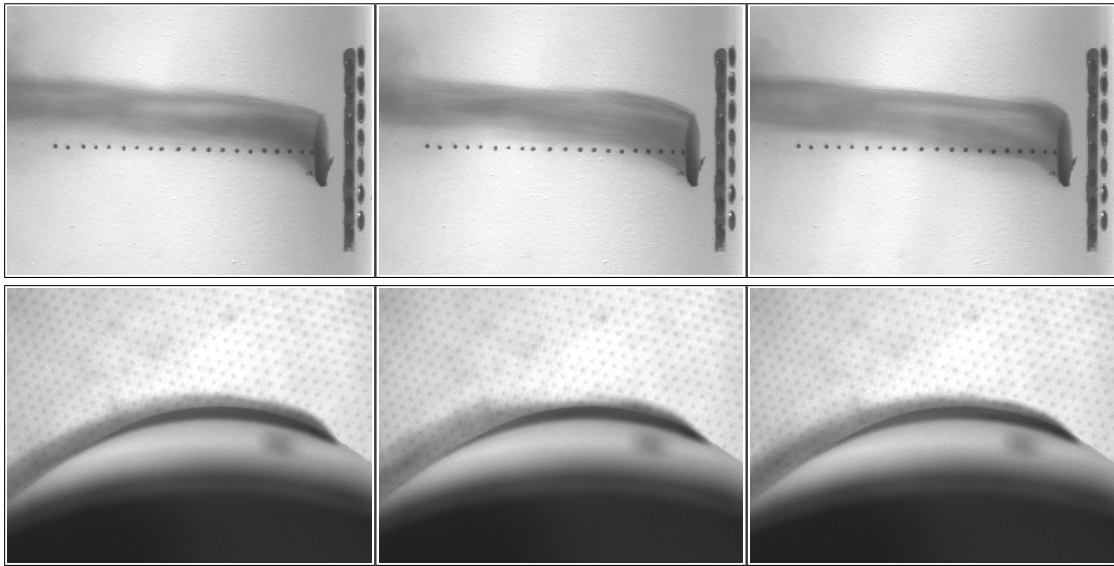
Figure 39   Two staggered rows of small cylindrical dimples - $M = 0.75$
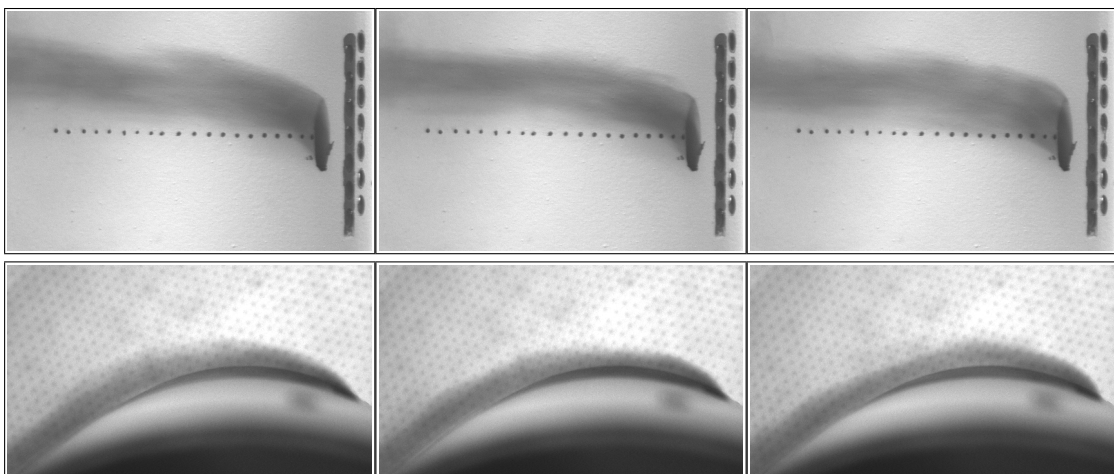
Figure 40   Two staggered rows of small cylindrical dimples - $M = 1.00$
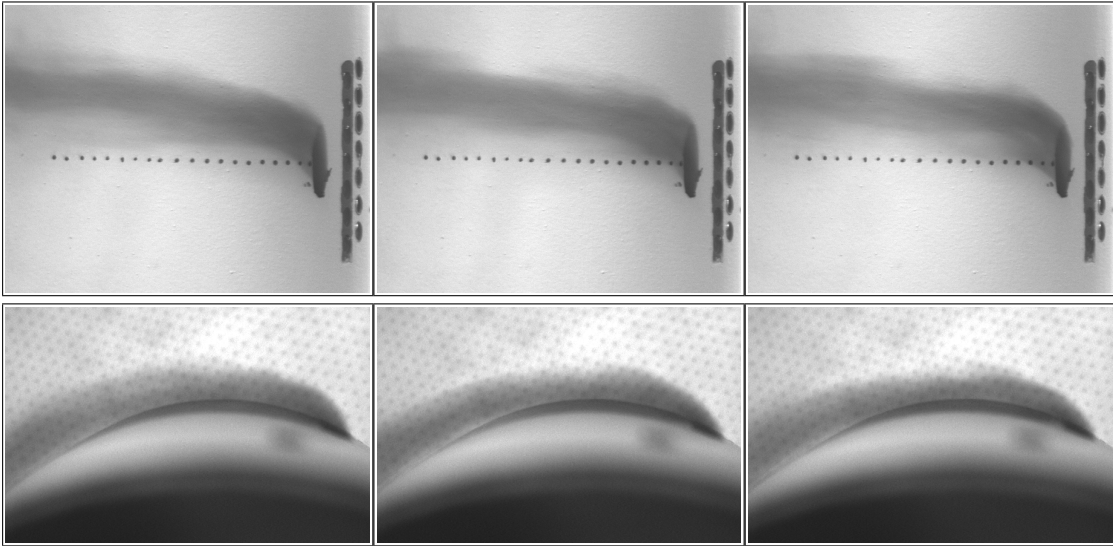
Figure 41   Two staggered rows of small cylindrical dimples - $M = 1.25$
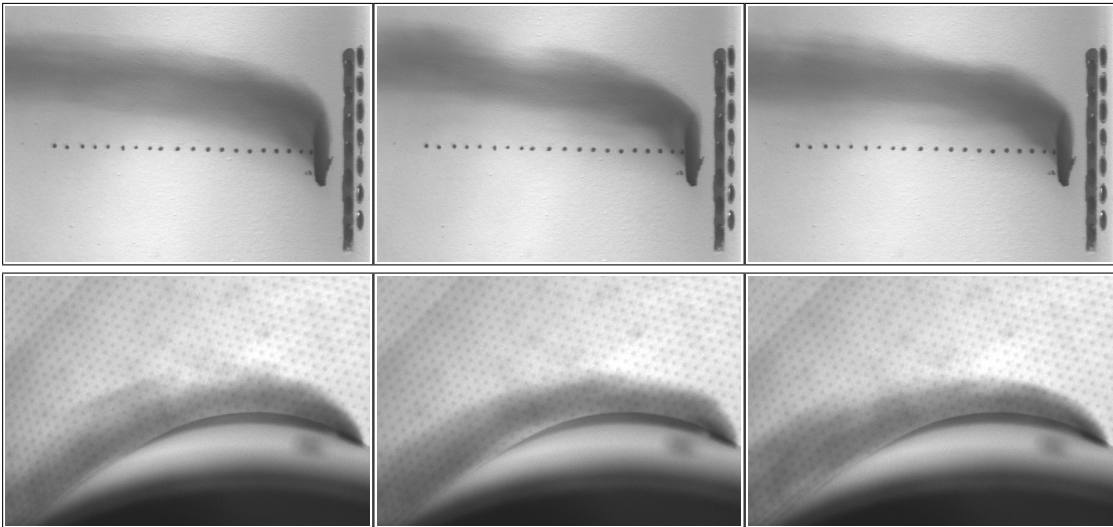
Figure 42   Two staggered rows of small cylindrical dimples - $M = 1.50$
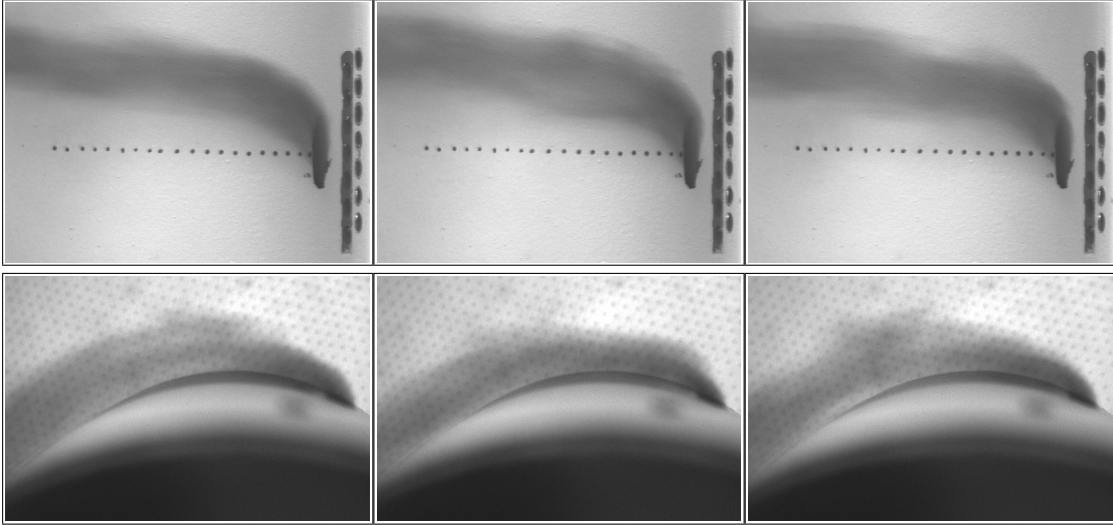
Figure 43   Two staggered rows of small cylindrical dimples - $M = 1.75$
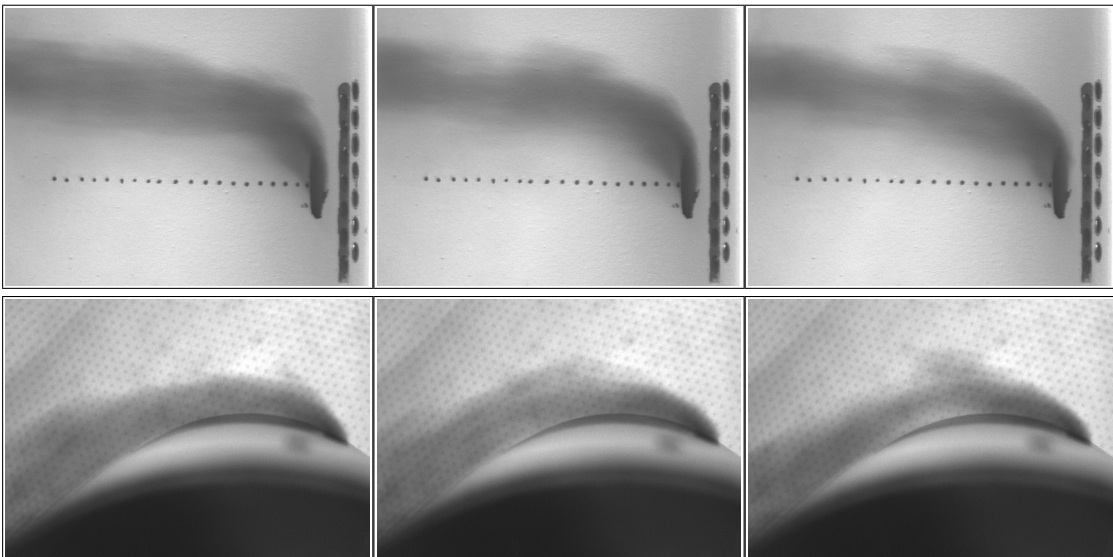
Figure 44   Two staggered rows of small cylindrical dimples - $M = 2.00$
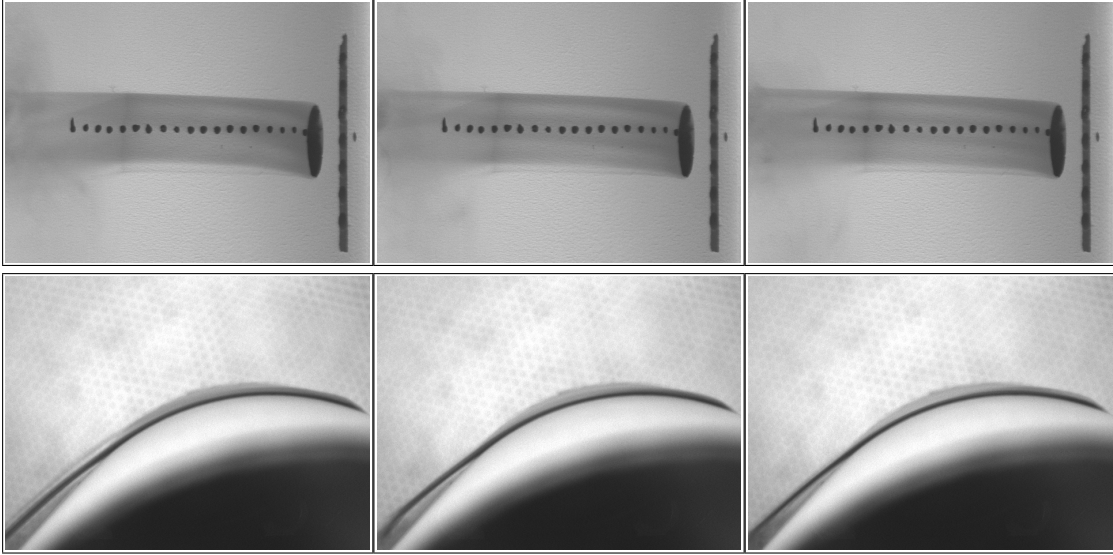
Figure 45   Small spherical dimples upstream of coolant hole - $M = 0.25$
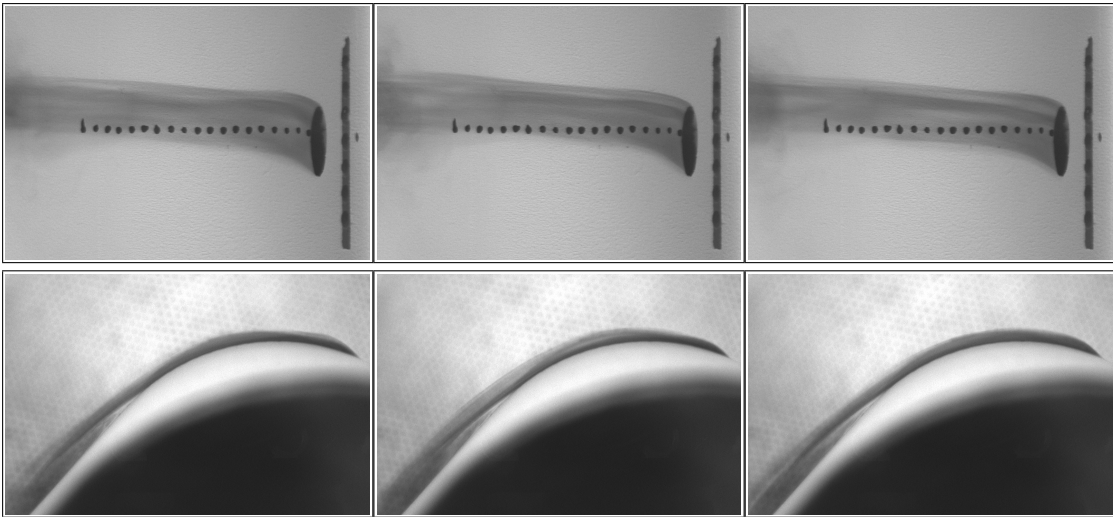
Figure 46   Small spherical dimples upstream of coolant hole - $M = 0.50$
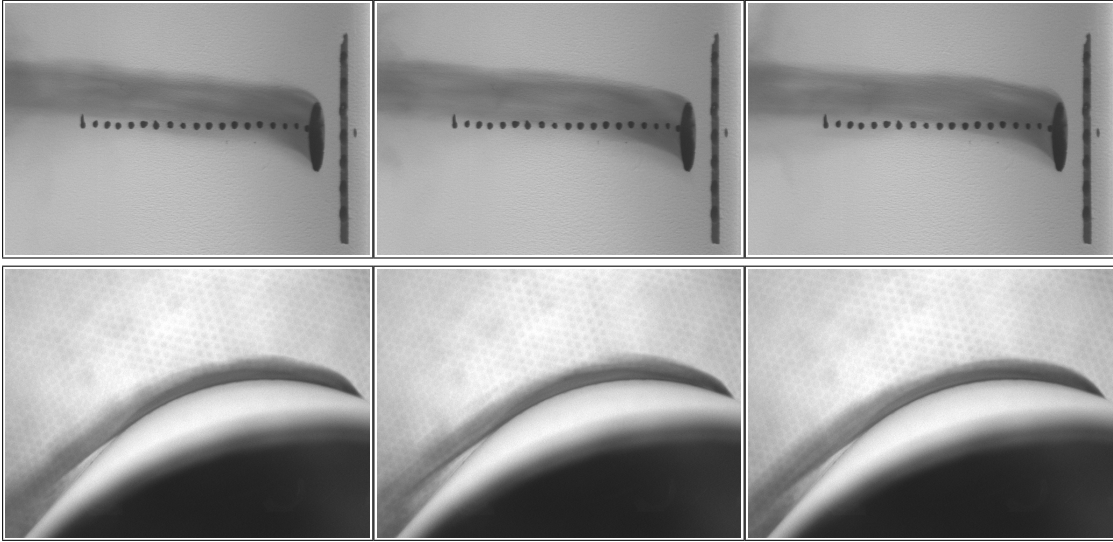
Figure 47   Small spherical dimples upstream of coolant hole - $M = 0.75$
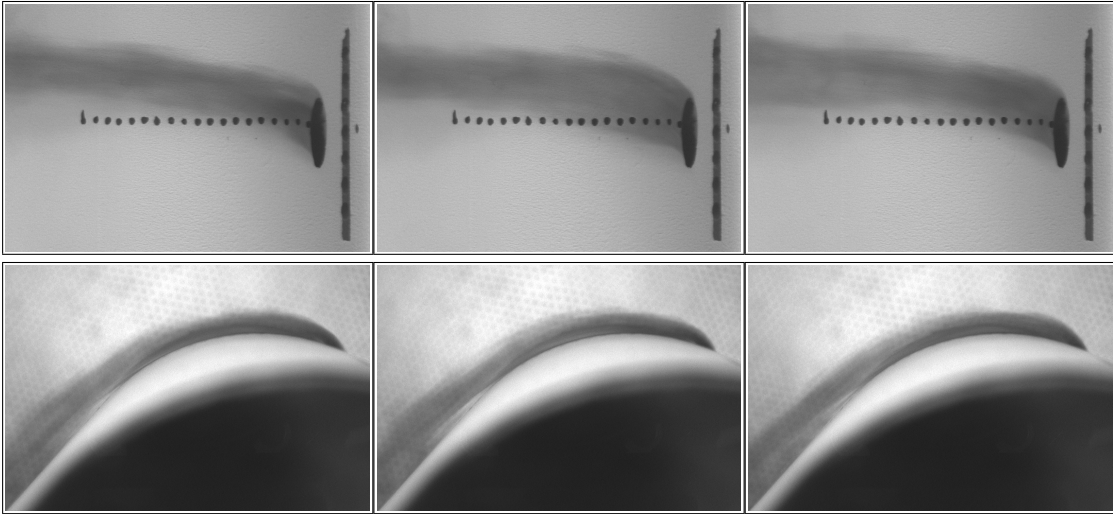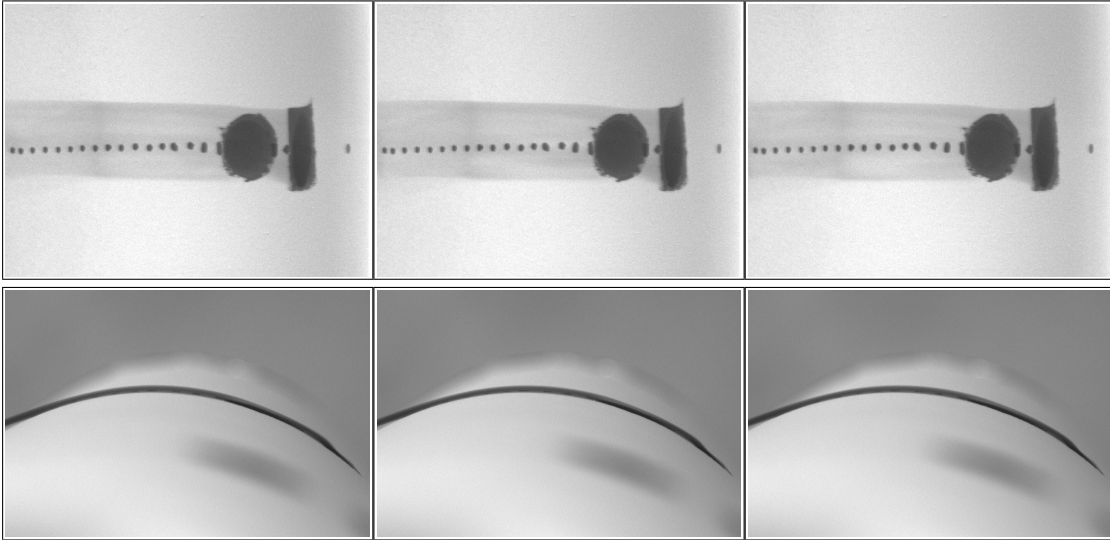

Figure 48   Small spherical dimples upstream of coolant hole - $M = 1.00$
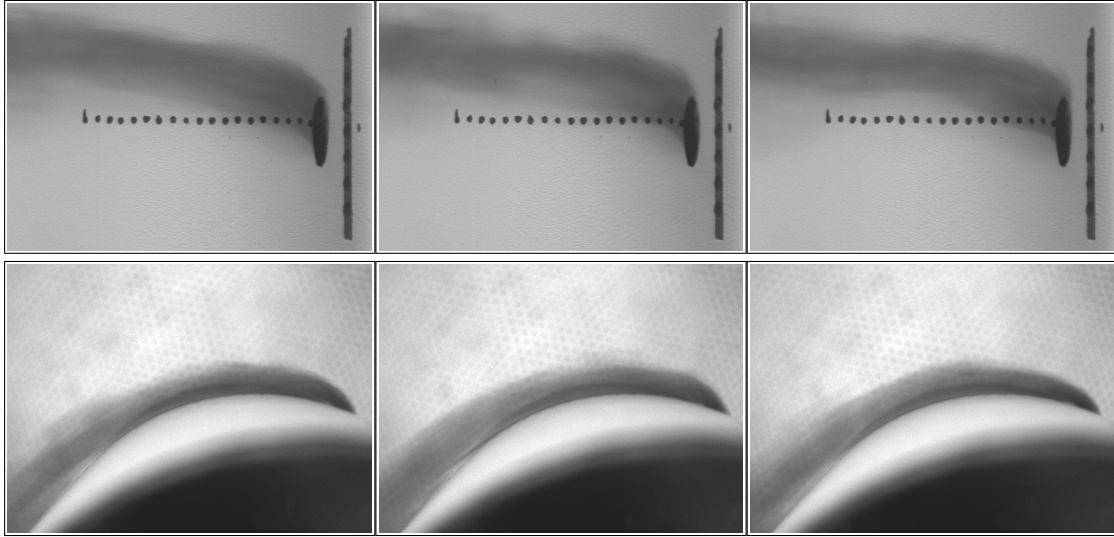
Figure 49   Small spherical dimples upstream of coolant hole - $M = 1.25$
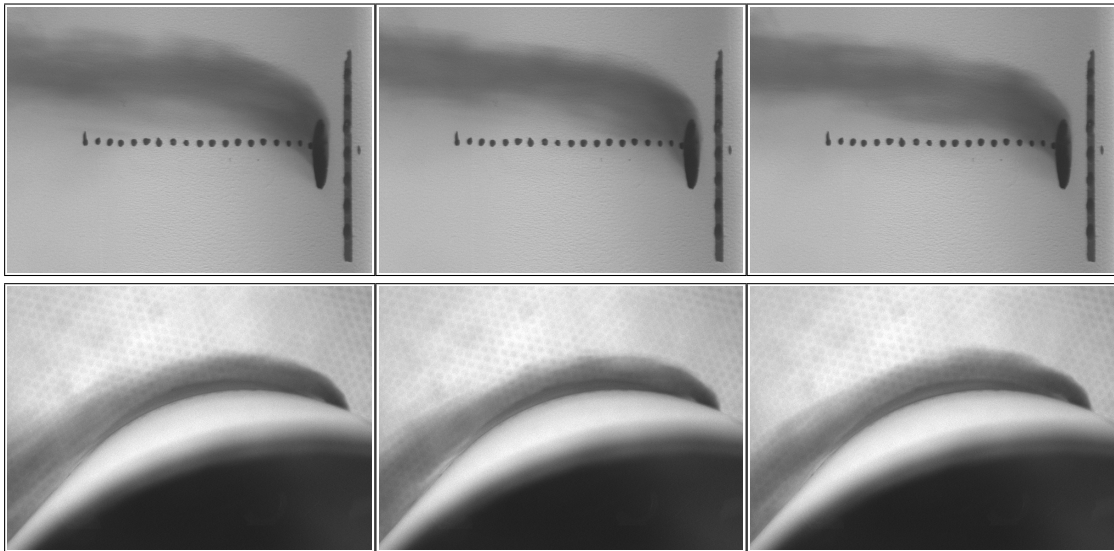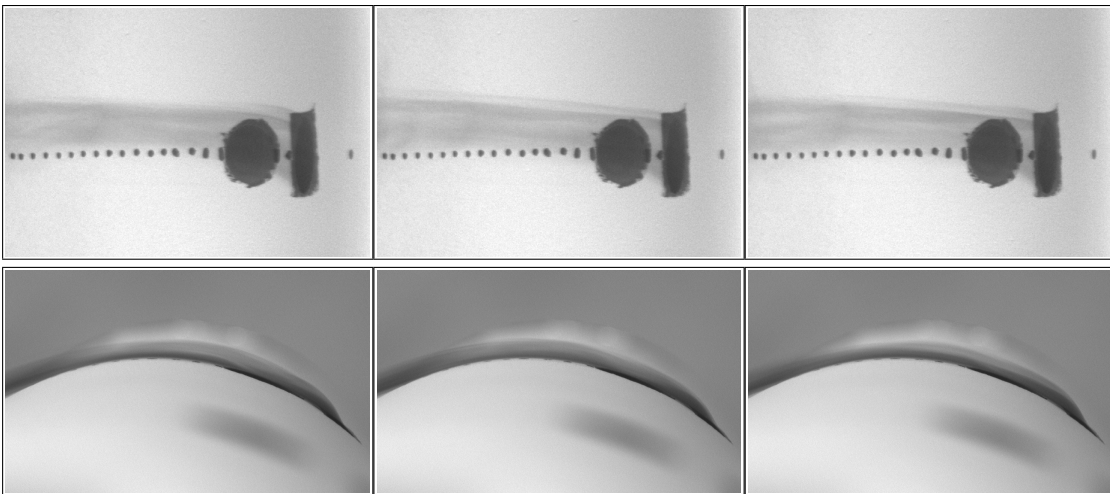

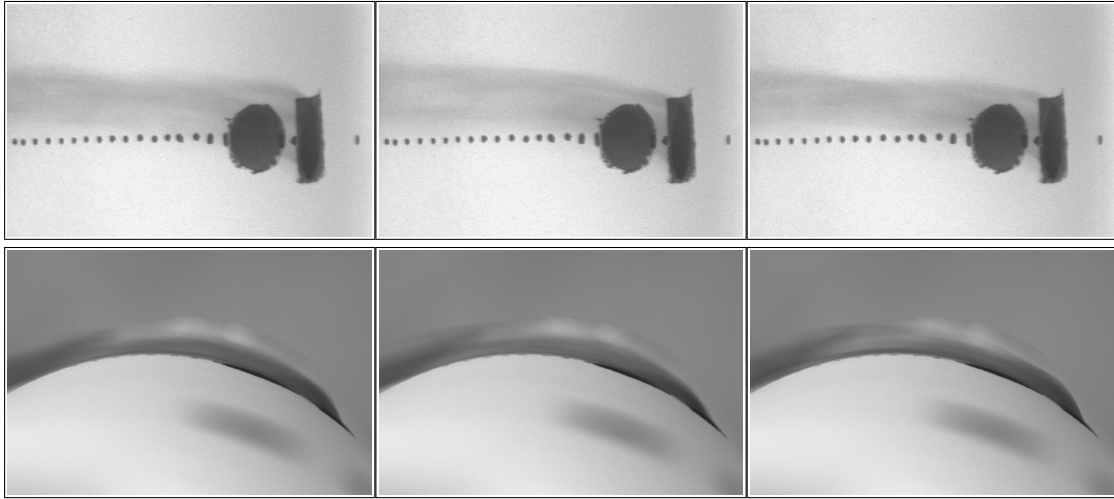Figure 50   Small spherical dimples upstream of coolant hole - $M = 1.50$
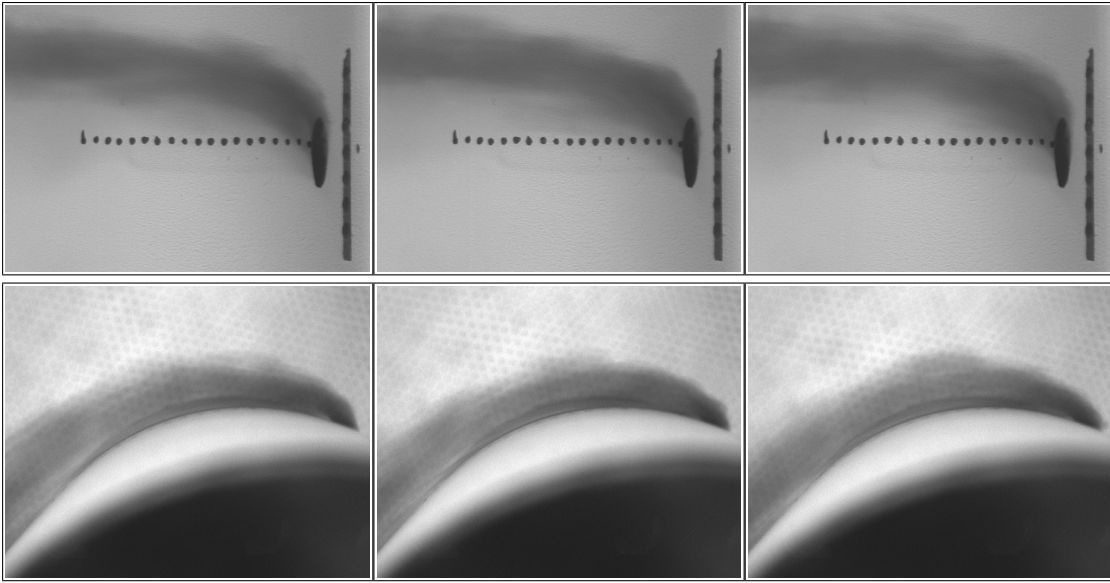
Figure 51   Small spherical dimples upstream of coolant hole - $M = 1.75$
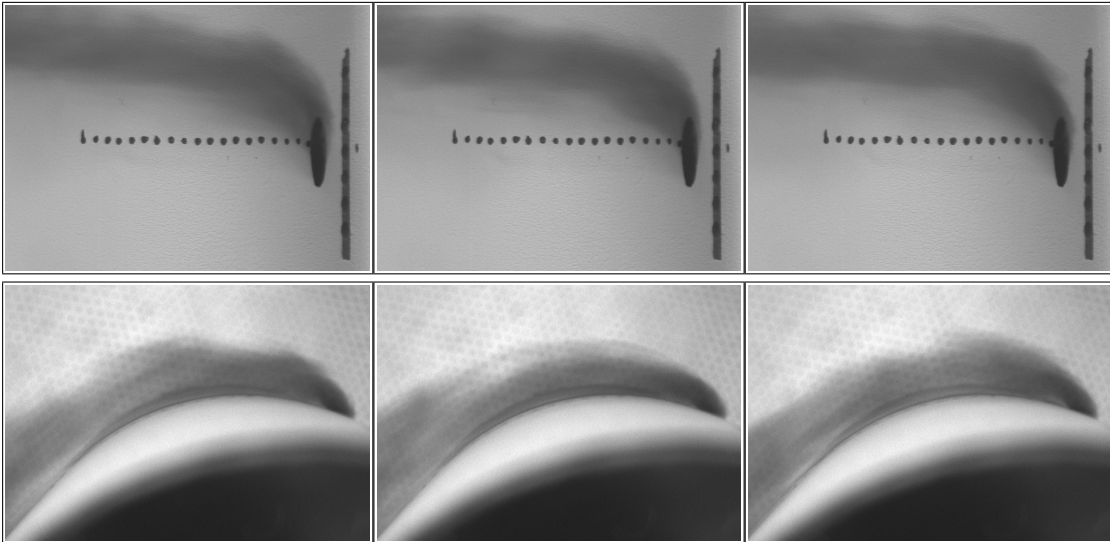
Figure 52   Small spherical dimples upstream of coolant hole - $M = 2.00$
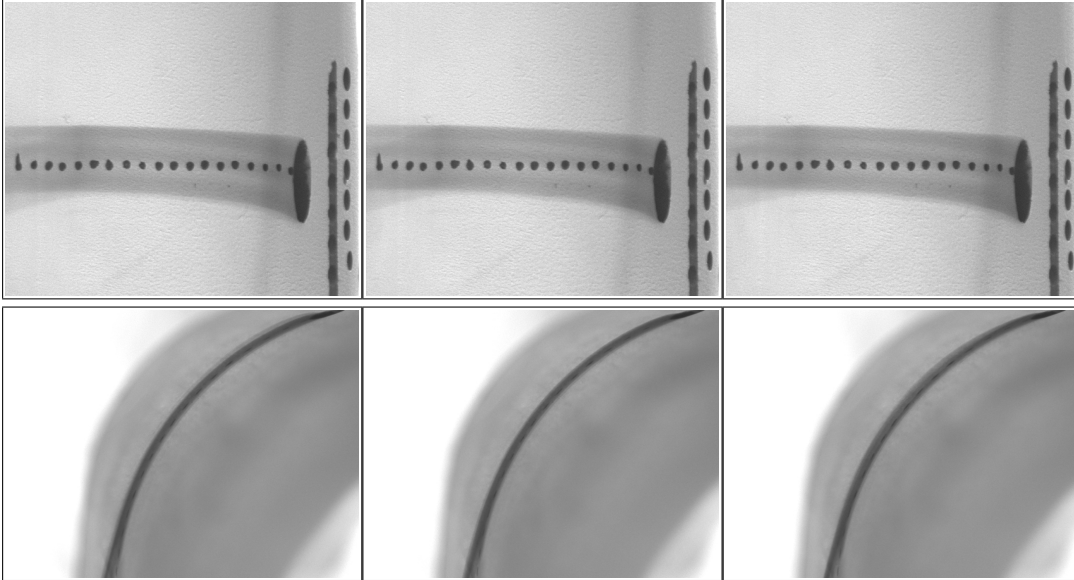
Figure 53   Two staggered rows of small spherical dimples - $M = 0.25$
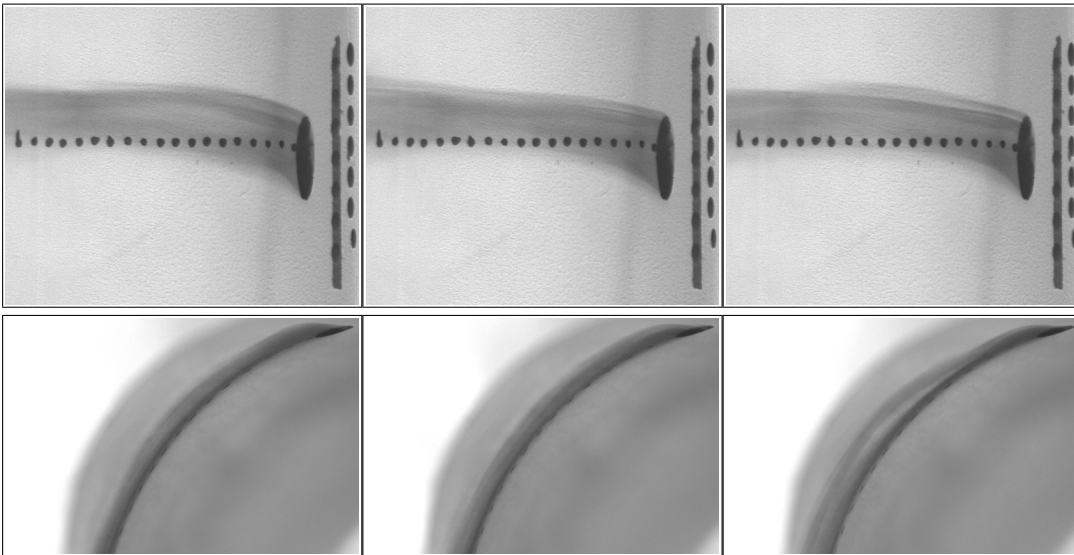
Figure 54   Two staggered rows of small spherical dimples - $M = 0.50$
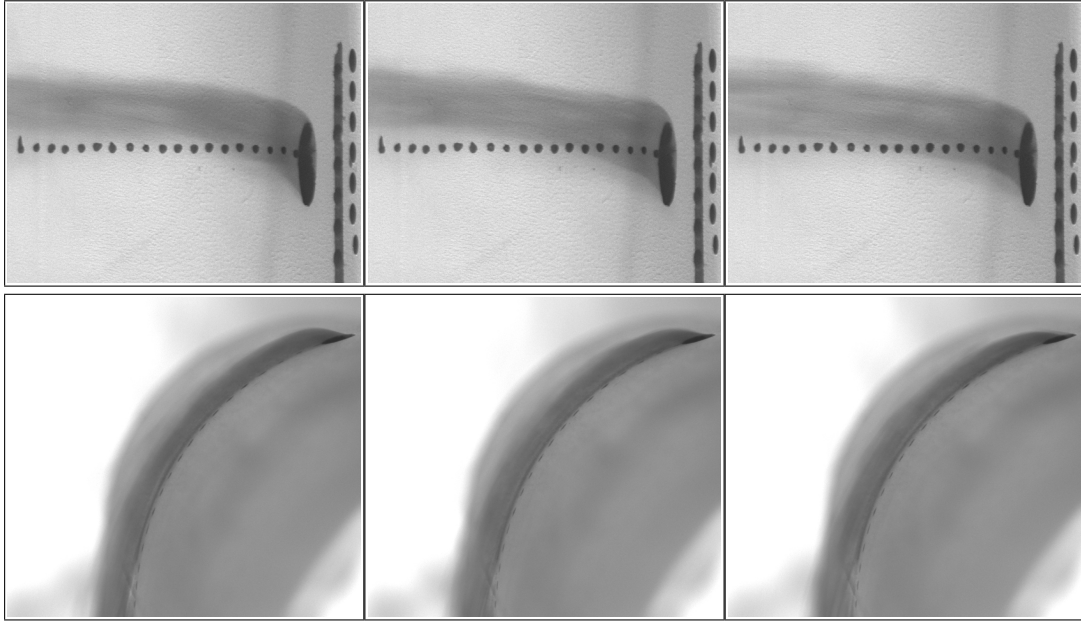
Figure 55   Two staggered rows of small spherical dimples - $M = 0.75$
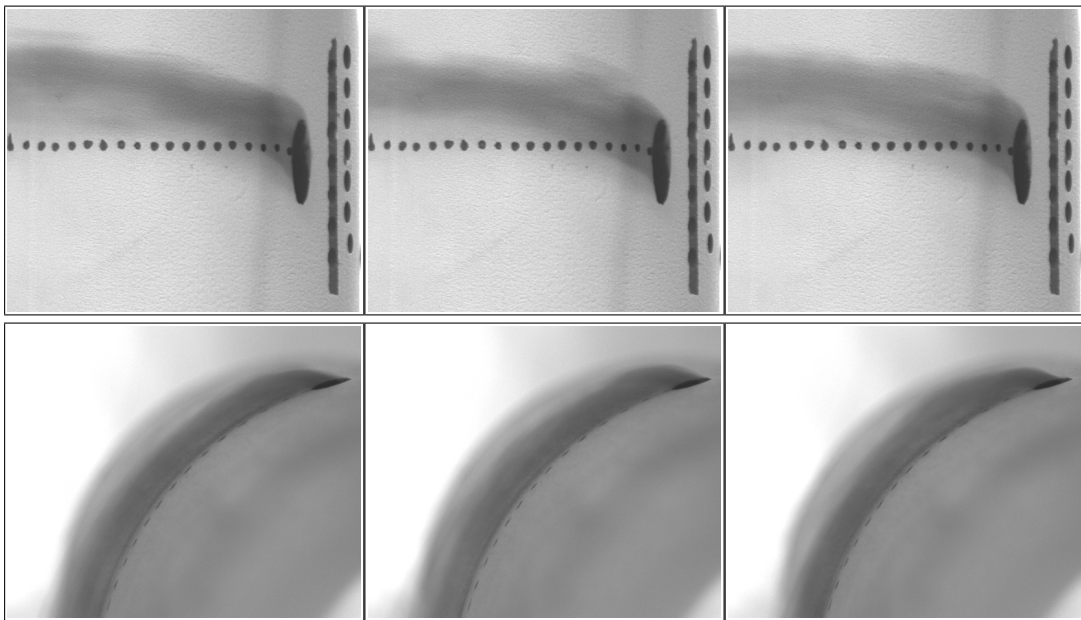
Figure 56   Two staggered rows of small spherical dimples - $M = 1.00$
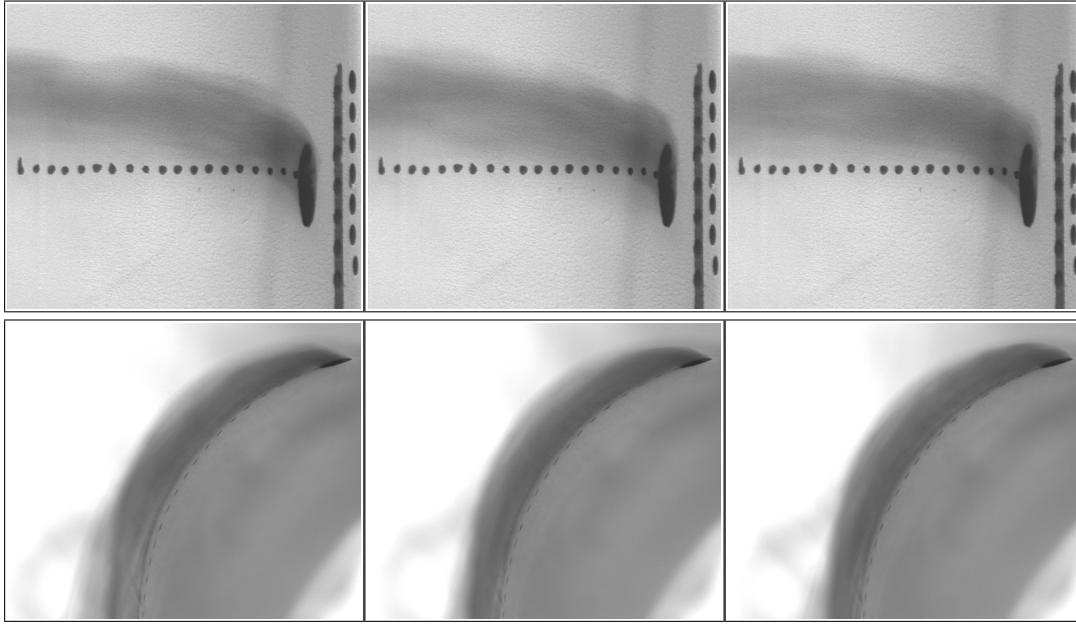
Figure 57   Two staggered rows of small spherical dimples - $M = 1.25$
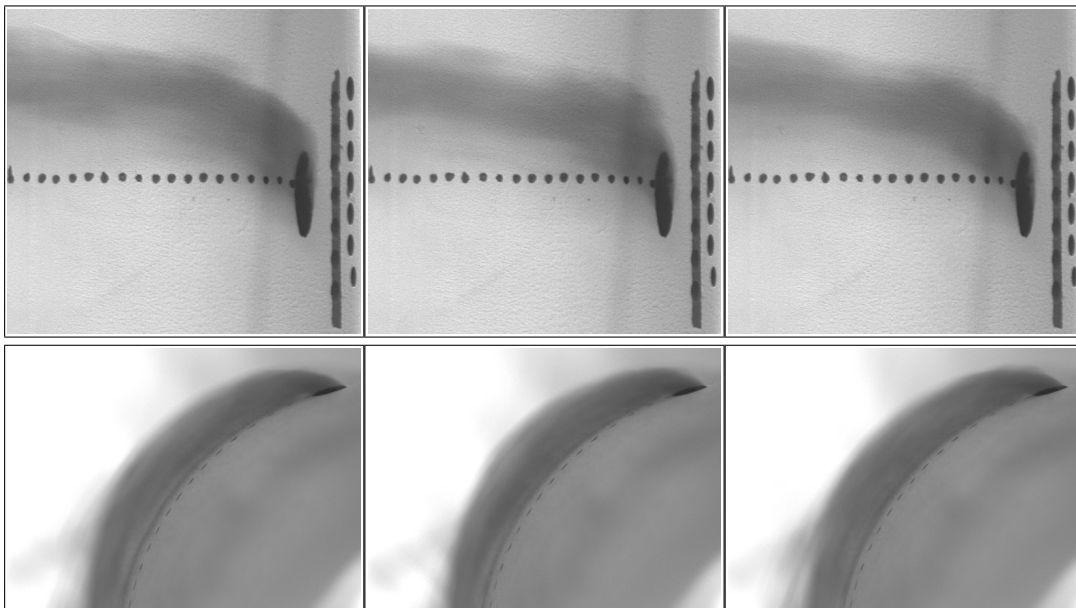
Figure 58   Two staggered rows of small spherical dimples - $M = 1.50$
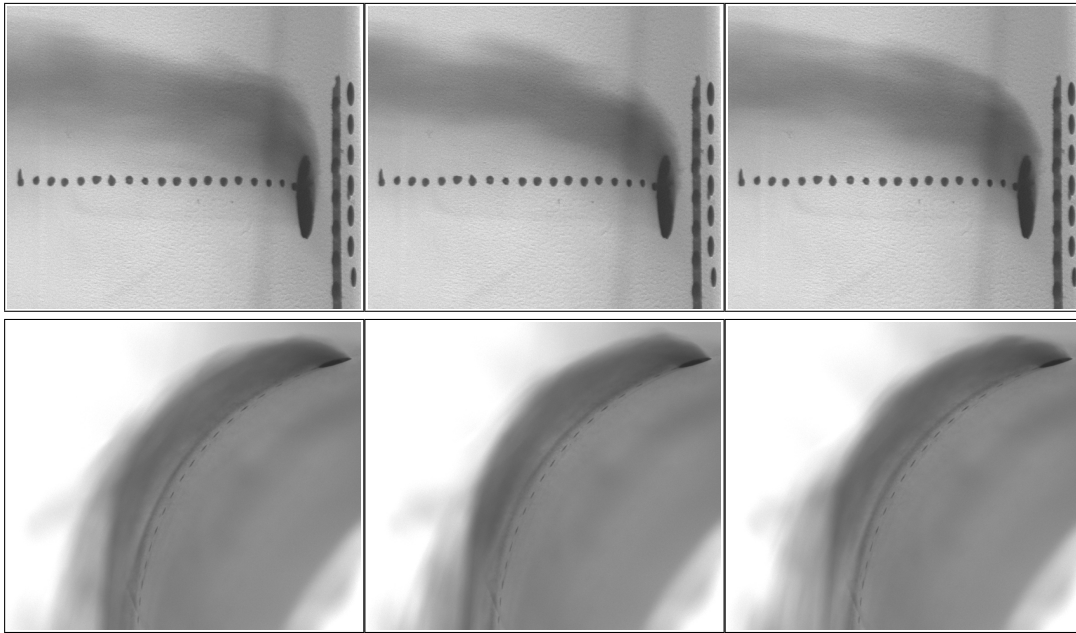
Figure 59   Two staggered rows of small spherical dimples - $M = 1.75$
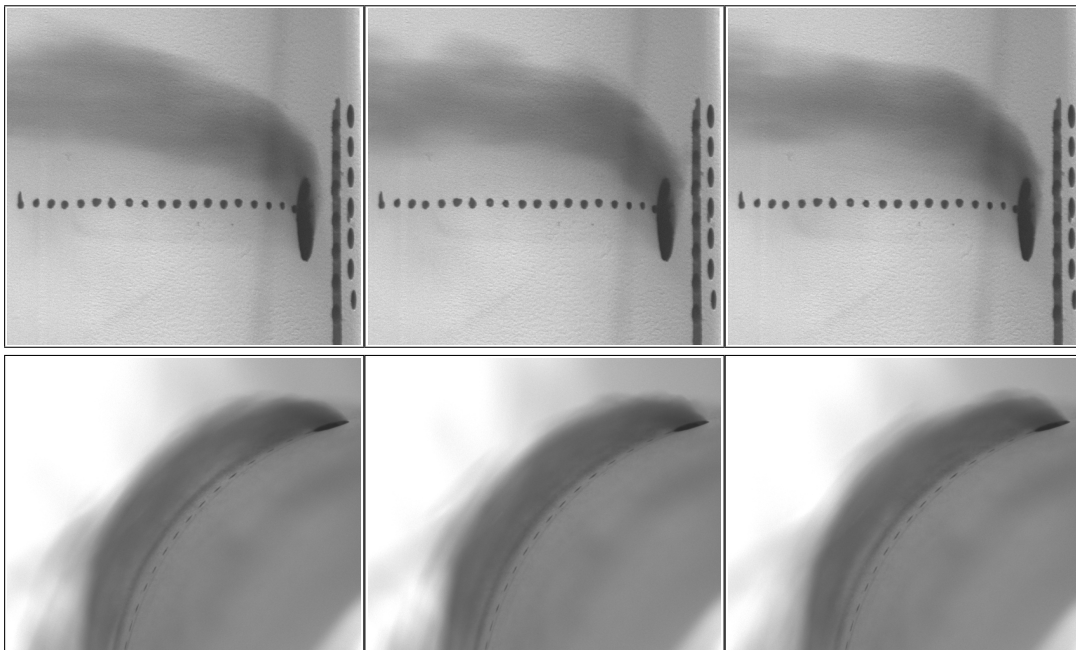
Figure 60   Two staggered rows of small spherical dimples - $M = 2.00$
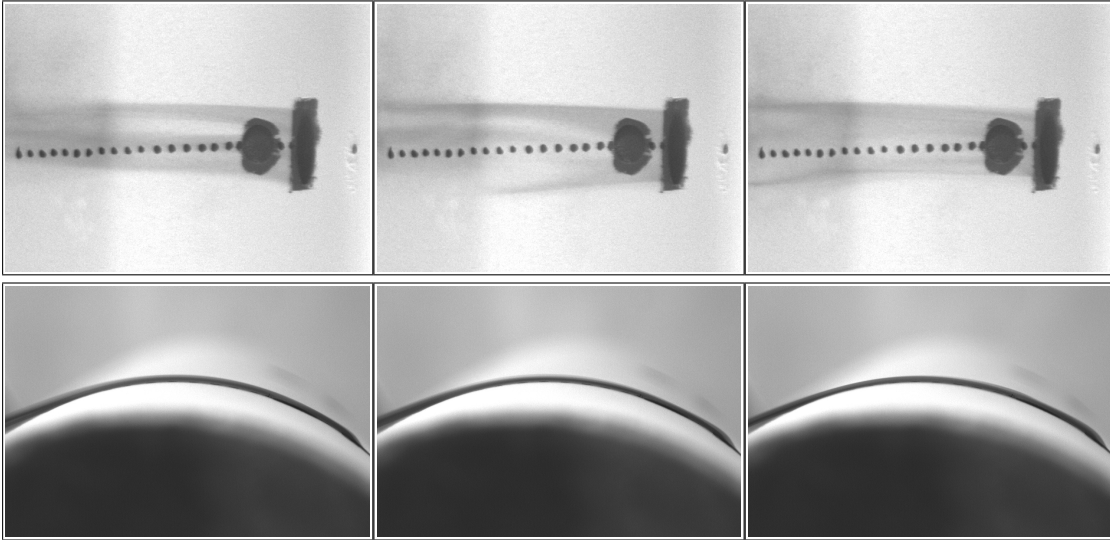
Figure 61   Medium cylindrical dimple downstream of coolant hole - $M = 0.25$
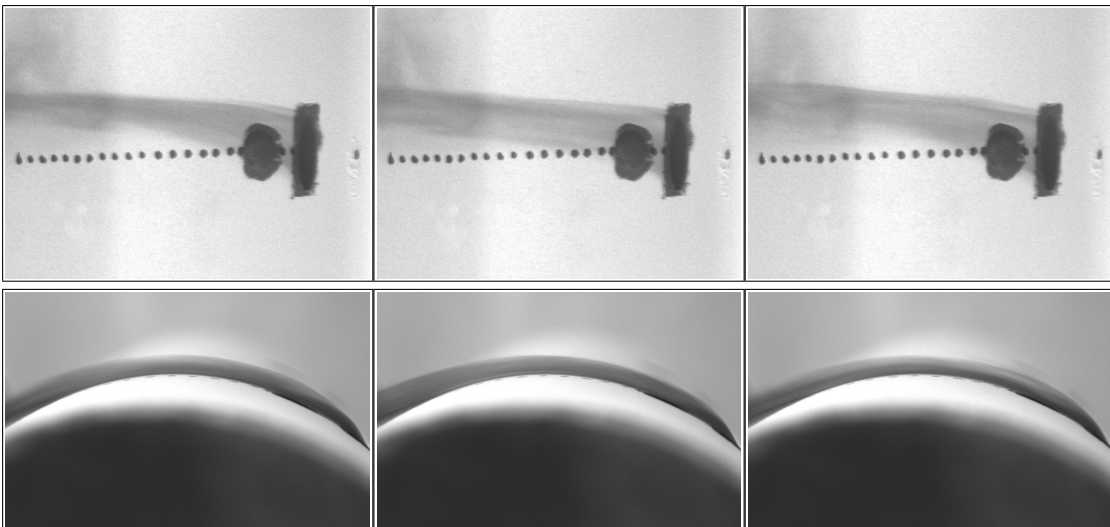
Figure 62   Medium cylindrical dimple downstream of coolant hole - $M = 0.50$

Figure 63   Medium cylindrical dimple downstream of coolant hole - $M = 0.75$

Figure 64   Medium cylindrical dimple downstream of coolant hole - $M = 1.00$

Figure 65   Medium cylindrical dimple downstream of coolant hole - $M = 1.25$

Figure 66   Medium cylindrical dimple downstream of coolant hole - $M = 1.50$

Figure 67   Medium cylindrical dimple downstream of coolant hole - $M = 1.75$

Figure 68   Medium cylindrical dimple downstream of coolant hole - $M = 2.00$
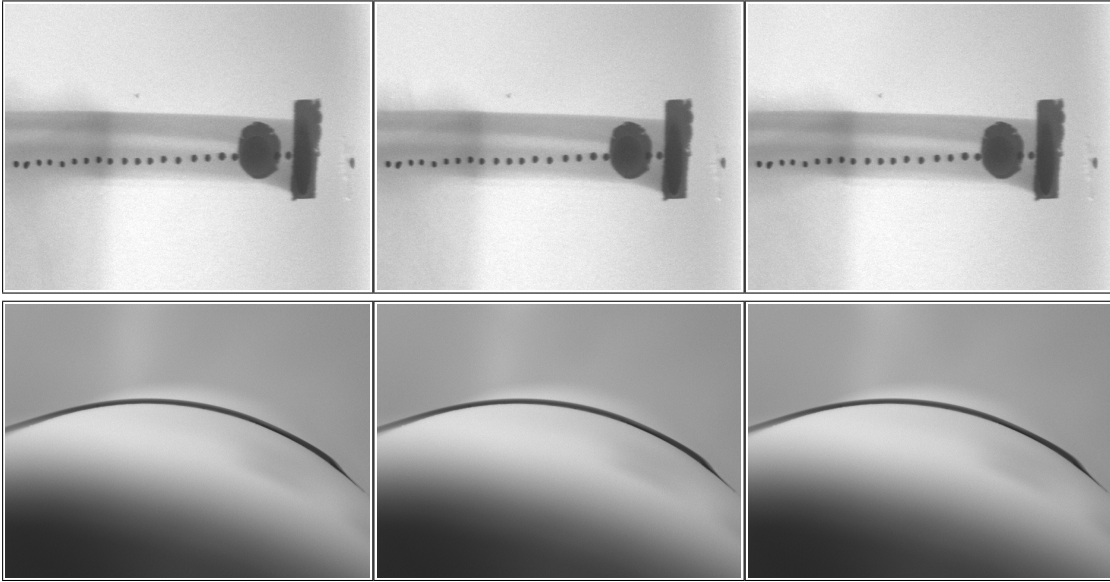
Figure 69   Medium spherical dimple downstream of coolant hole - $M = 0.25$
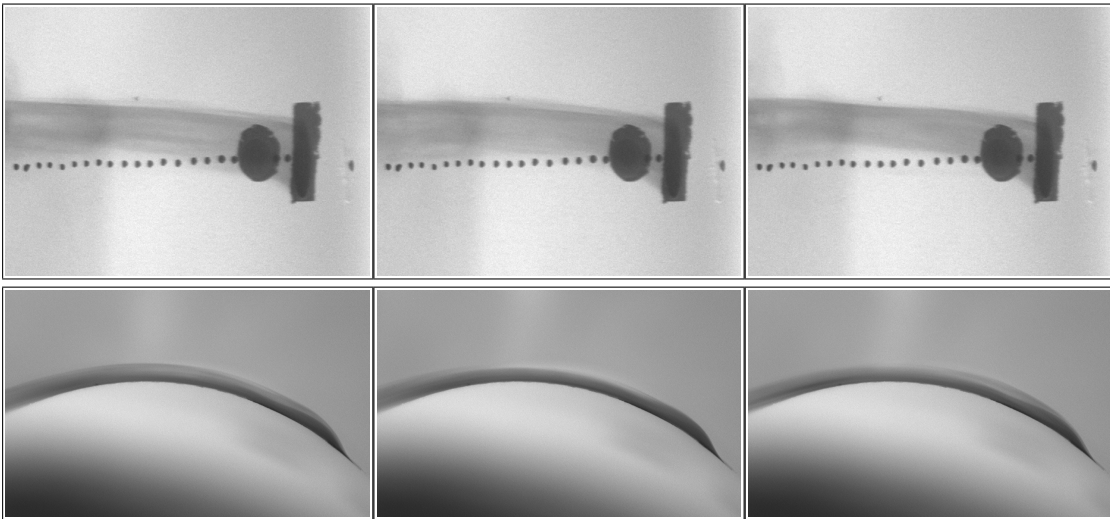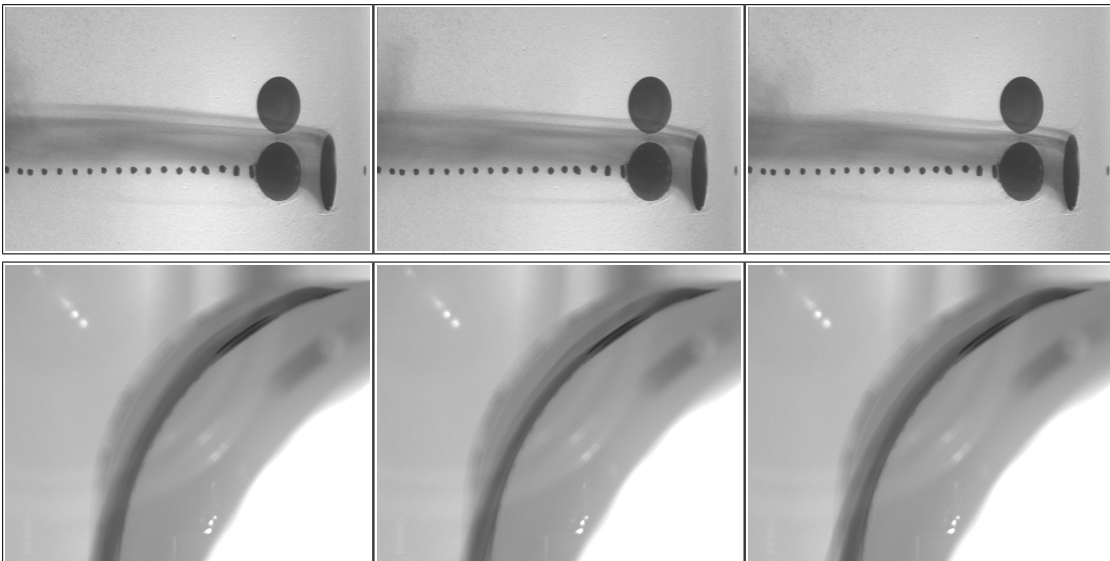

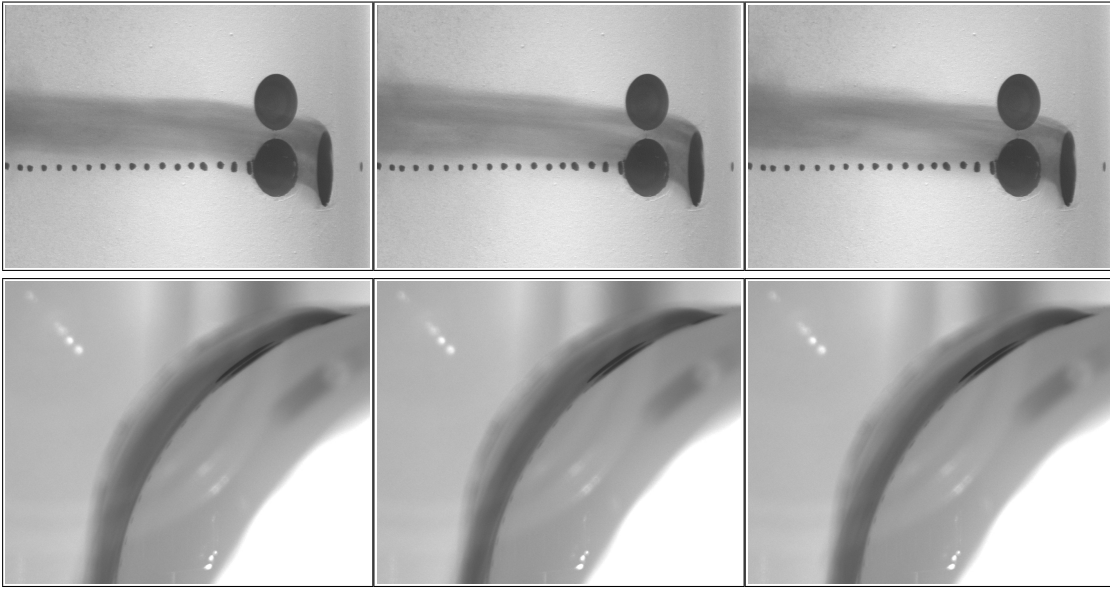Figure 70   Medium spherical dimple downstream of coolant hole - $M = 0.50$
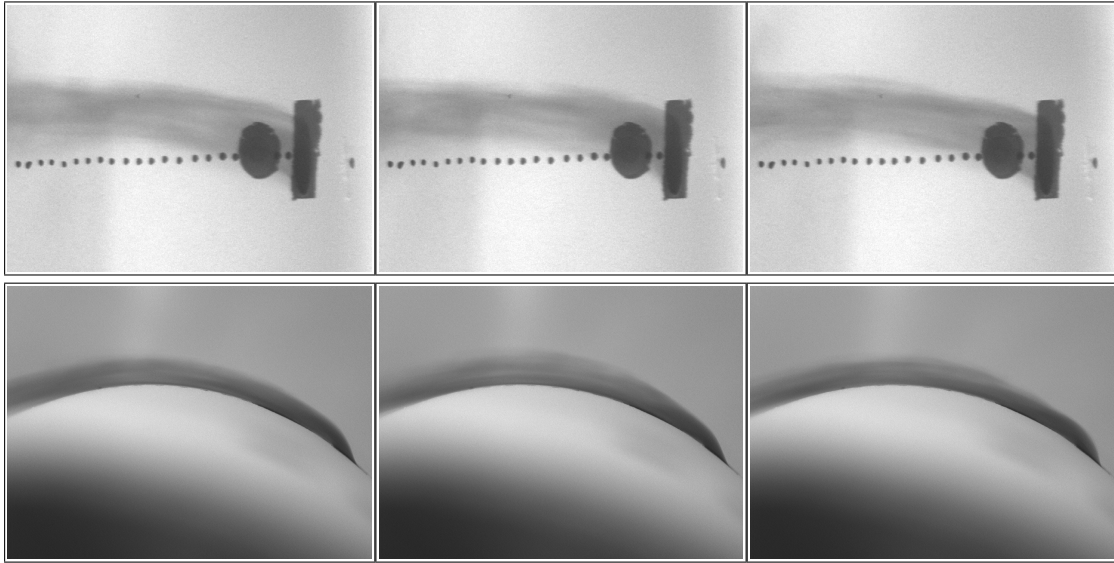
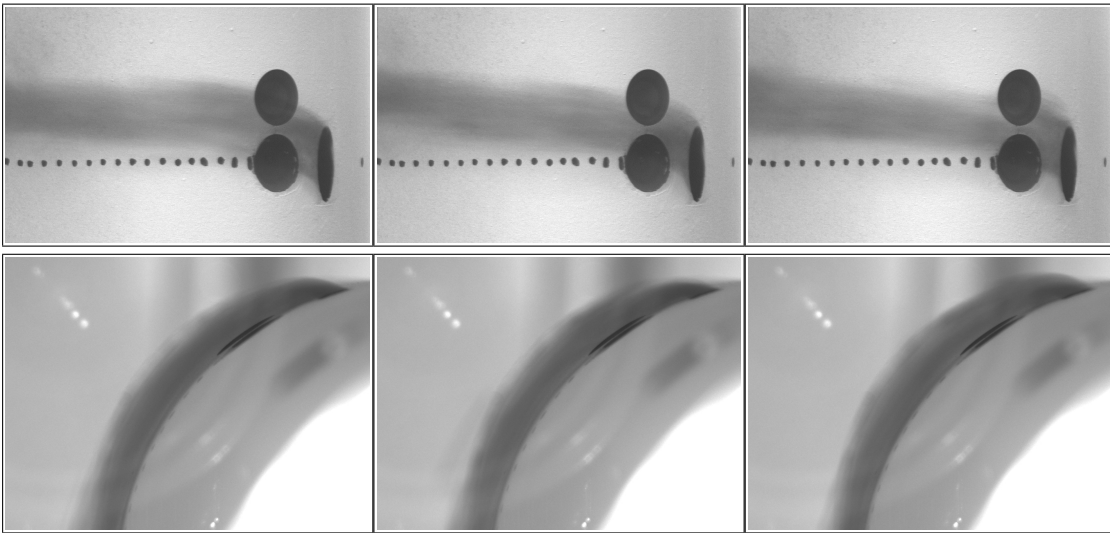Figure 71   Medium spherical dimple downstream of coolant hole - $M = 0.75$
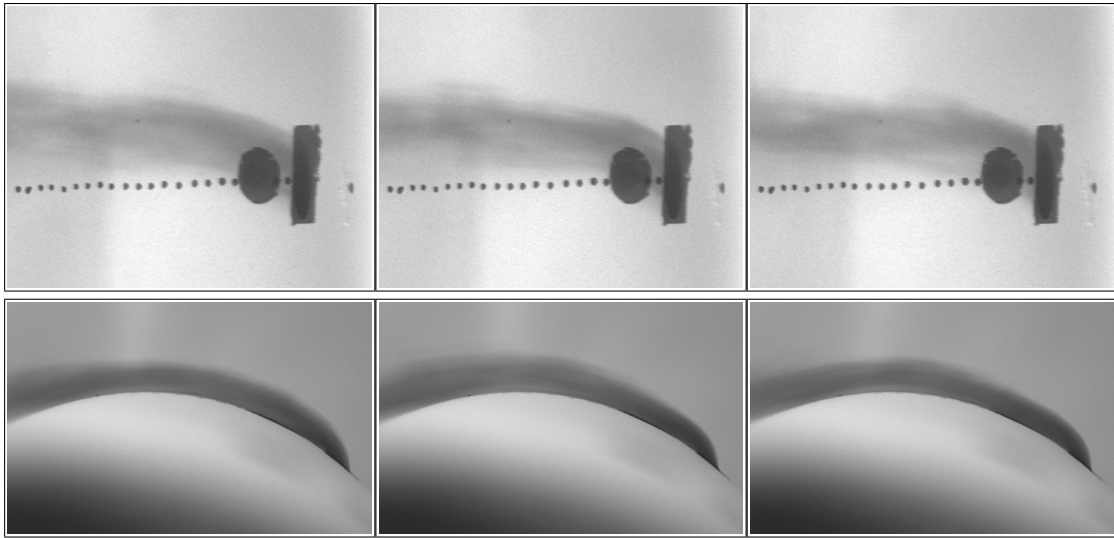
Figure 72   Medium spherical dimple downstream of coolant hole - $M = 1.00$
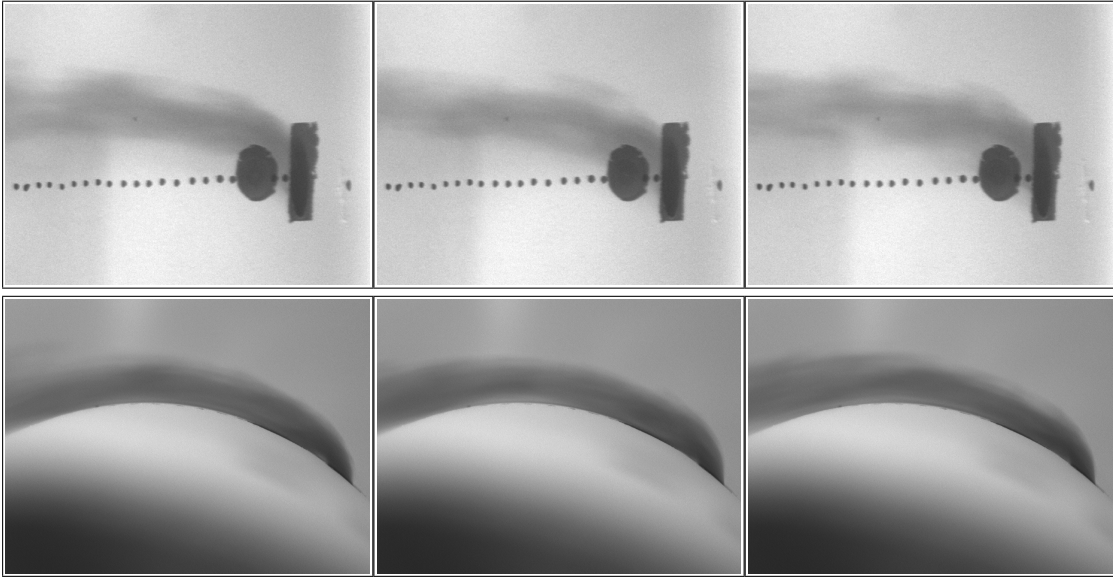
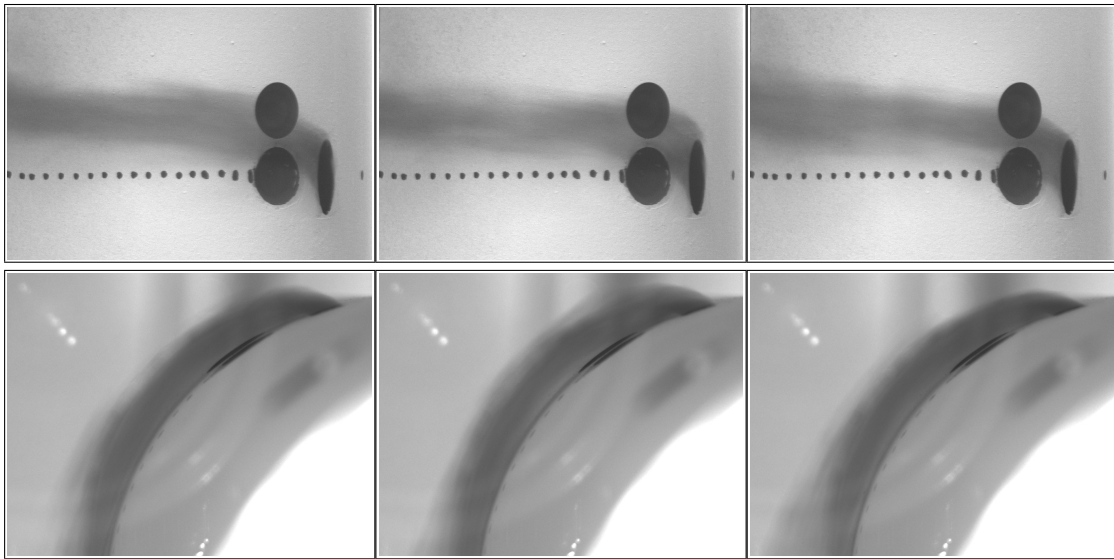Figure 73   Medium spherical dimple downstream of coolant hole - $M = 1.25$
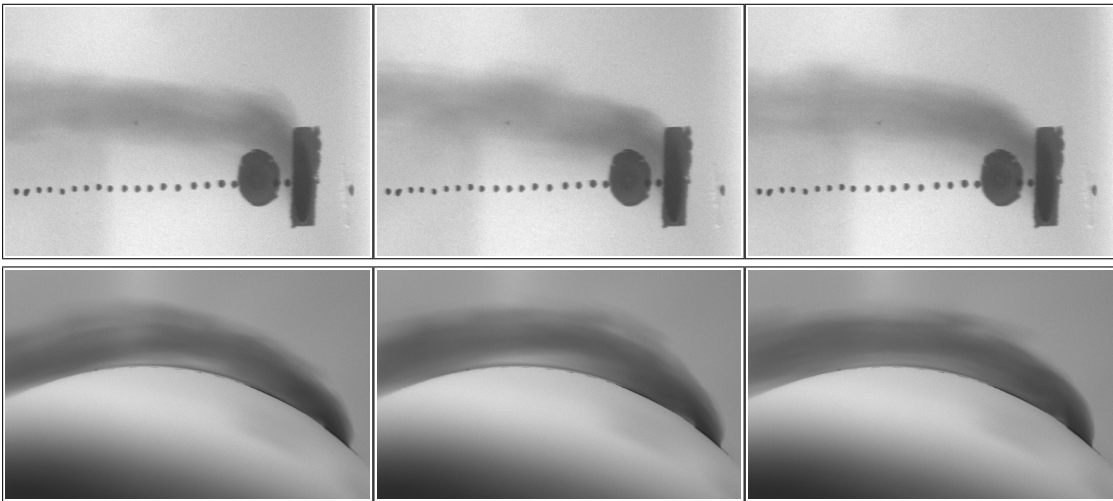
Figure 74   Medium spherical dimple downstream of coolant hole - $M = 1.50$
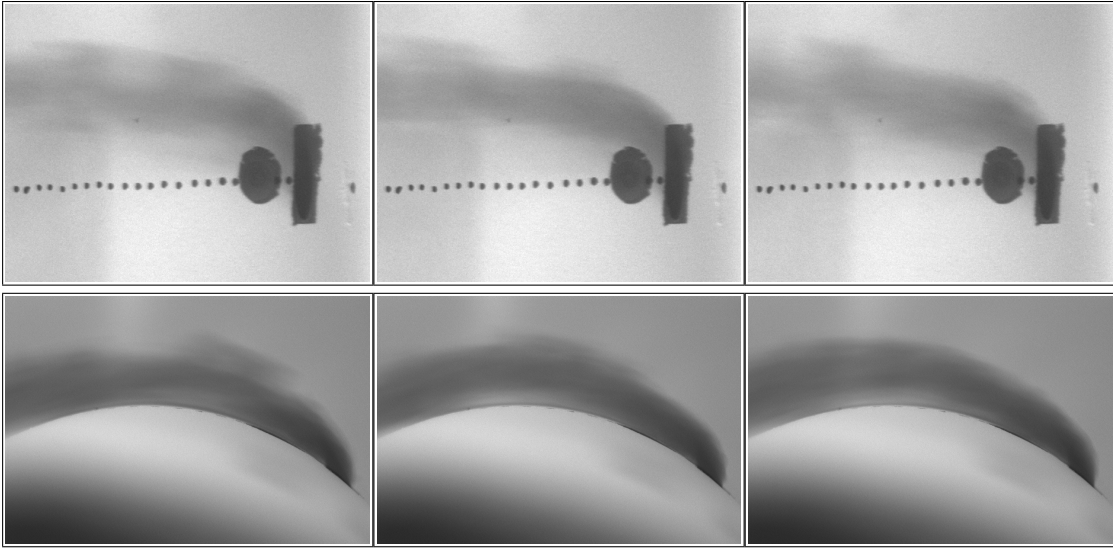
Figure 75   Medium spherical dimple downstream of coolant hole - $M = 1.75$
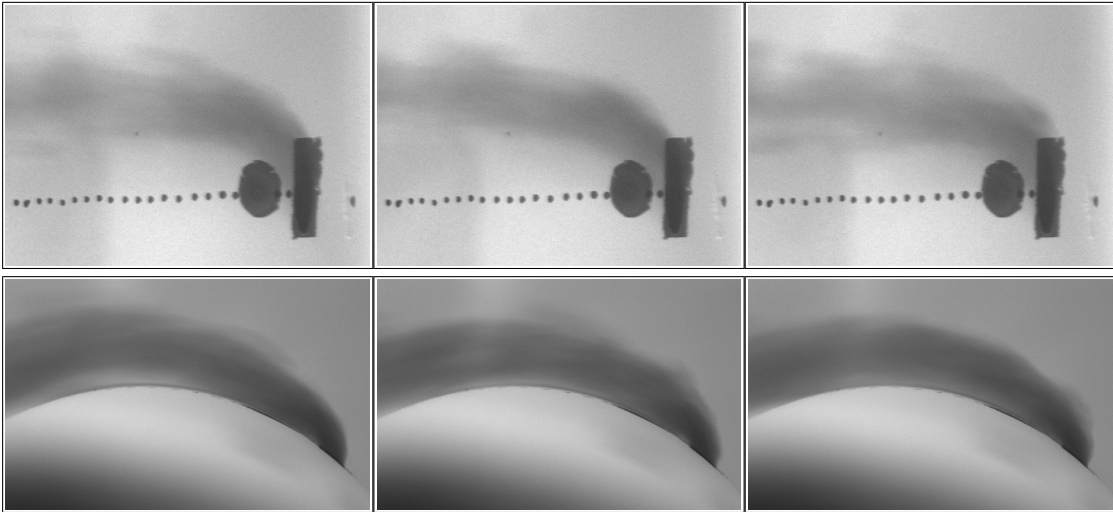
Figure 76   Medium spherical dimple downstream of coolant hole - $M = 2.00$
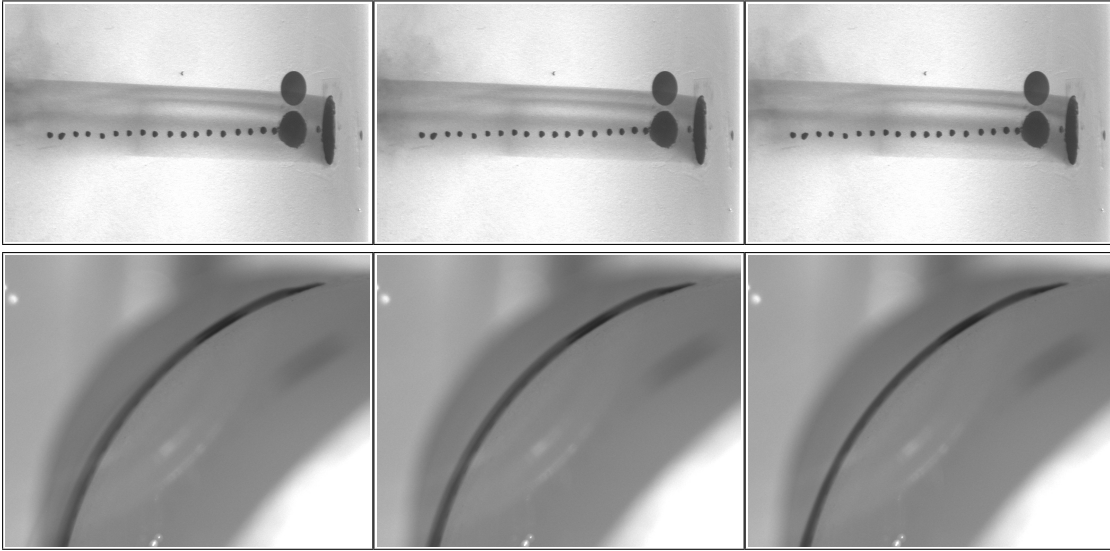
Figure 77   Two medium spherical dimples downstream of coolant hole - $M = 0.25$
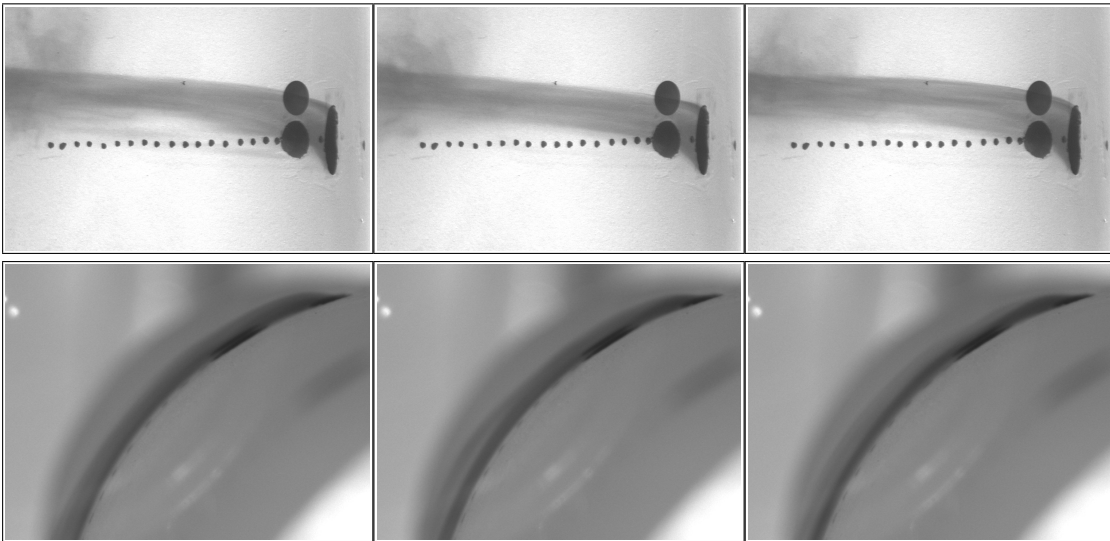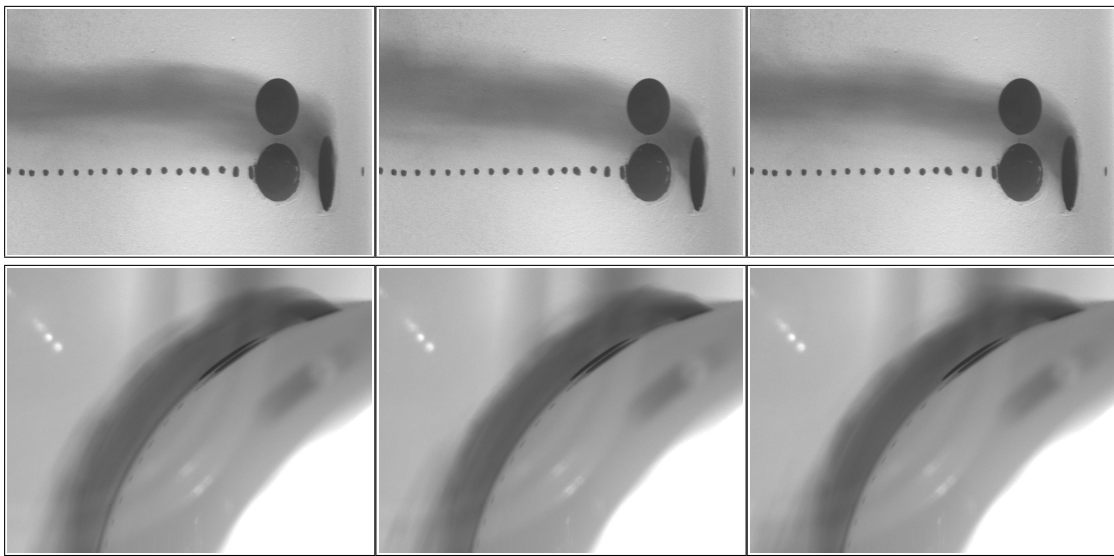

Figure 78   Two medium spherical dimples downstream of coolant hole - $M = 0.50$
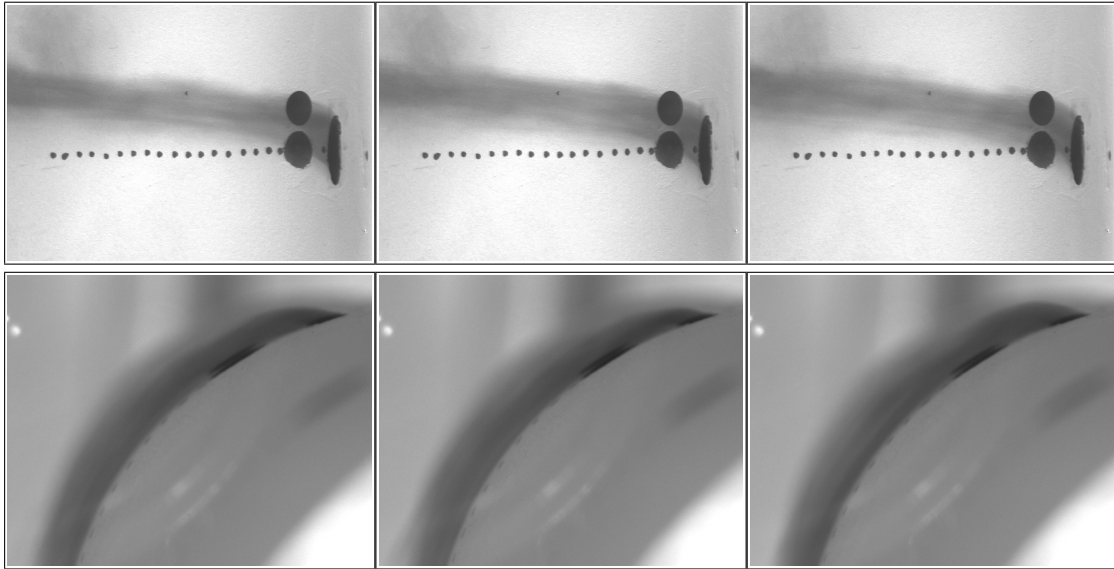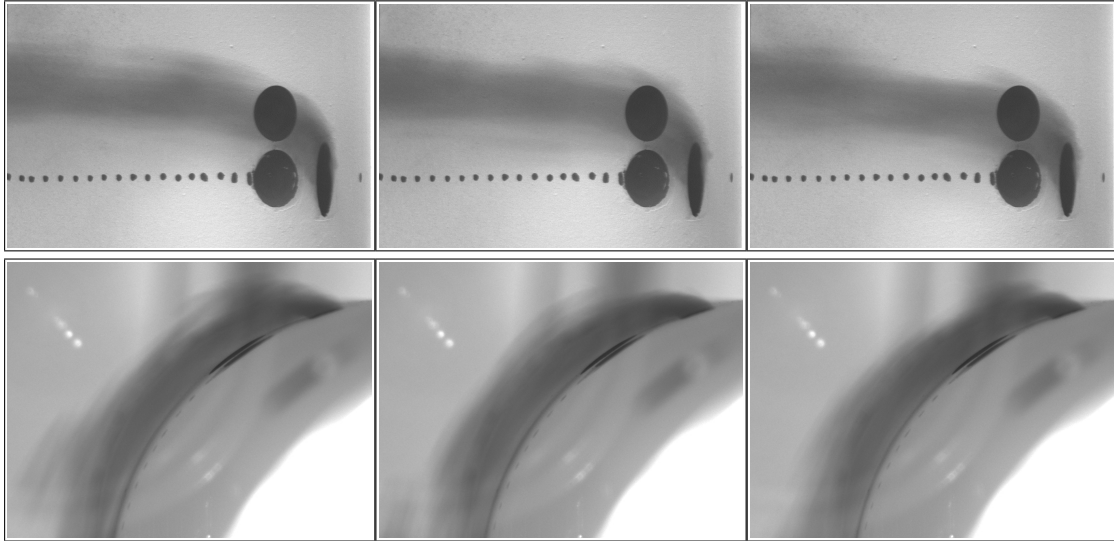
Figure 79   Two medium spherical dimples downstream of coolant hole - $M = 0.75$
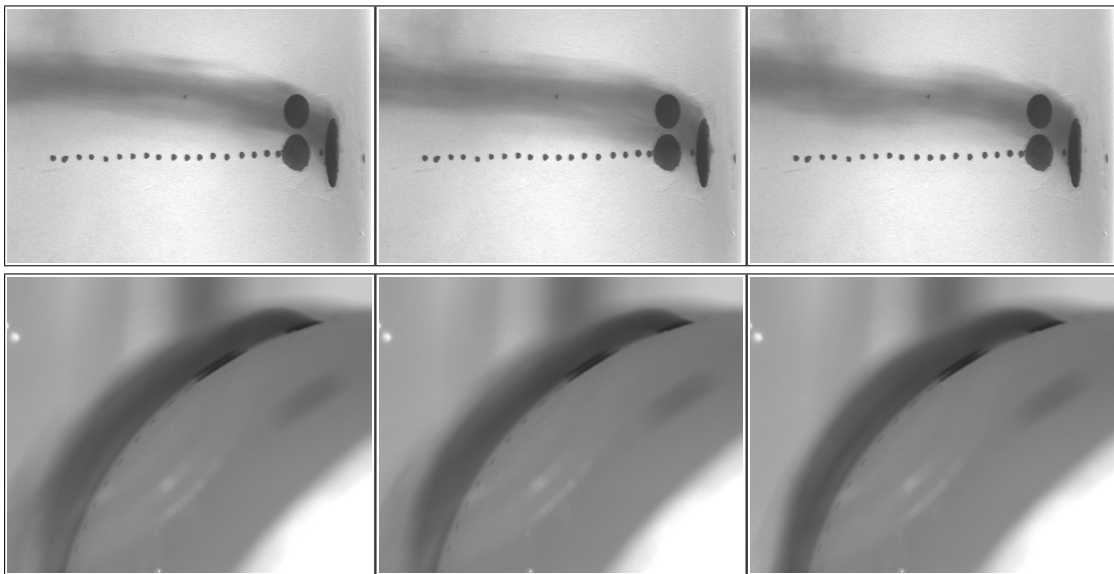
Figure 80   Two medium spherical dimples downstream of coolant hole - $M = 1.00$
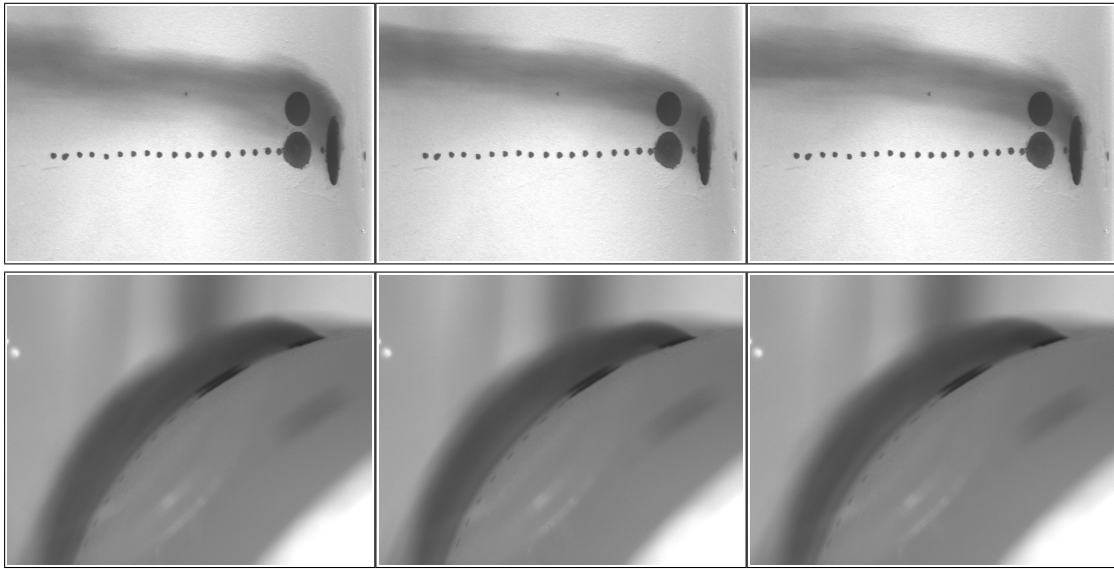
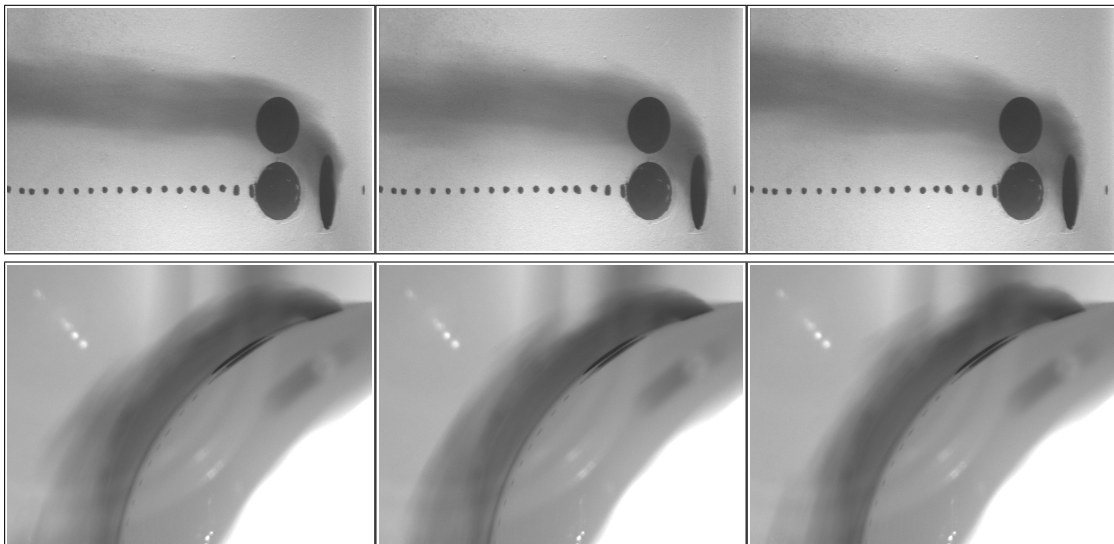Figure 81   Two medium spherical dimples downstream of coolant hole - $M = 1.25$
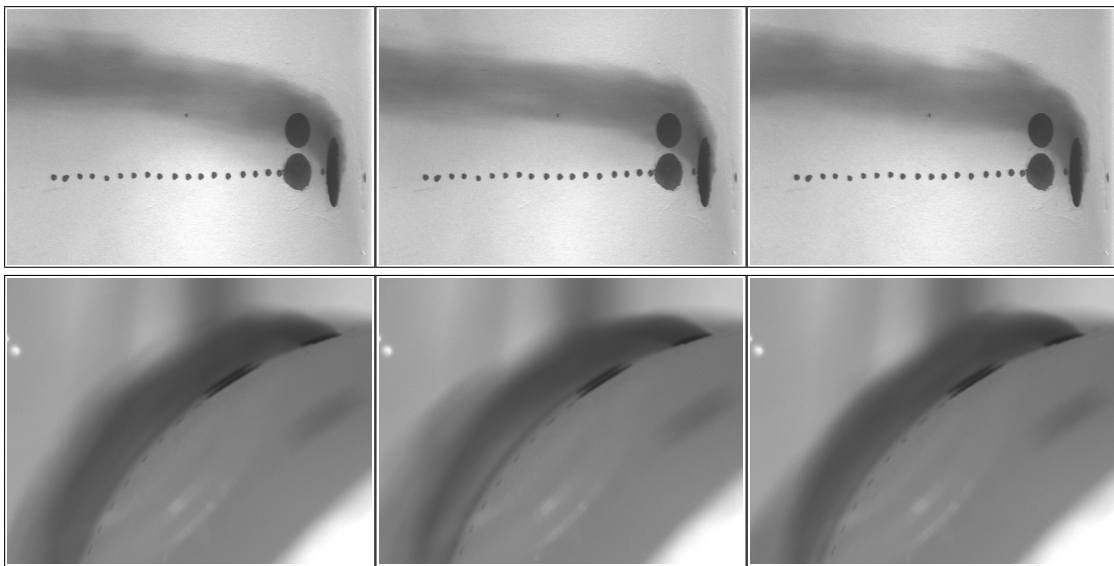
Figure 82   Two medium spherical dimples downstream of coolant hole - $M = 1.50$
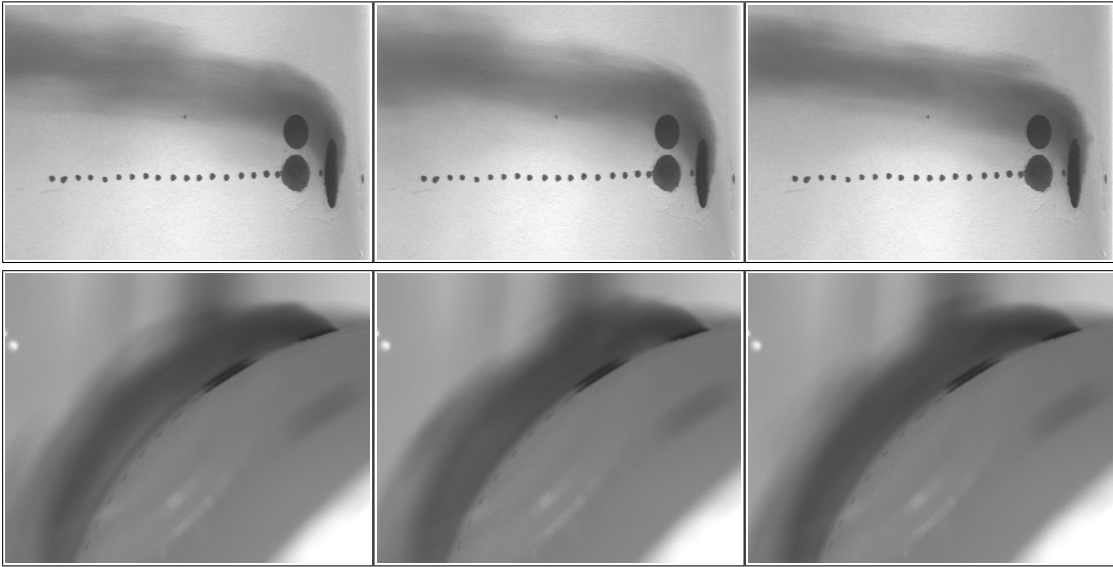
Figure 83   Two medium spherical dimples downstream of coolant hole - $M = 1.75$
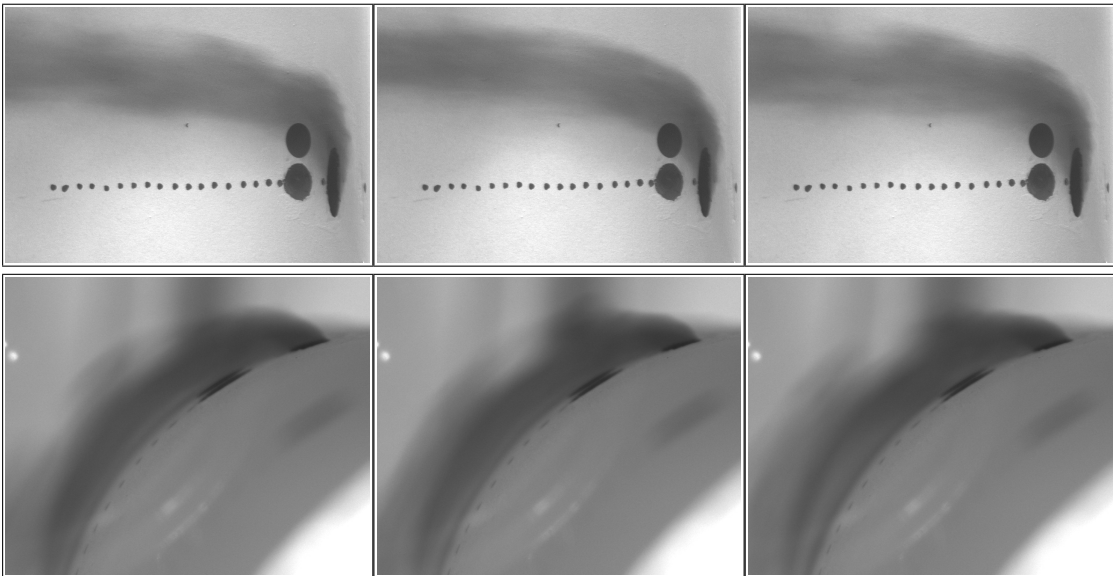
Figure 84   Two medium spherical dimples downstream of coolant hole - $M = 2.00$

Figure 85   Large cylindrical dimple downstream of coolant hole - $M = 0.25$

Figure 86   Large cylindrical dimple downstream of coolant hole - $M = 0.50$

Figure 87   Large cylindrical dimple downstream of coolant hole - $M = 0.75$

Figure 88   Large cylindrical dimple downstream of coolant hole - $M = 1.00$

Figure 89   Large cylindrical dimple downstream of coolant hole - $M = 1.25$

Figure 90   Large cylindrical dimple downstream of coolant hole - $M = 1.50$
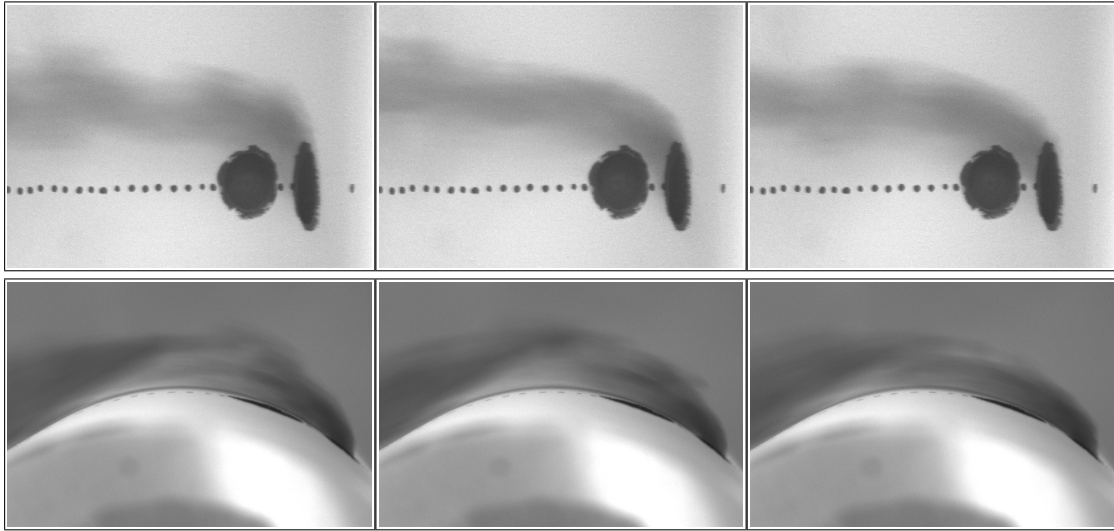
Figure 91   Large cylindrical dimple downstream of coolant hole - $M = 1.75$
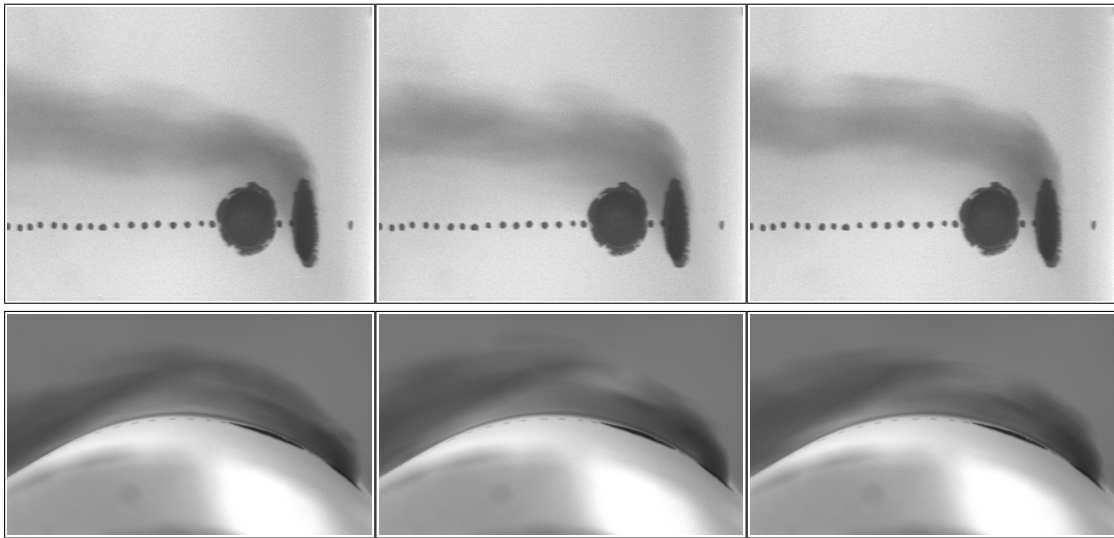
Figure 92   Large cylindrical dimple downstream of coolant hole - $M = 2.00$

Figure 93   Large spherical dimple downstream of coolant hole - $M = 0.25$

Figure 94   Large spherical dimple downstream of coolant hole - $M = 0.50$

Figure 95   Large spherical dimple downstream of coolant hole - $M = 0.75$
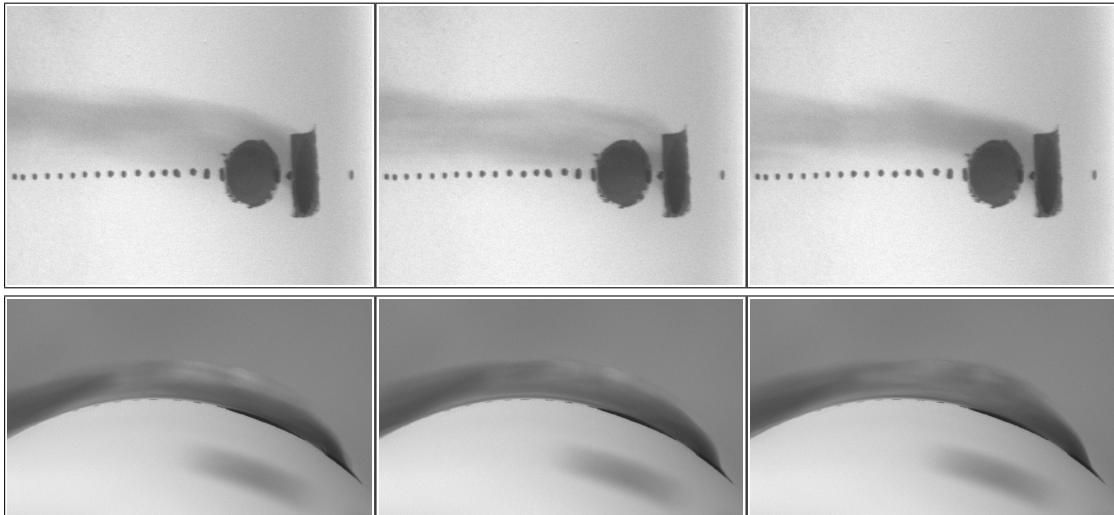
Figure 96   Large spherical dimple downstream of coolant hole - $M = 1.00$
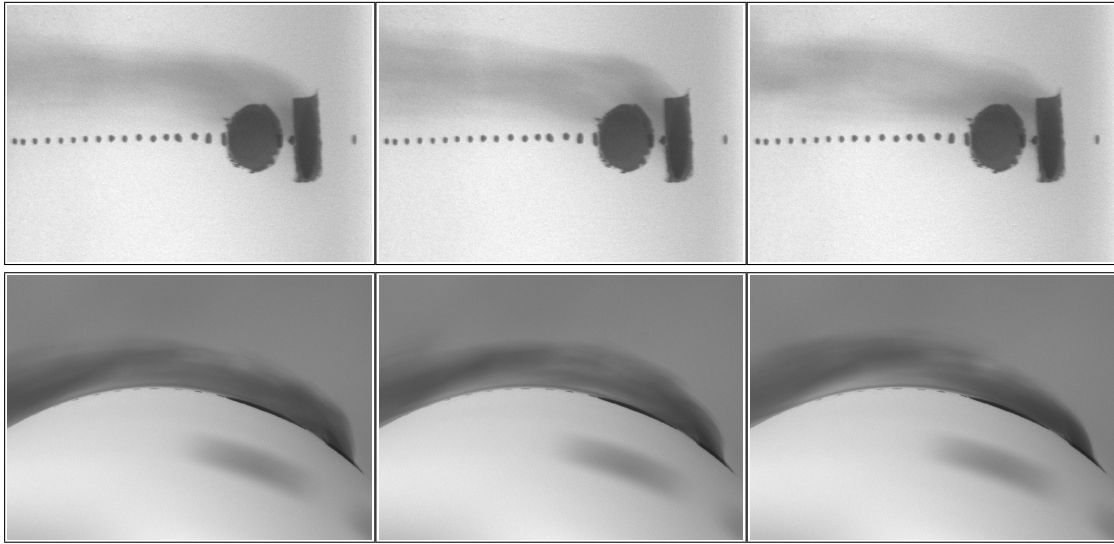
Figure 97   Large spherical dimple downstream of coolant hole - $M = 1.25$
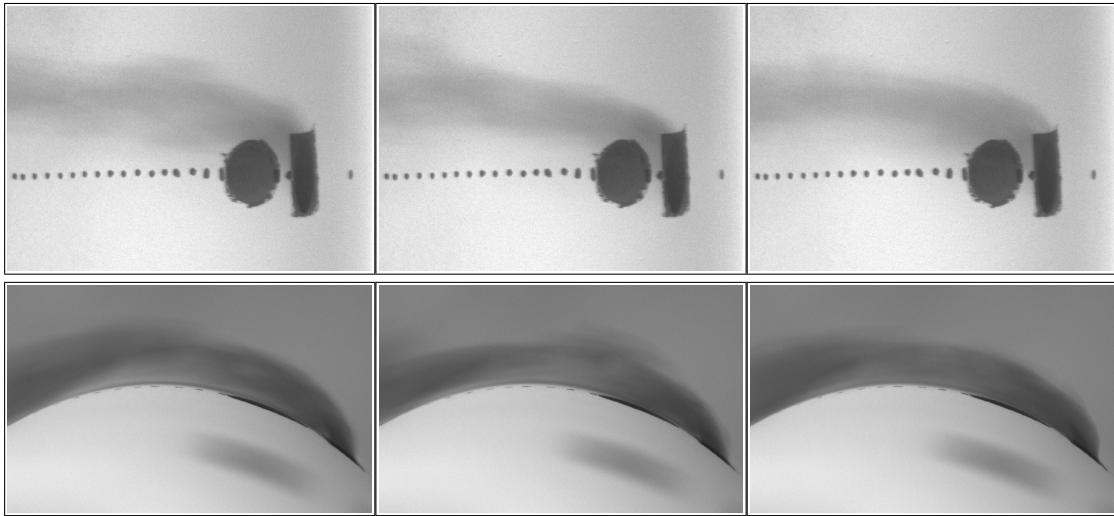
Figure 98   Large spherical dimple downstream of coolant hole - $M = 1.50$
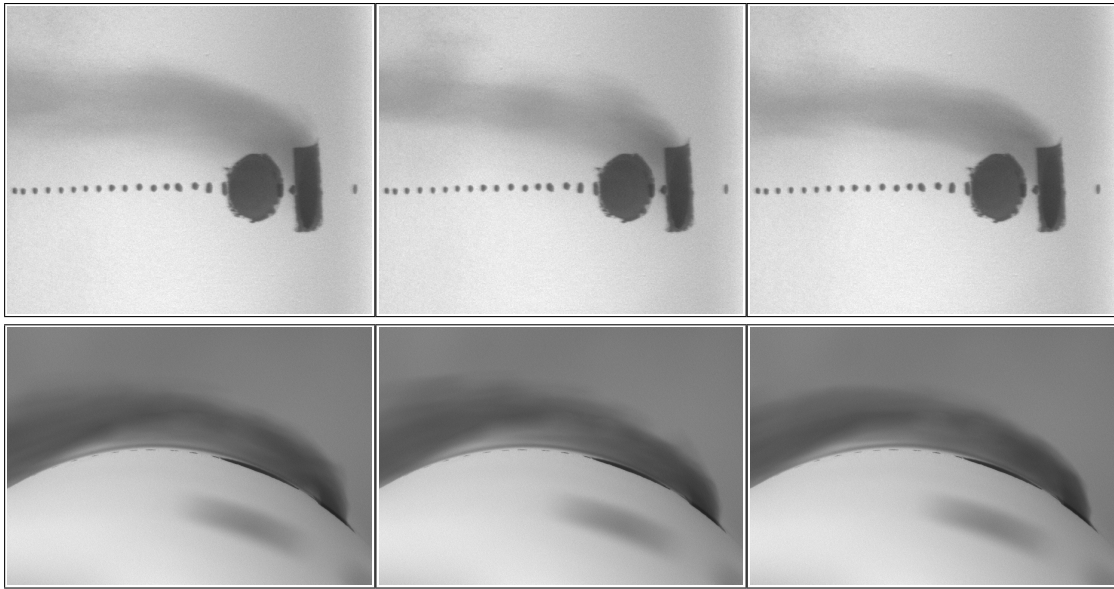
Figure 99   Large spherical dimple downstream of coolant hole - $M = 1.75$
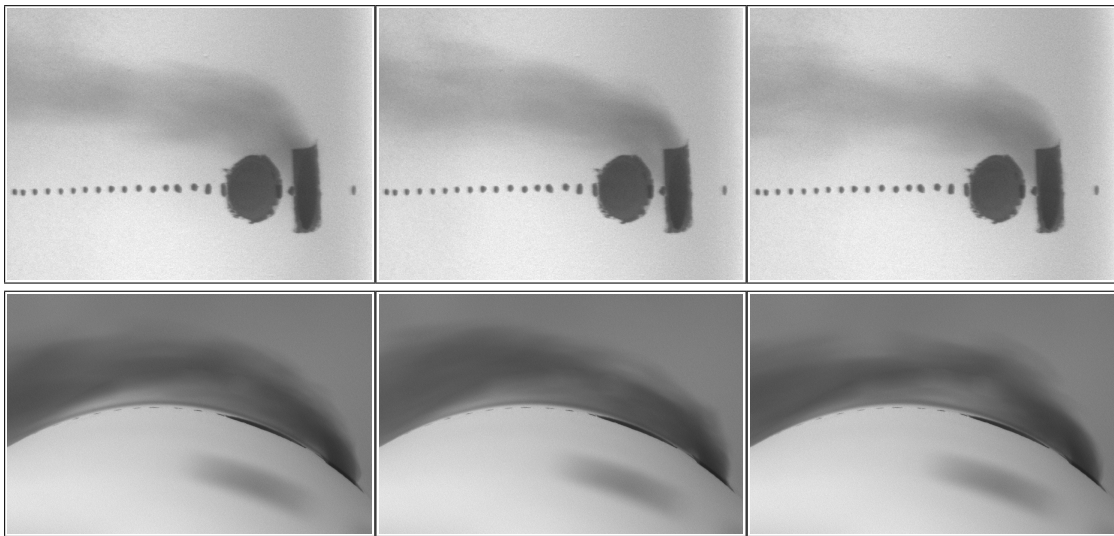
Figure 100   Large spherical dimple downstream of coolant hole - $M = 2.00$
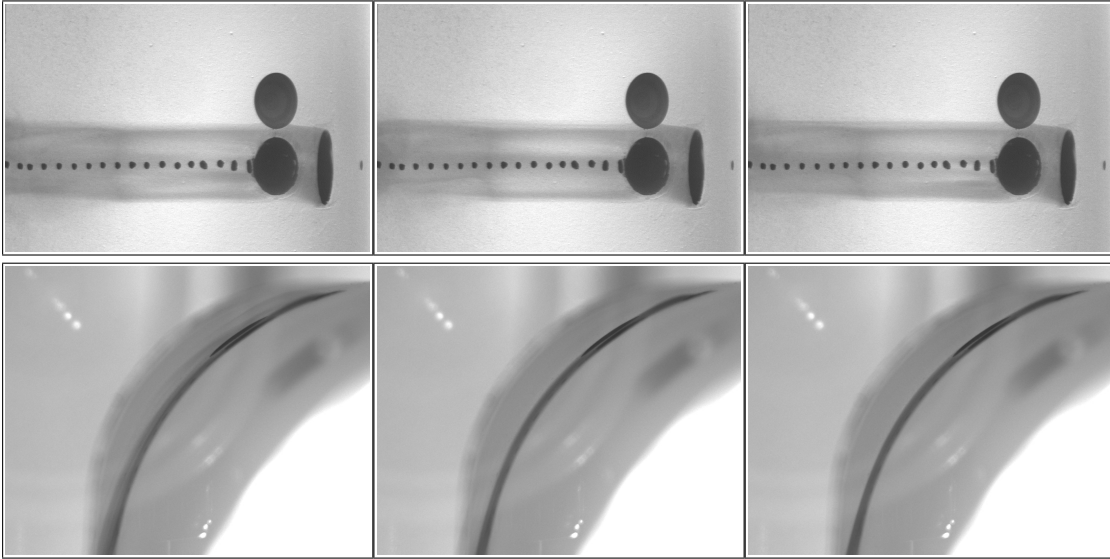
Figure 101   Two large spherical dimples downstream of coolant hole - $M = 0.25$

Figure 102   Two large spherical dimples downstream of coolant hole - $M = 0.50$

Figure 103   Two large spherical dimples downstream of coolant hole - $M = 0.75$

Figure 104   Two large spherical dimples downstream of coolant hole - $M = 1.00$

Figure 105   Two large spherical dimples downstream of coolant hole - $M = 1.25$

Figure 106   Two large spherical dimples downstream of coolant hole - $M = 1.50$

Figure 107   Two large spherical dimples downstream of coolant hole - $M = 1.75$

Figure 108   Two large spherical dimples downstream of coolant hole - $M = 2.00$
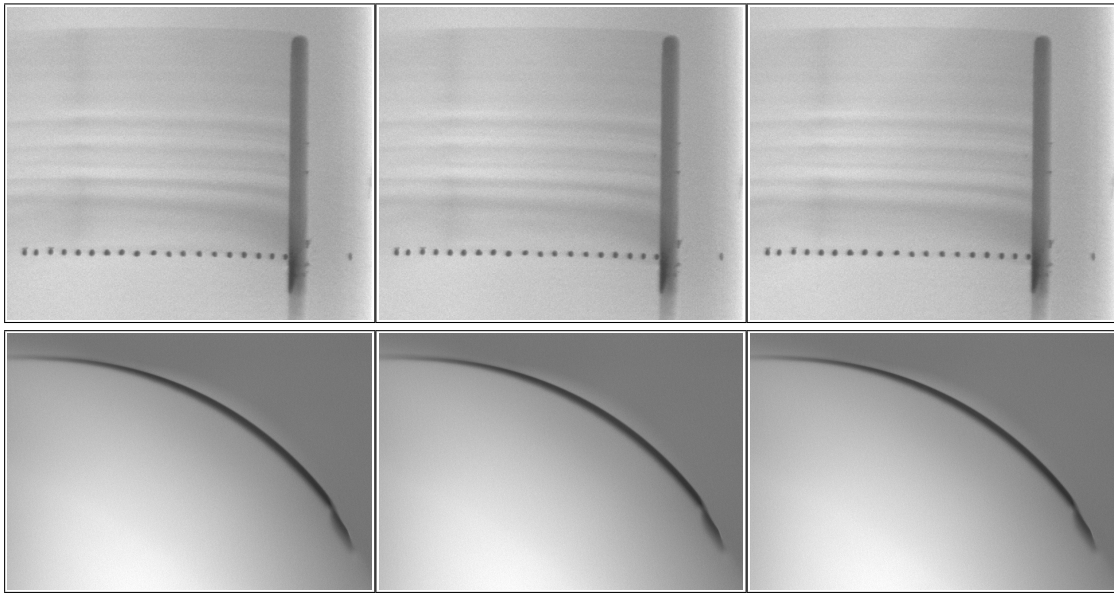
Figure 109   Single-depth transverse trench - $M = 0.25$
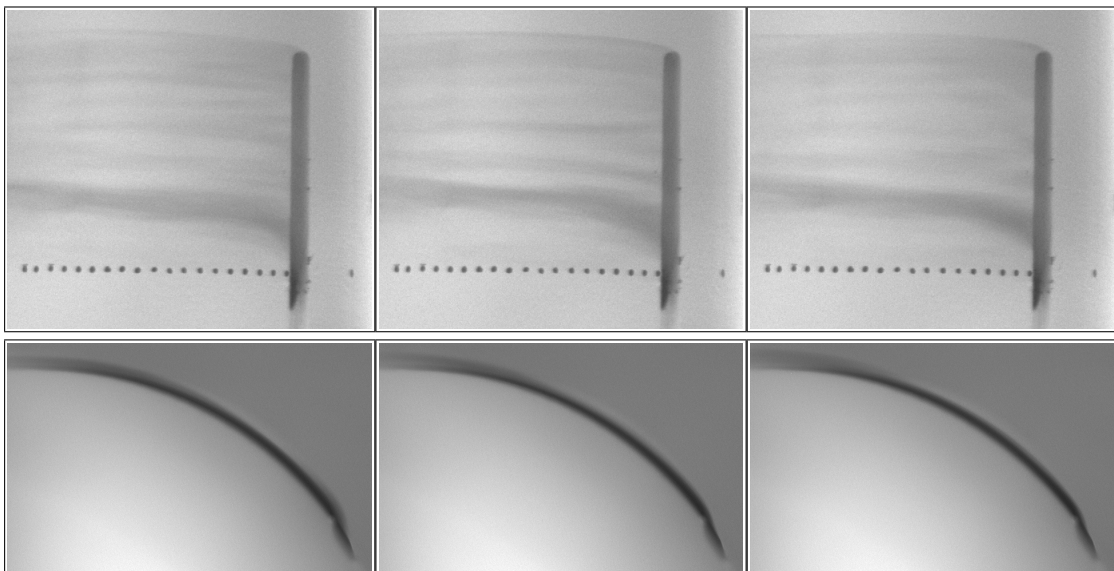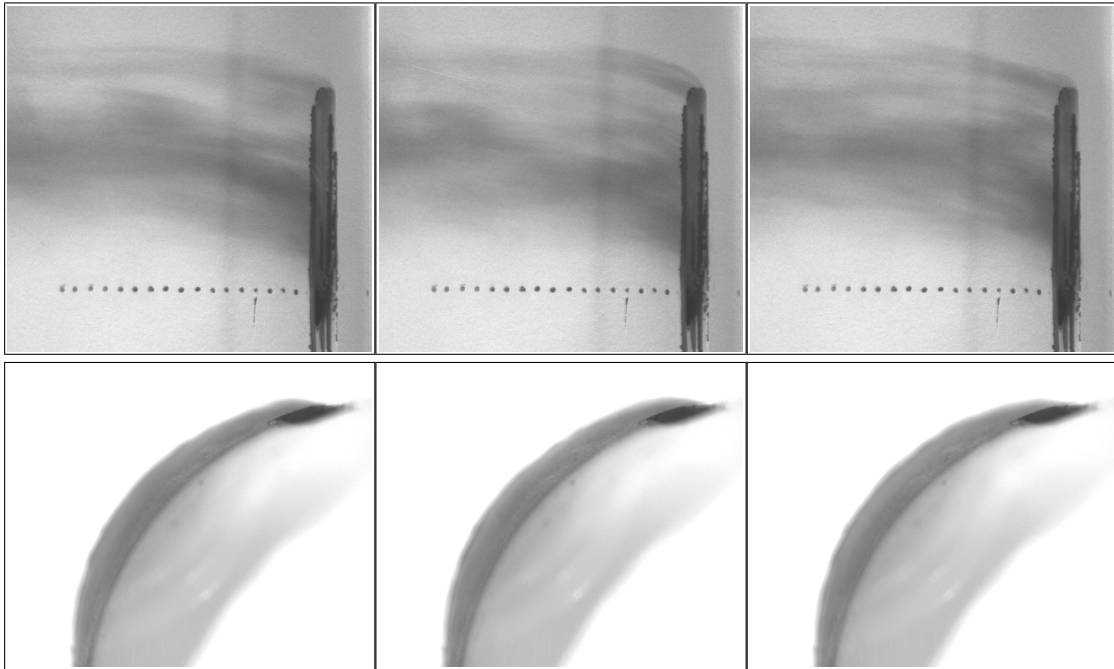
Figure 110   Single-depth transverse trench - $M = 0.50$
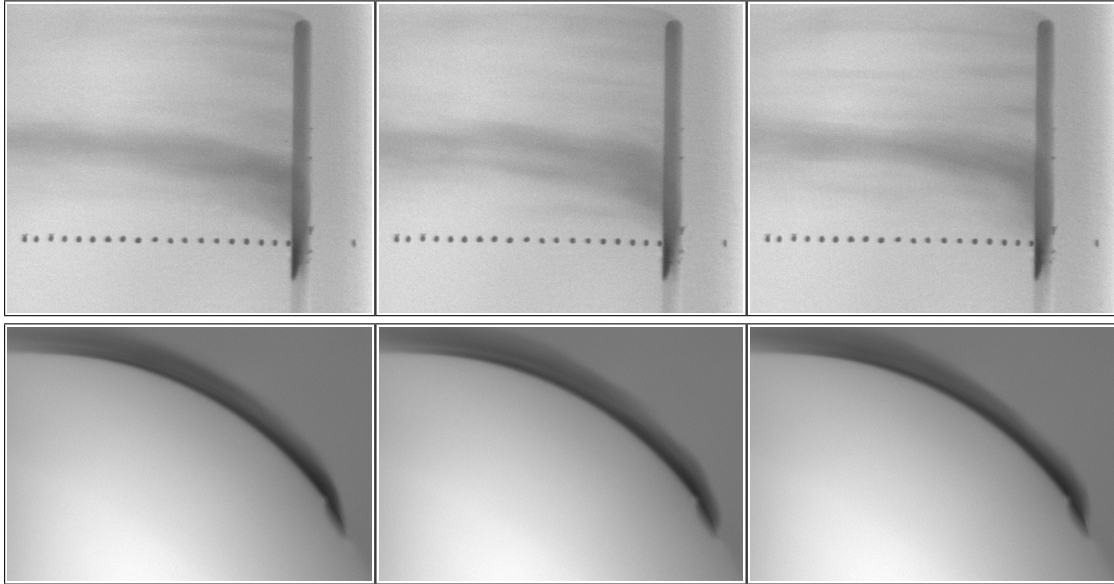
Figure 111   Single-depth transverse trench - $M = 0.75$
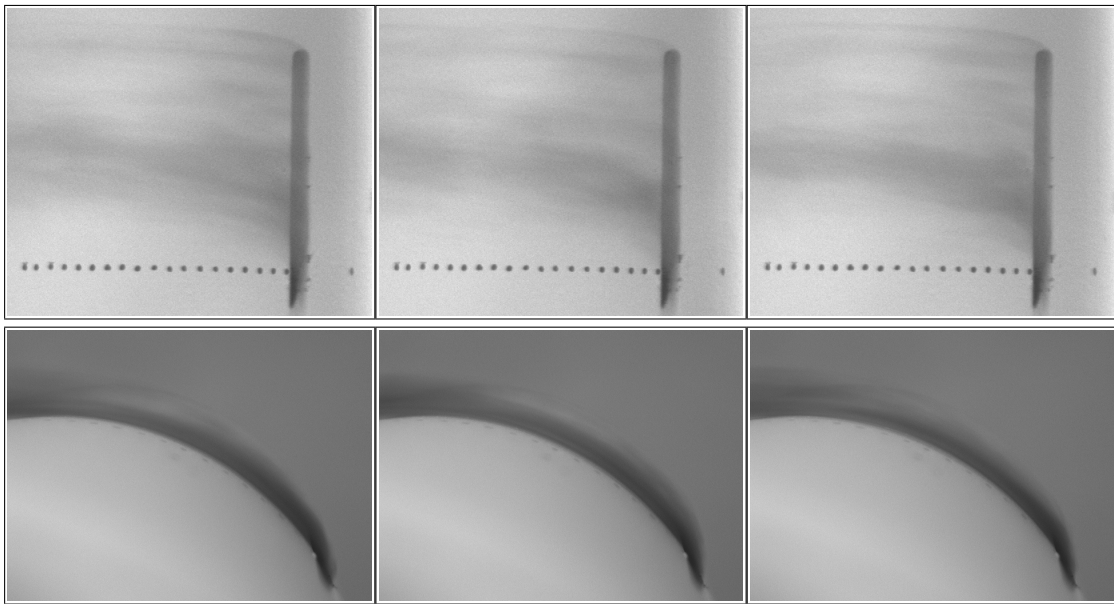
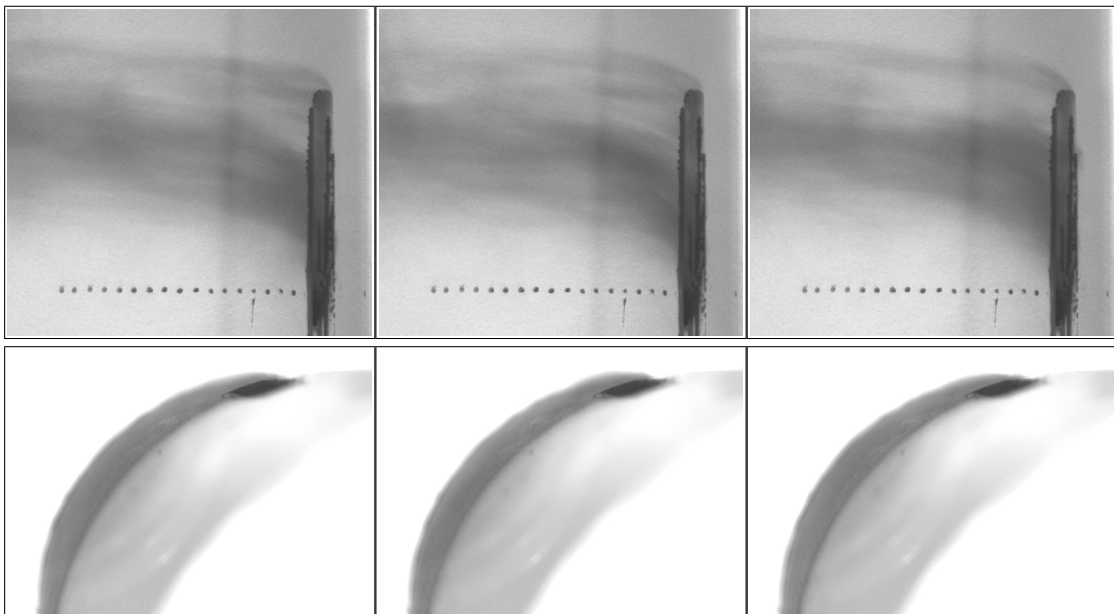Figure 112   Single-depth transverse trench - $M = 1.00$
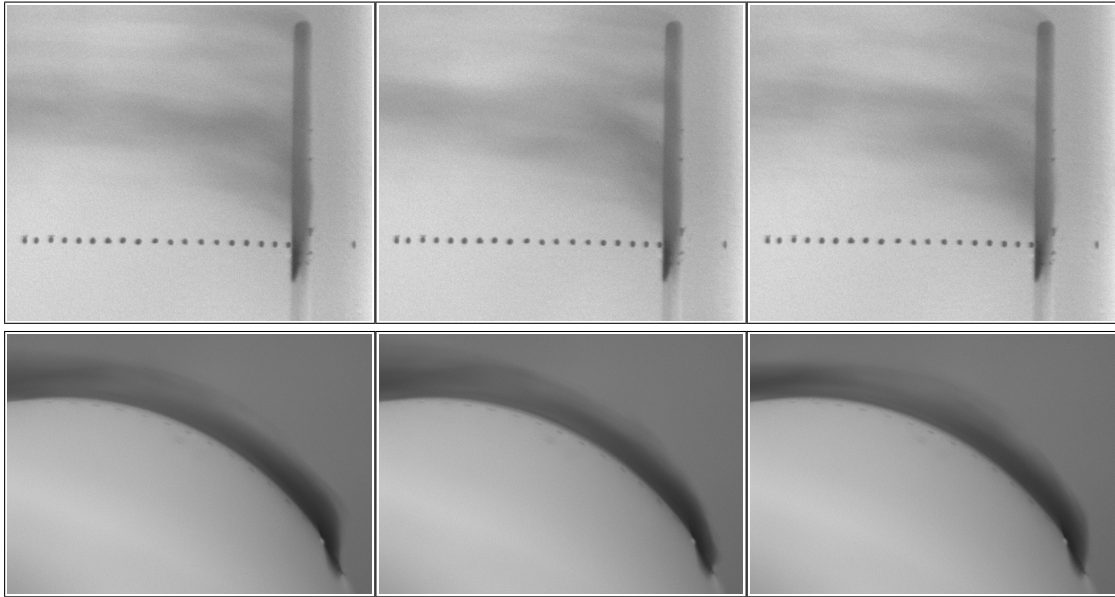
Figure 113   Single-depth transverse trench - $M = 1.25$
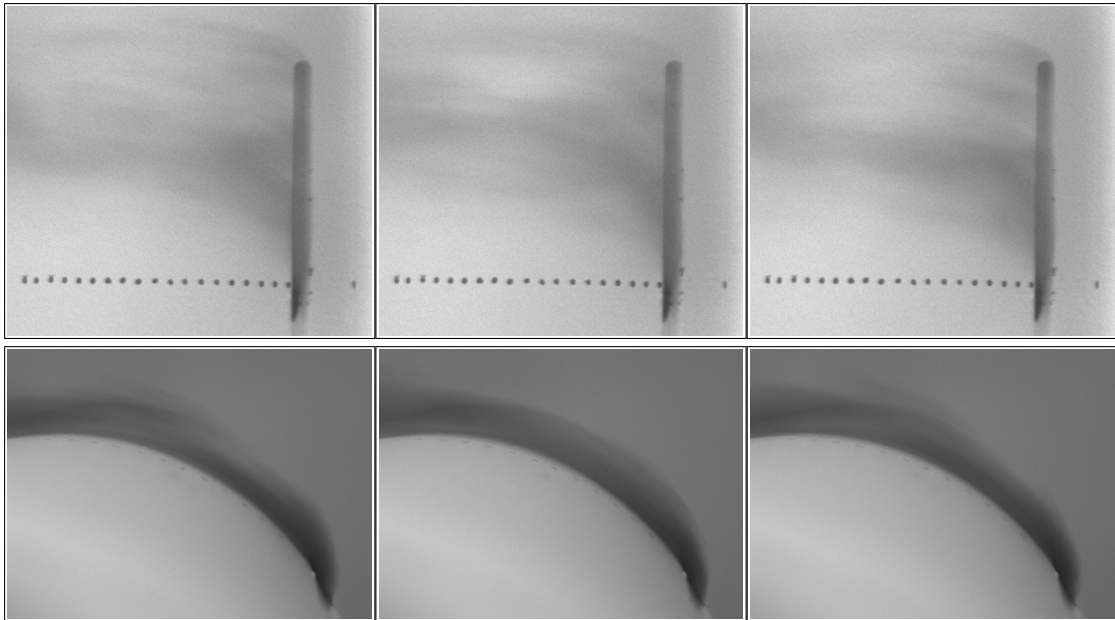
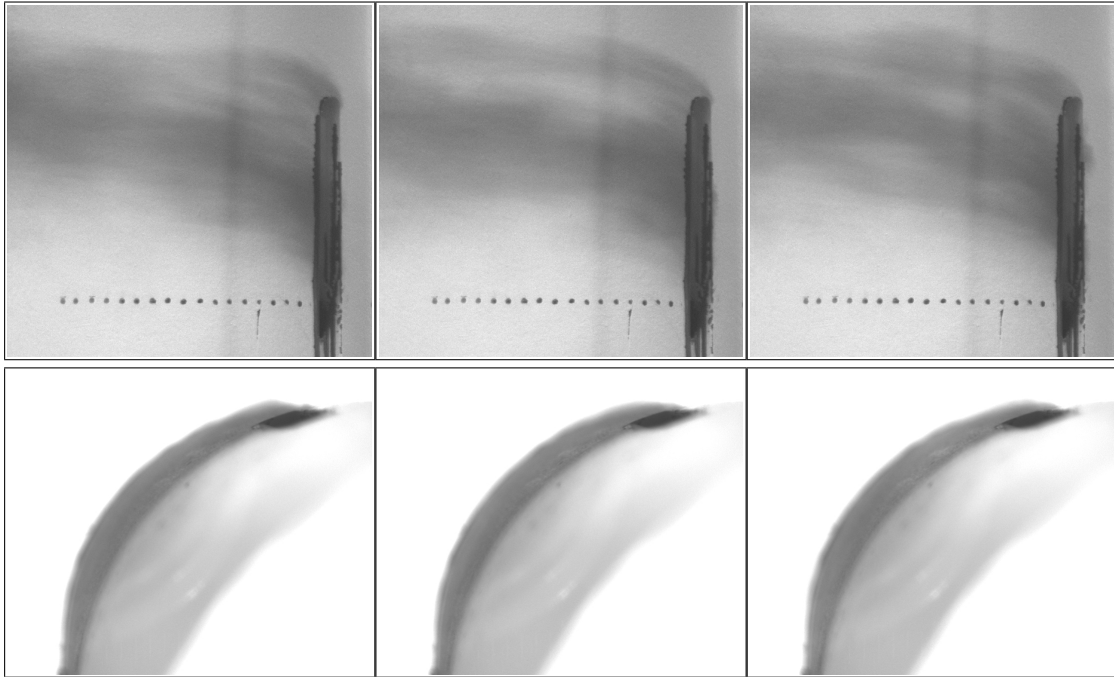Figure 114   Single-depth transverse trench - $M = 1.50$
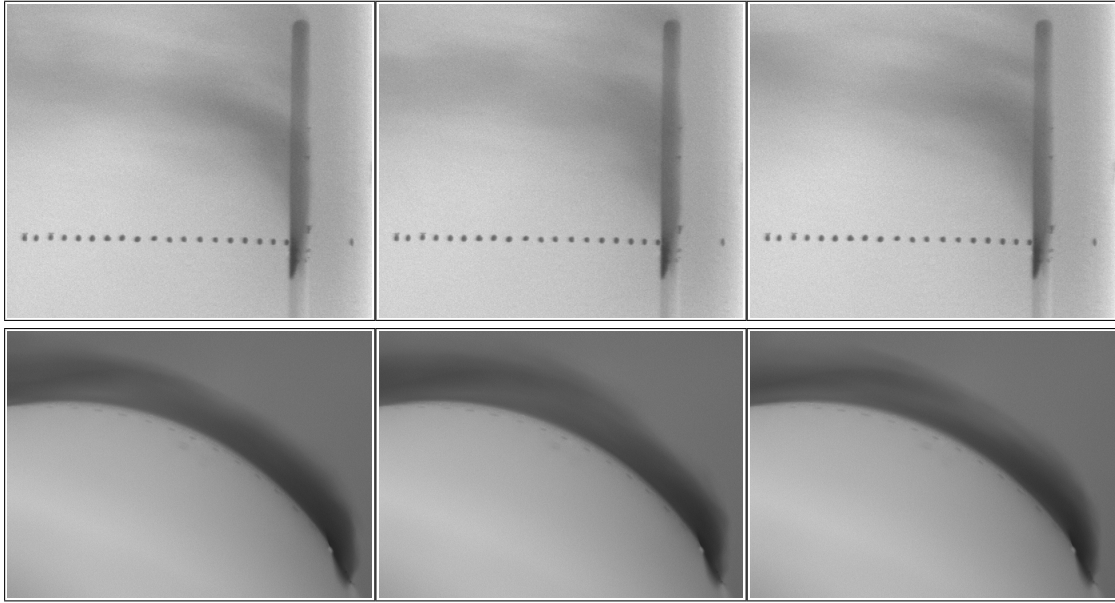
Figure 115   Single-depth transverse trench - $M = 1.75$
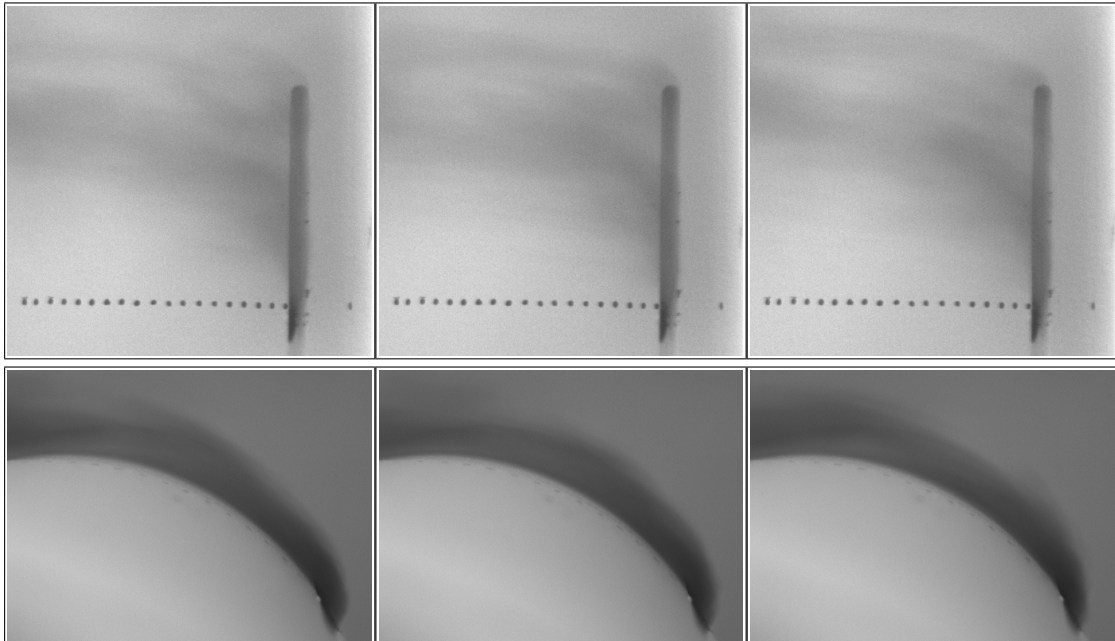
Figure 116   Single-depth transverse trench - $M = 2.00$
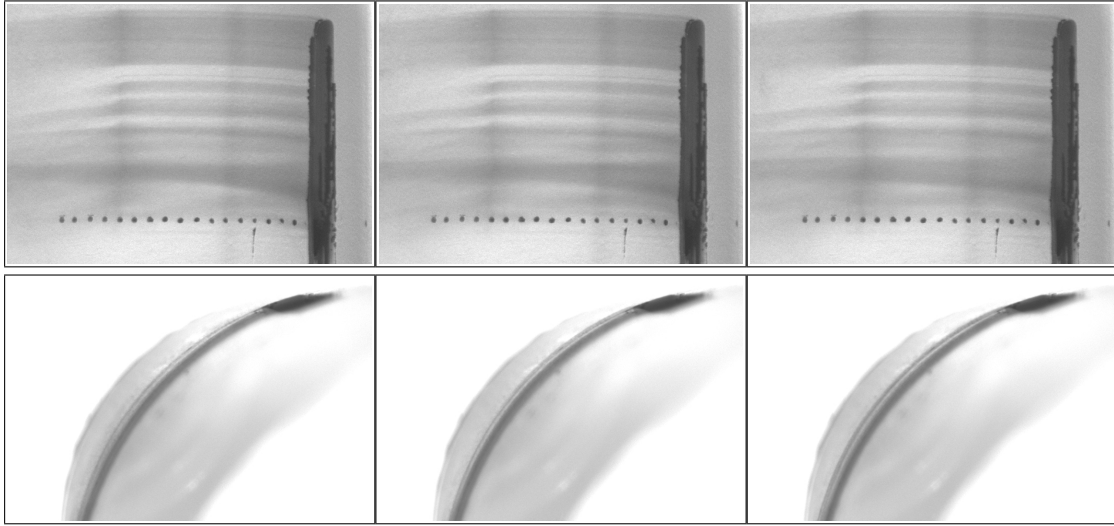
Figure 117   Filleted single-depth transverse trench - $M = 0.25$
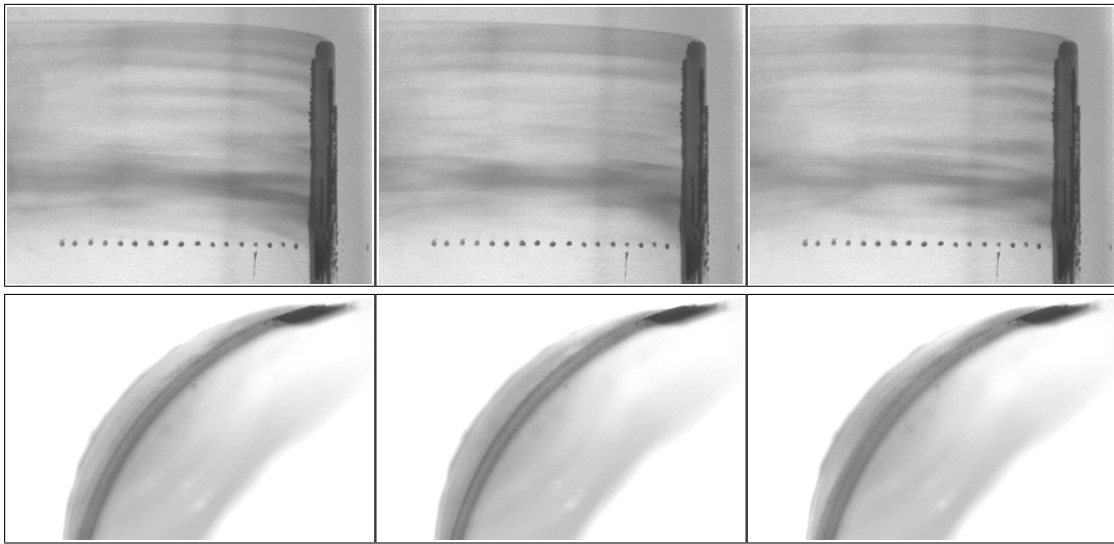
Figure 118   Filleted single-depth transverse trench - $M = 0.50$
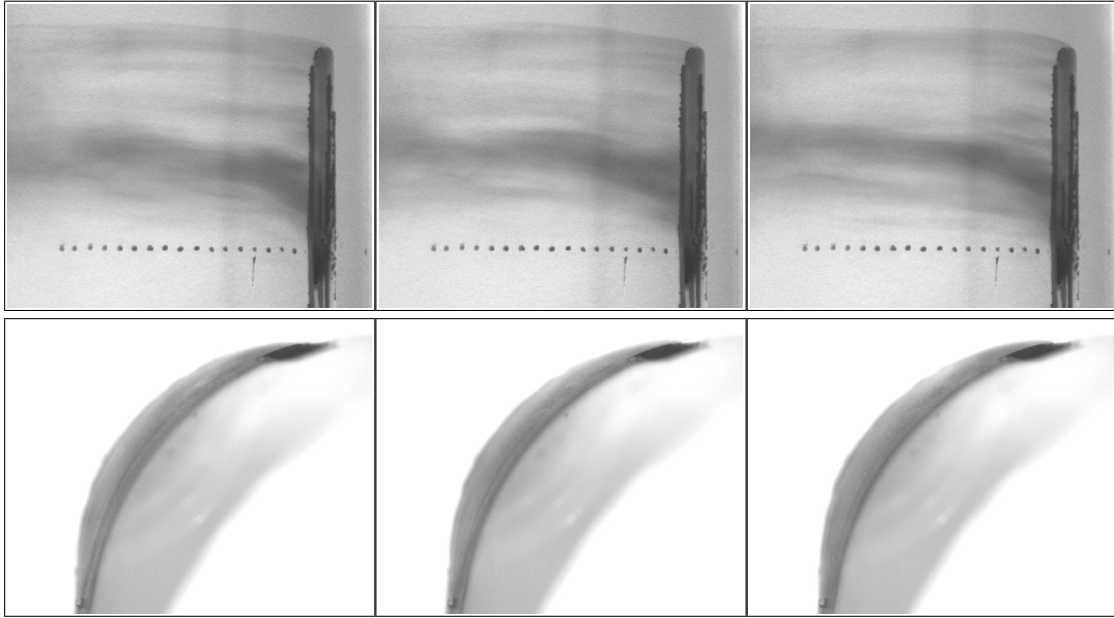
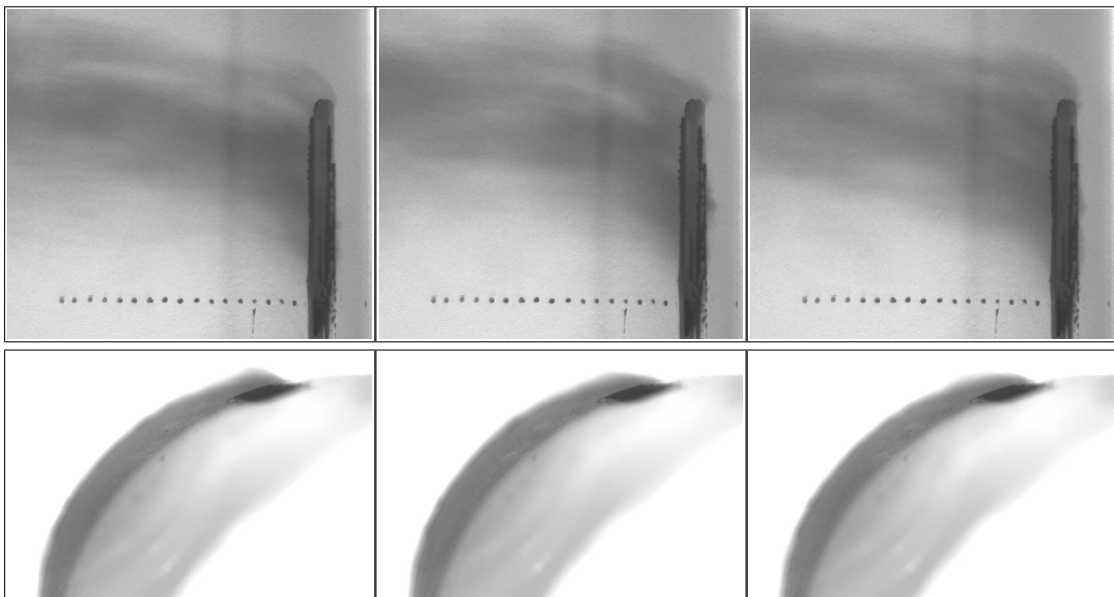Figure 119   Filleted single-depth transverse trench - $M = 0.75$
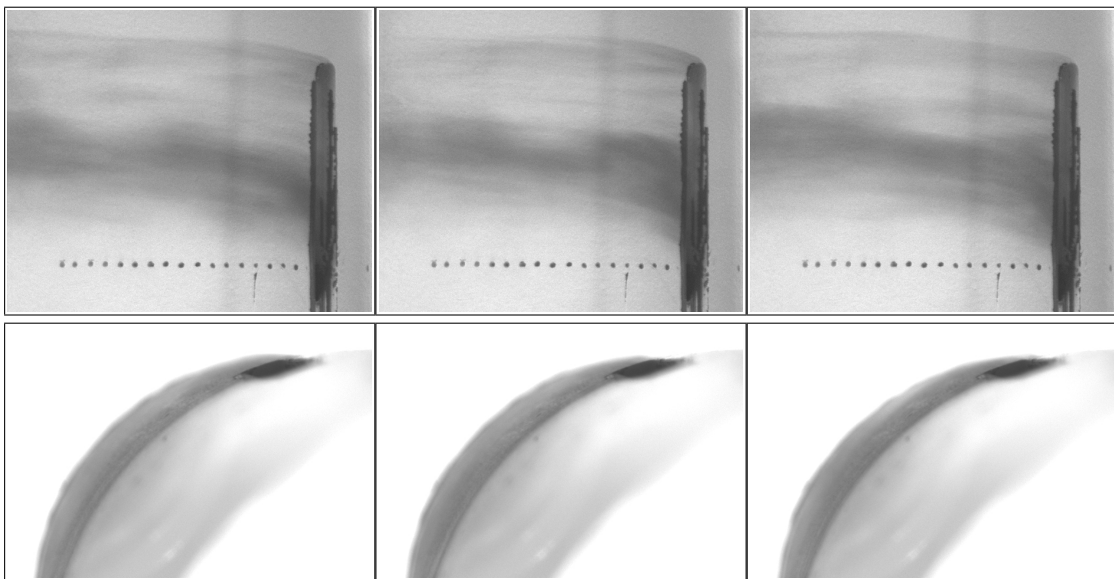
Figure 120   Filleted single-depth transverse trench - $M = 1.00$

Figure 121   Filleted single-depth transverse trench - $M = 1.25$

Figure 122   Filleted single-depth transverse trench - $M = 1.50$

Figure 123   Filleted single-depth transverse trench - $M = 1.75$

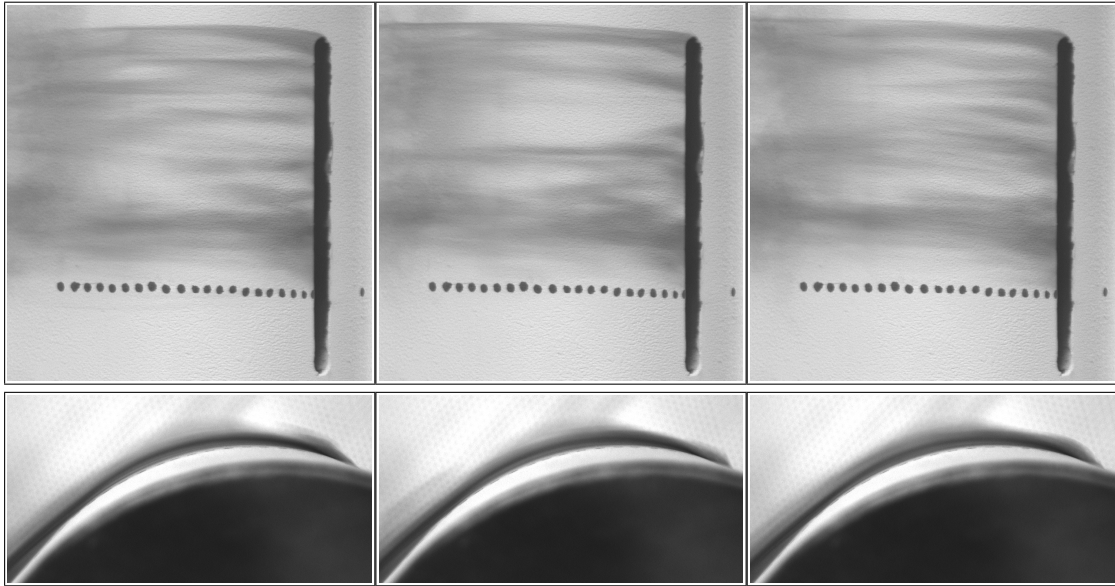Figure 124   Filleted single-depth transverse trench - $M = 2.00$
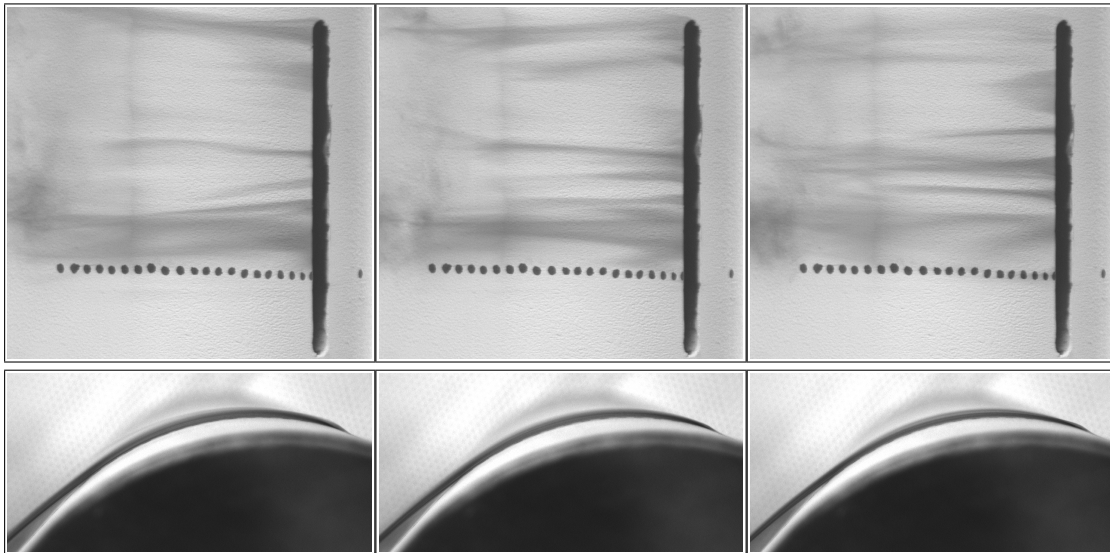
Figure 125   Tapered-depth transverse trench - $M = 0.25$
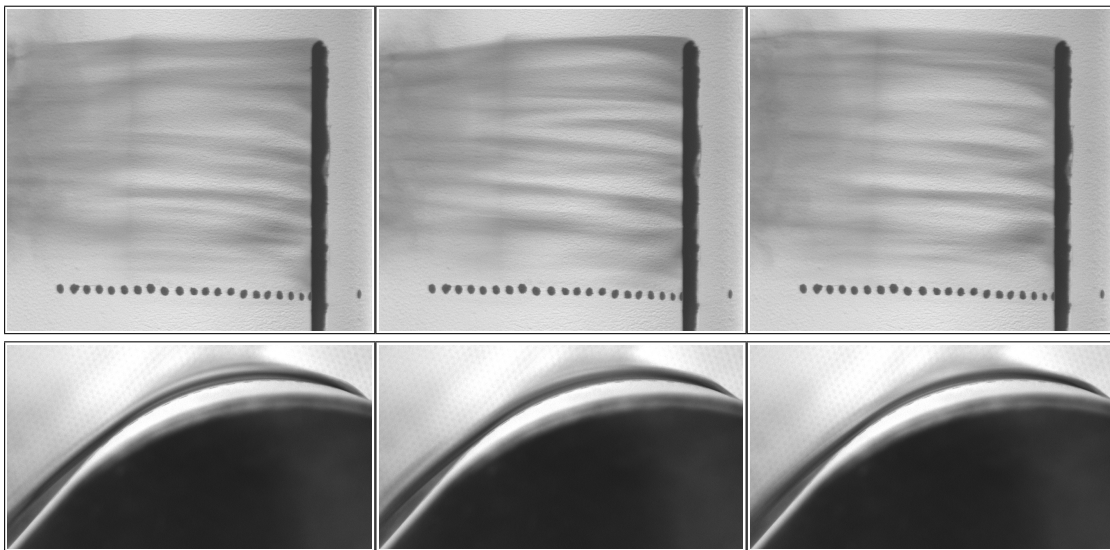
Figure 126   Tapered-depth transverse trench - $M = 0.50$

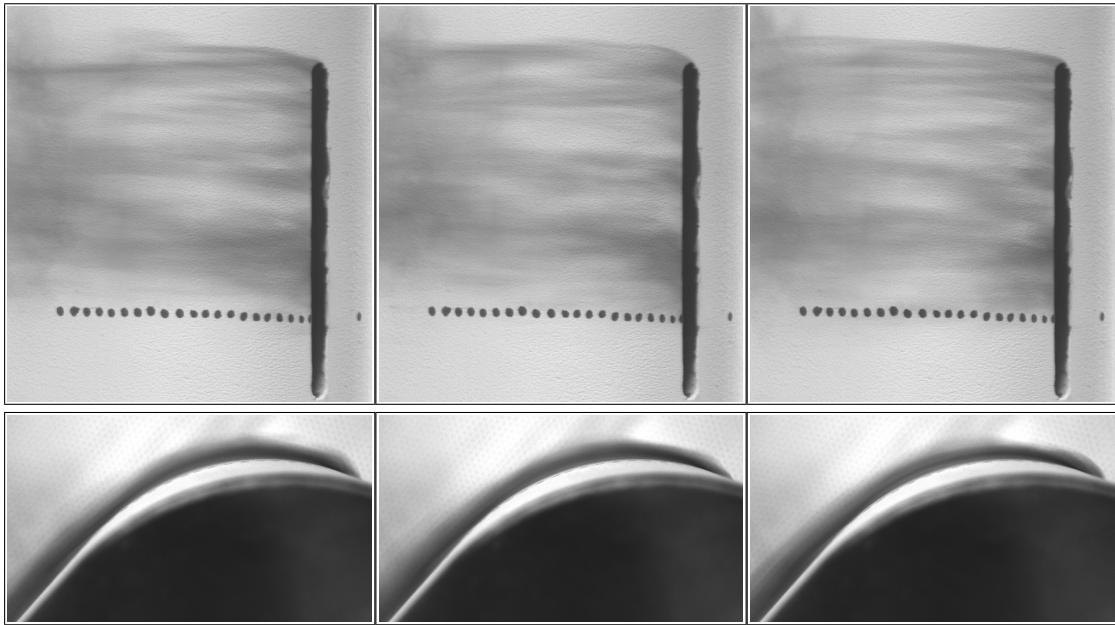Figure 127   Tapered-depth transverse trench - $M = 0.75$

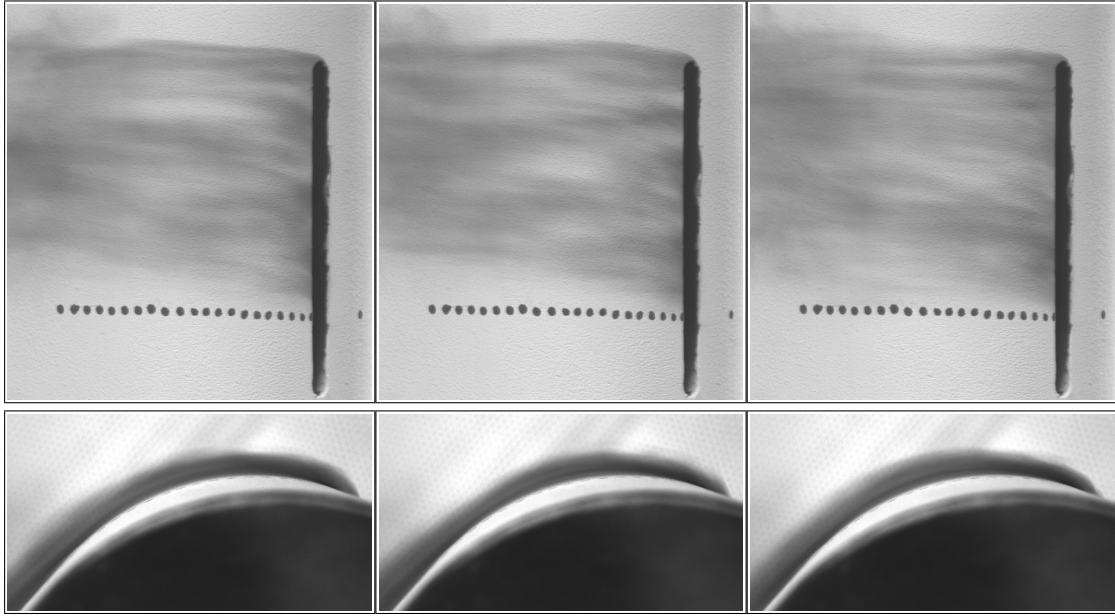Figure 128   Tapered-depth transverse trench - $M = 1.00$

Figure 129   Tapered-depth transverse trench - $M = 1.25$
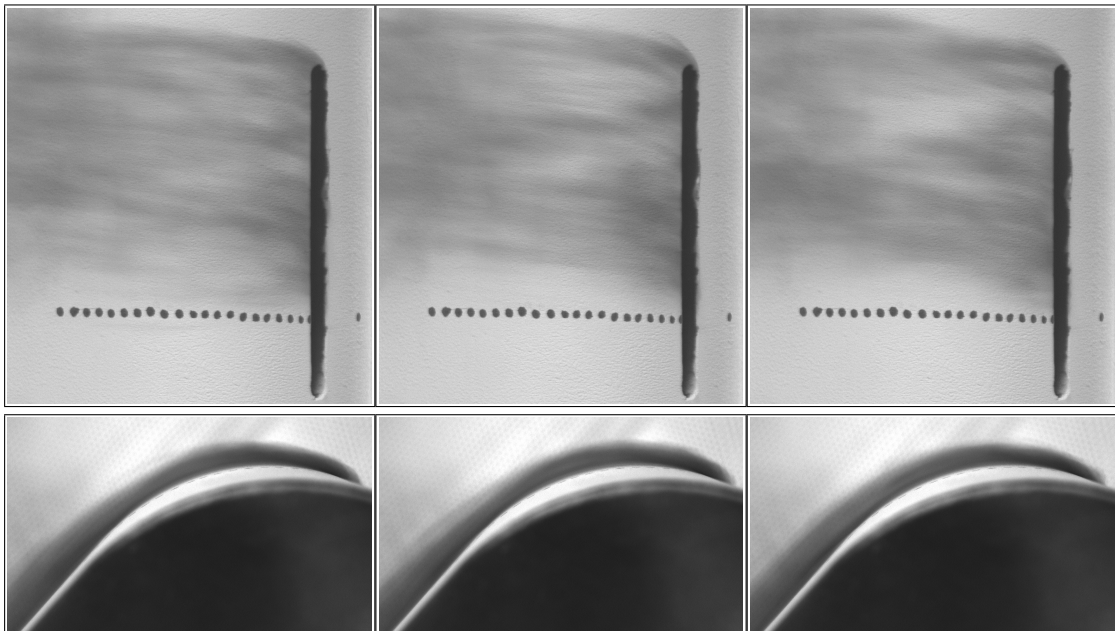

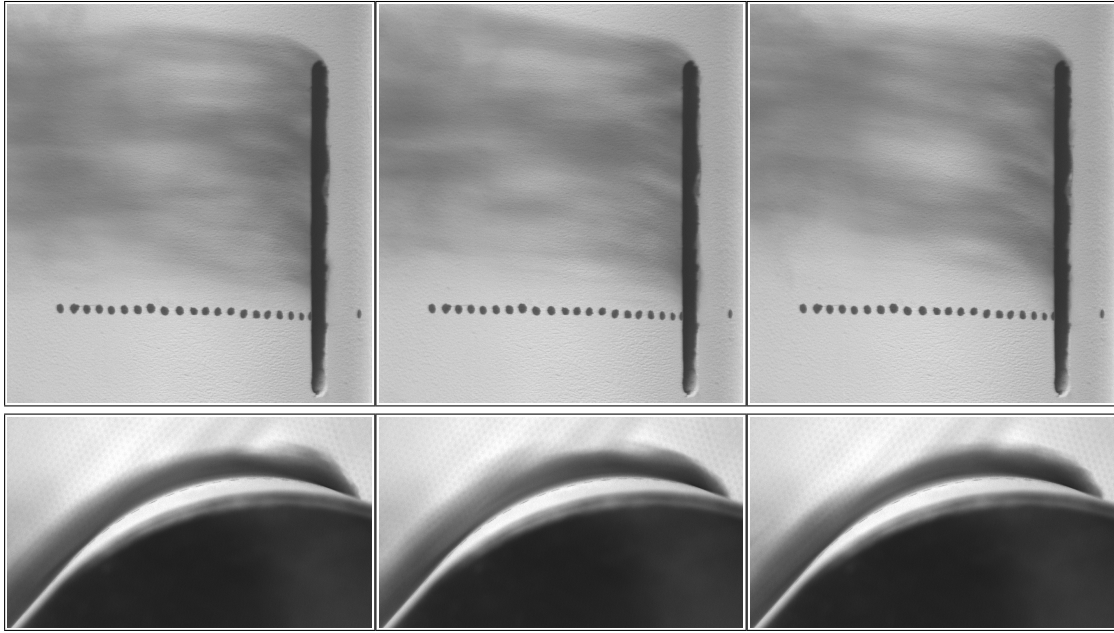Figure 130   Tapered-depth transverse trench - $M = 1.50$

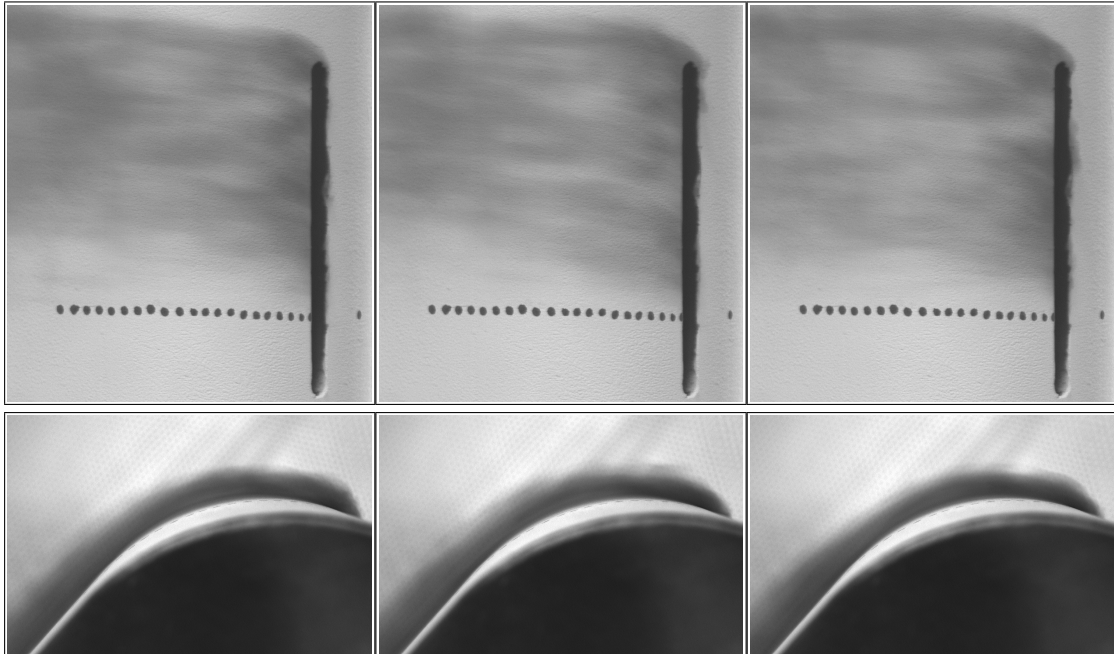Figure 131   Tapered-depth transverse trench - $M = 1.75$

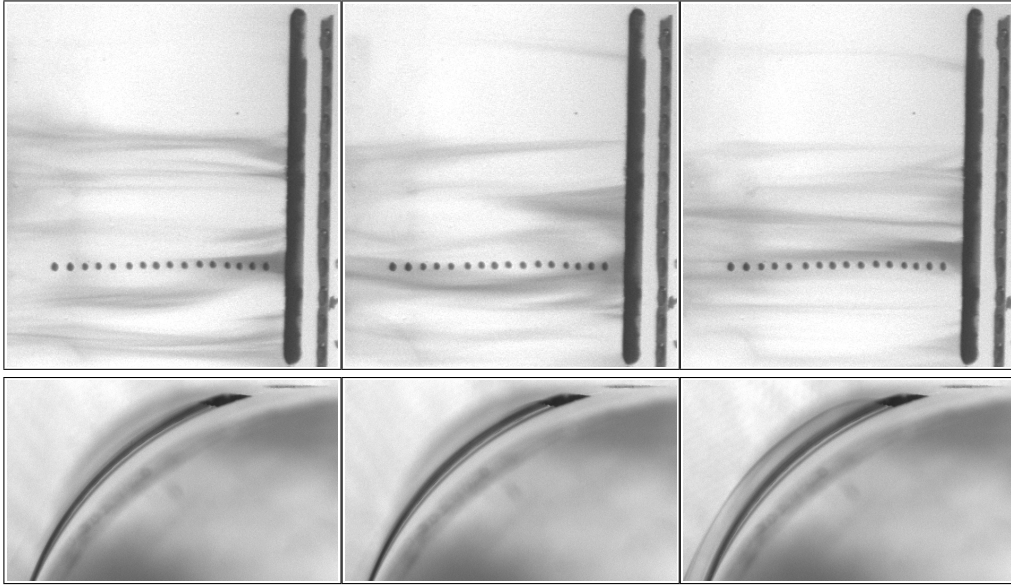Figure 132   Tapered-depth transverse trench - $M = 2.00$

Figure 133   Dimpled tapered-depth transverse trench - $M = 0.25$

Figure 134   Dimpled tapered-depth transverse trench - $M = 0.50$

Figure 135   Dimpled tapered-depth transverse trench - $M = 0.75$

Figure 136   Dimpled tapered-depth transverse trench - $M = 1.00$

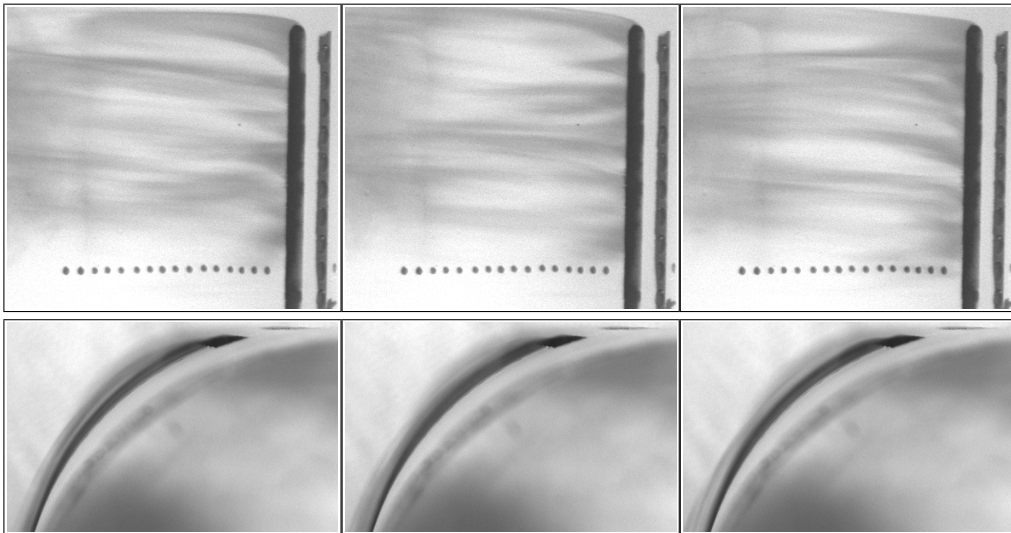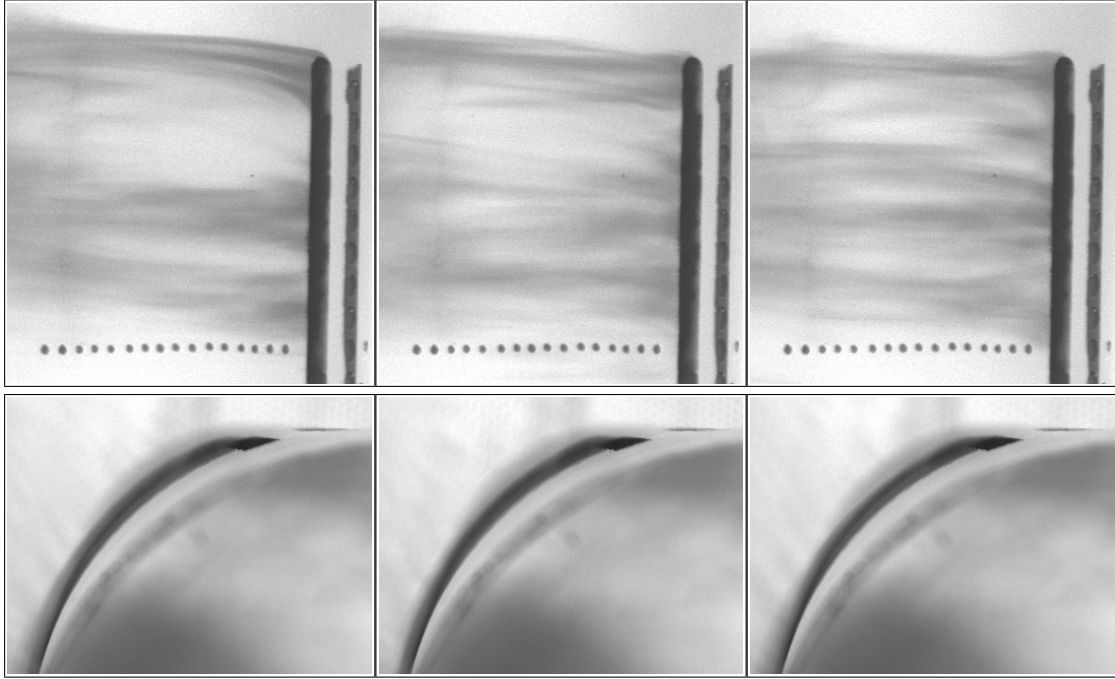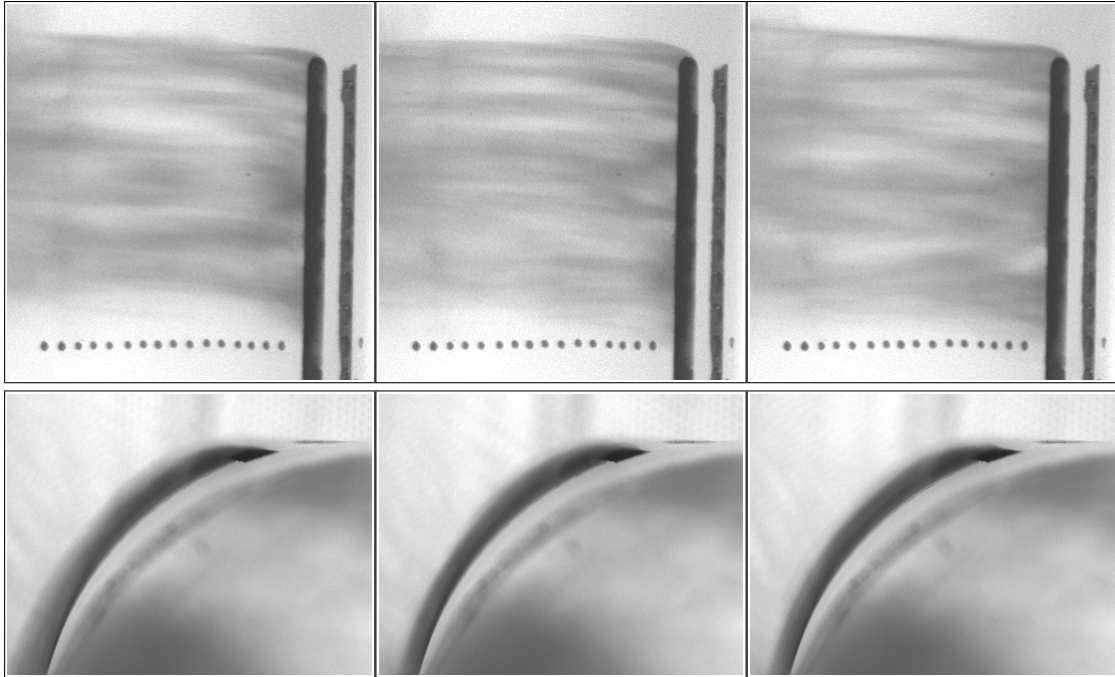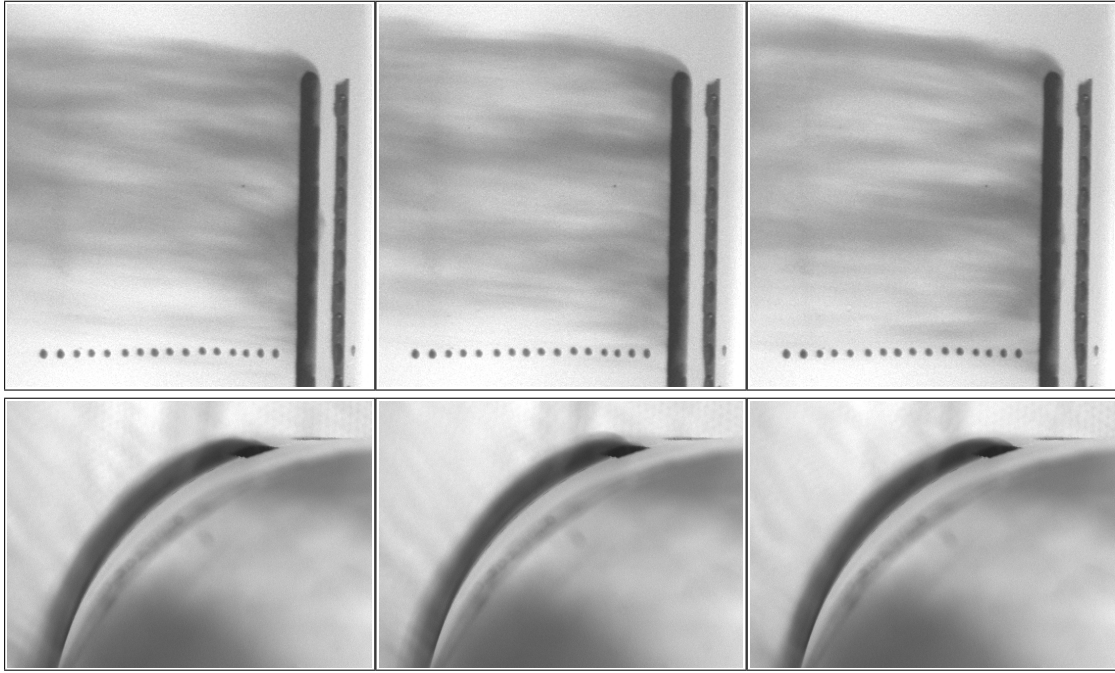Figure 137   Dimpled tapered-depth transverse trench - $M = 1.25$

Figure 138   Dimpled tapered-depth transverse trench - $M = 1.50$

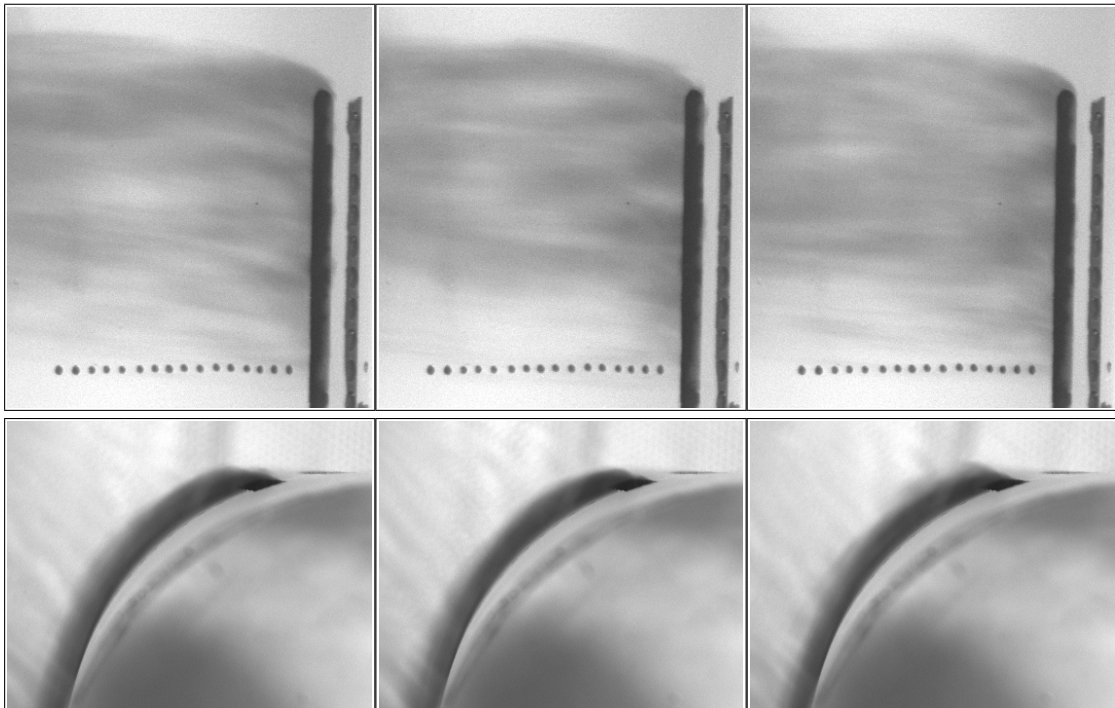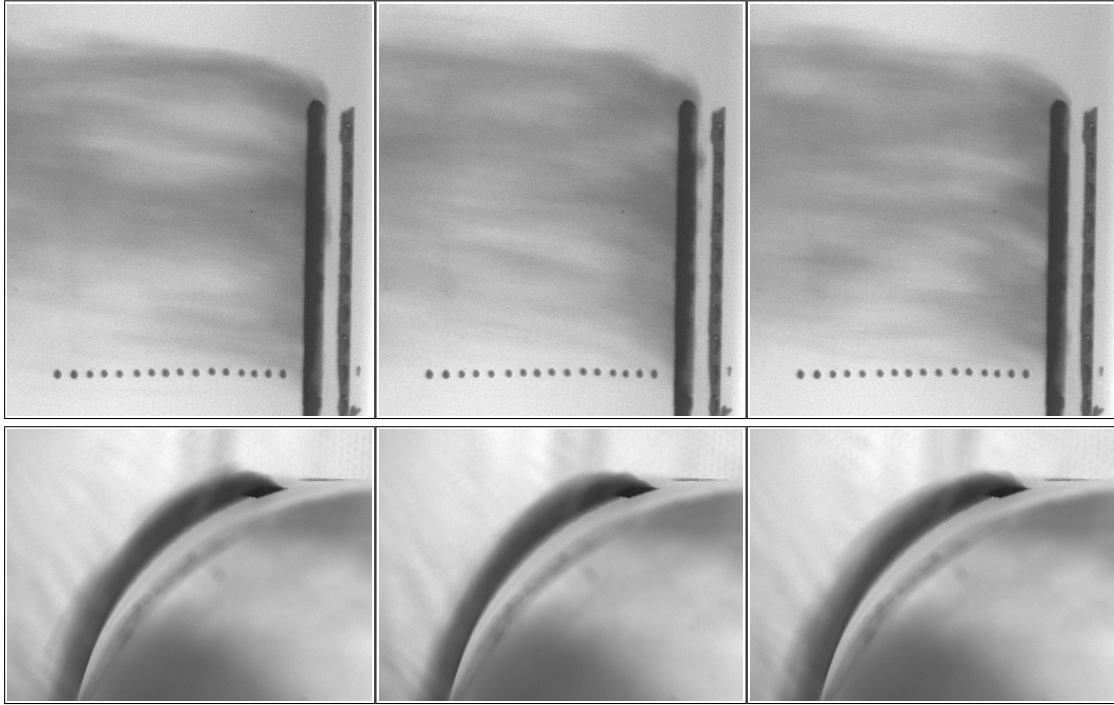Figure 139   Dimpled tapered-depth transverse trench - $M = 1.75$

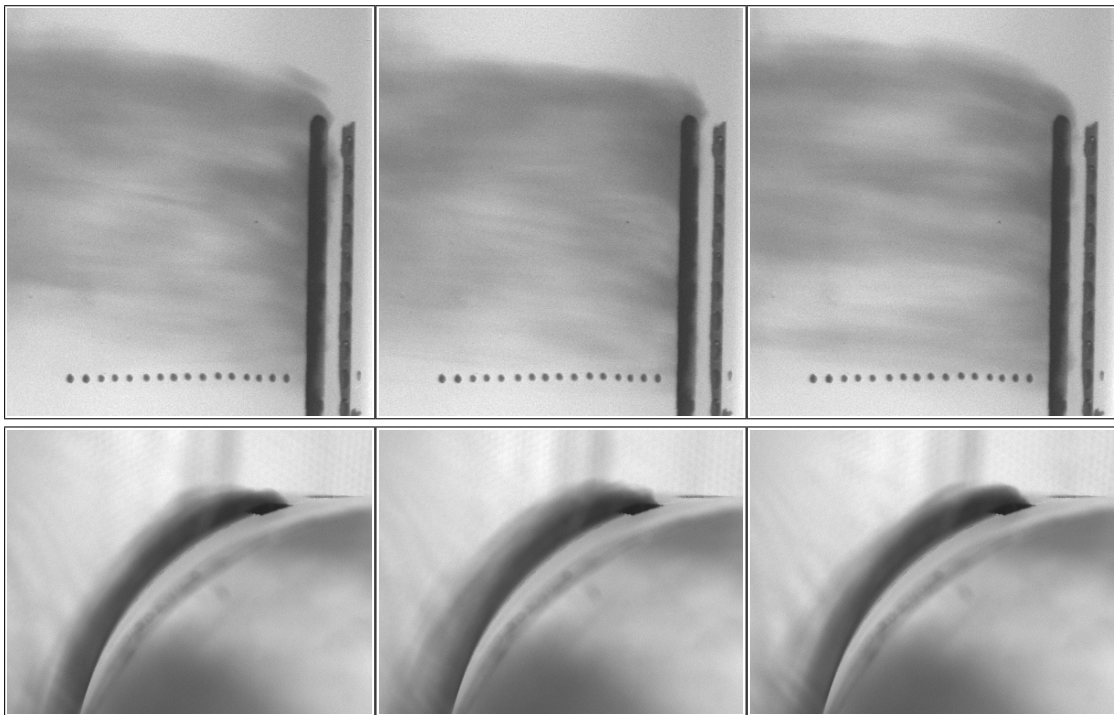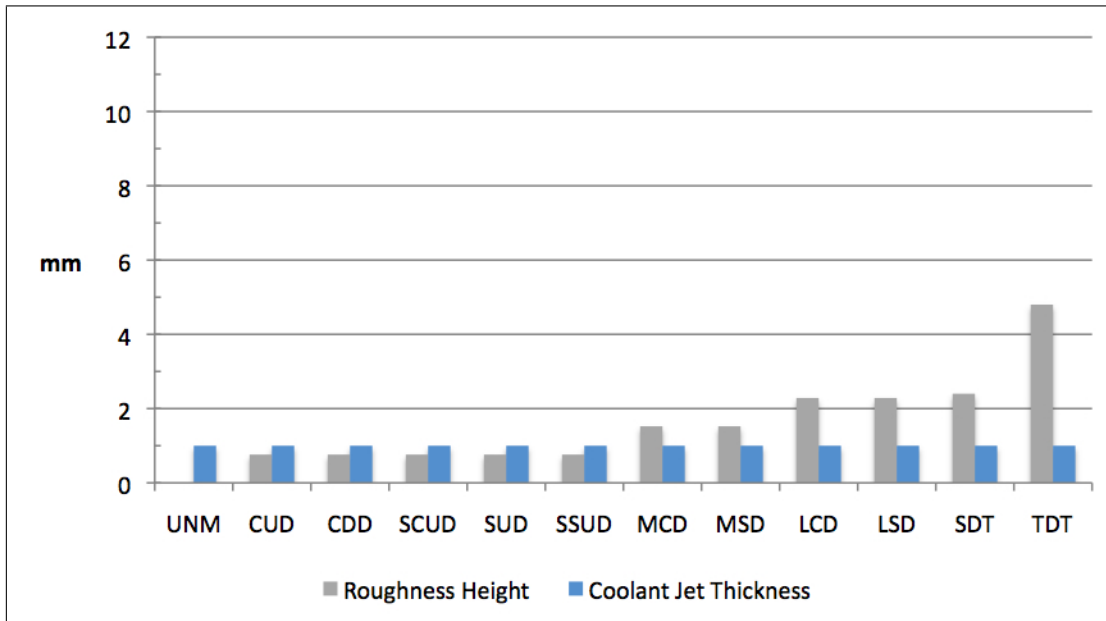Figure 140   Dimpled tapered-depth transverse trench - $M = 2.00$

Figure 141   Comparison of coolant jet thickness at $M = 0.25$.
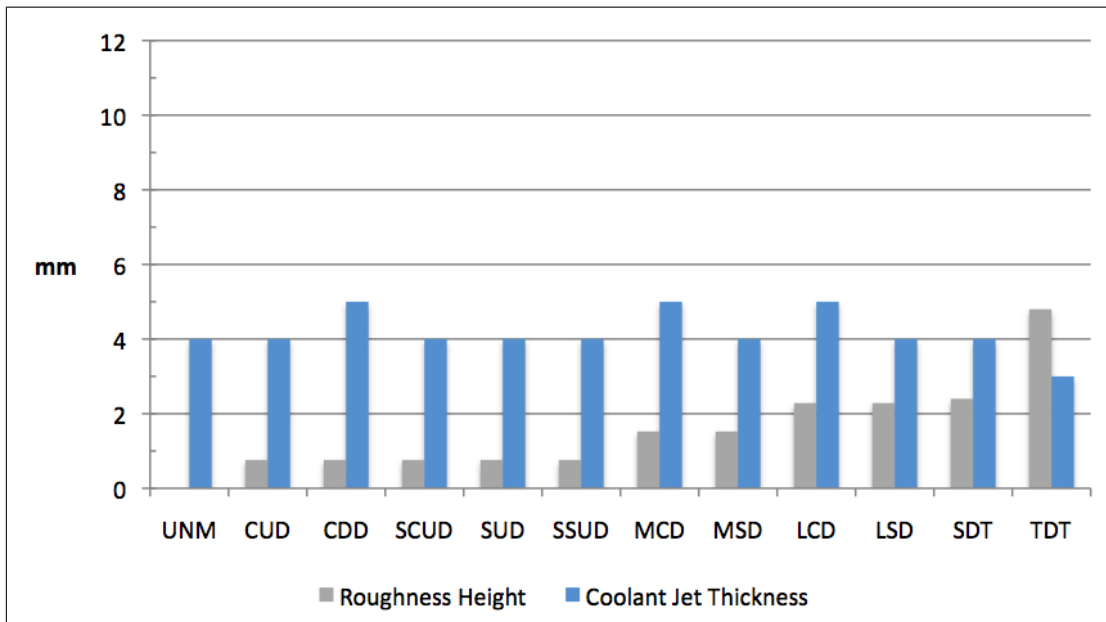

Figure 142   Comparison of coolant jet thickness at $M = 0.75$.
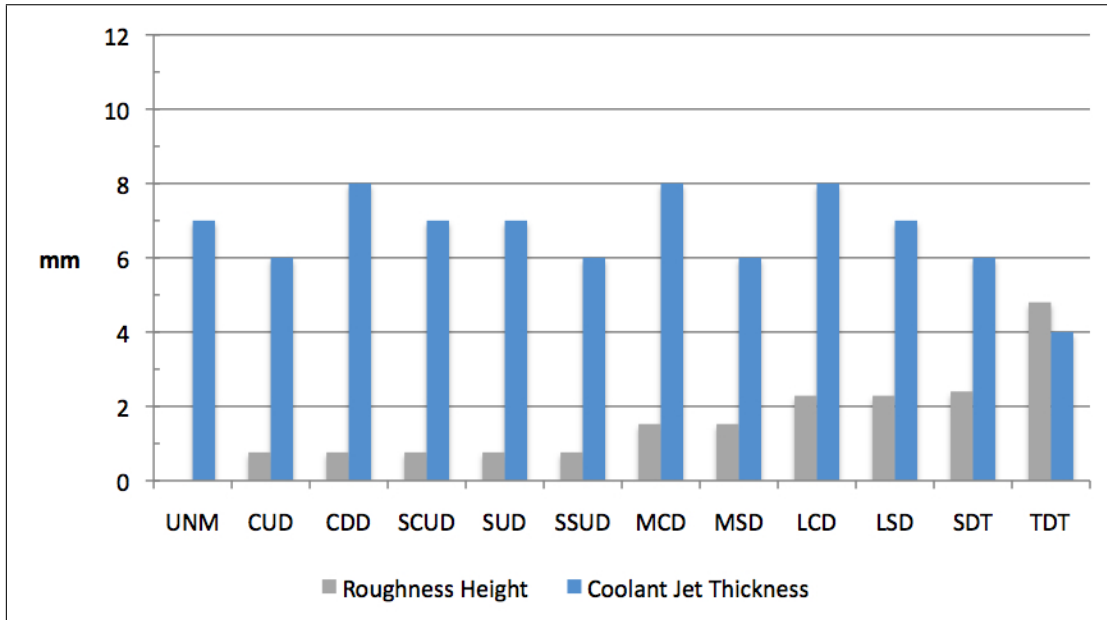
Figure 143   Comparison of coolant jet thickness at $M = 1.25$.
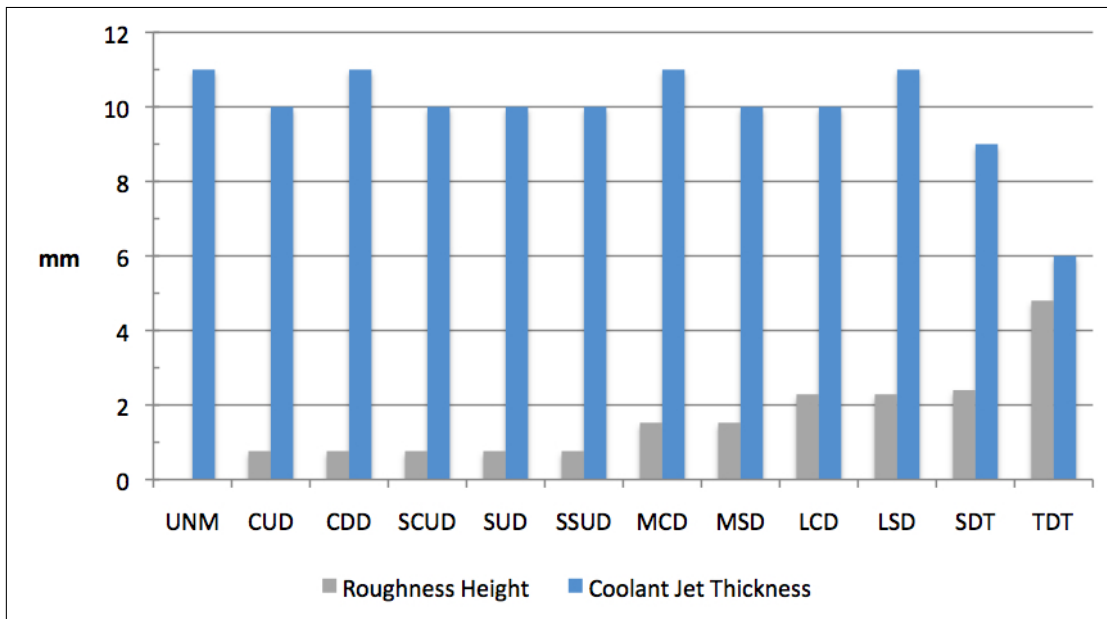
Figure 144   Comparison of coolant jet thickness at $M = 2.00$.

Model Schematics and Pictures

The specific geometries pictured in the *Water Channel Flow Visualization Data* section (pg. 28) do not appear the same as those presented here, since after initial machining the gray models were painted white for better contrast. Each geometry was masked to prevent the white paint from settling in the dimples/trenches and changing the specifications of the geometry. After testing was completed, each geometry was touched-up with white paint in order to provide more distinguishable pictures for this section. This issue would have been prevented by painting the gray PVC models white prior to machining.

Figure 145   Views of the leading edge template used for water channel testing. Up to four coolant holes were placed on each template, each being fed by an independent plenum.
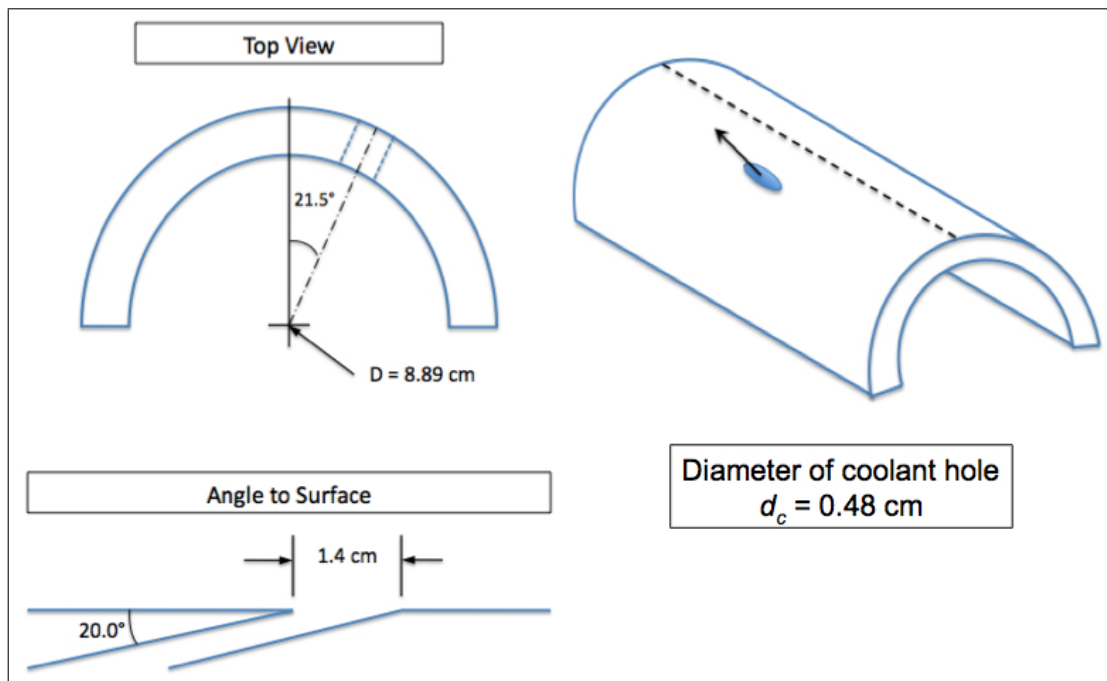
Figure 146   Coolant hole geometry. Coolant holes were drilled 21.5° off stagnation, angled at 20° to the surface, providing a coolant hole length of $11.64d_c$.
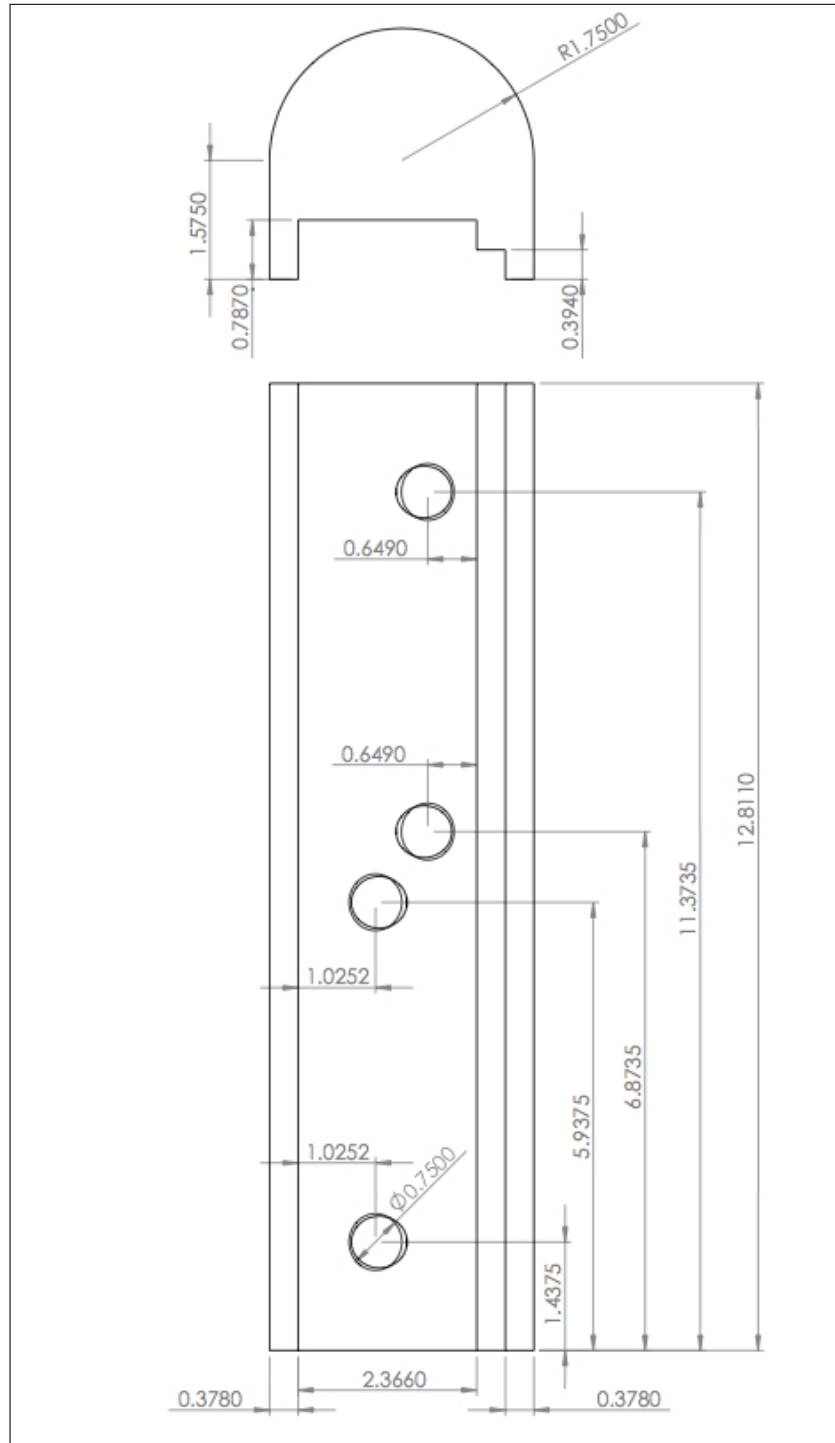
Figure 147   Dimensions shown for top and rear view of the leading edge model. Dimensions are in inches. The coolant hole plenums were milled on a 21.5° angle to the rear surface and threaded for 0.75" Swagelock connectors. Looking at the rear view, coolant flow is into the page.
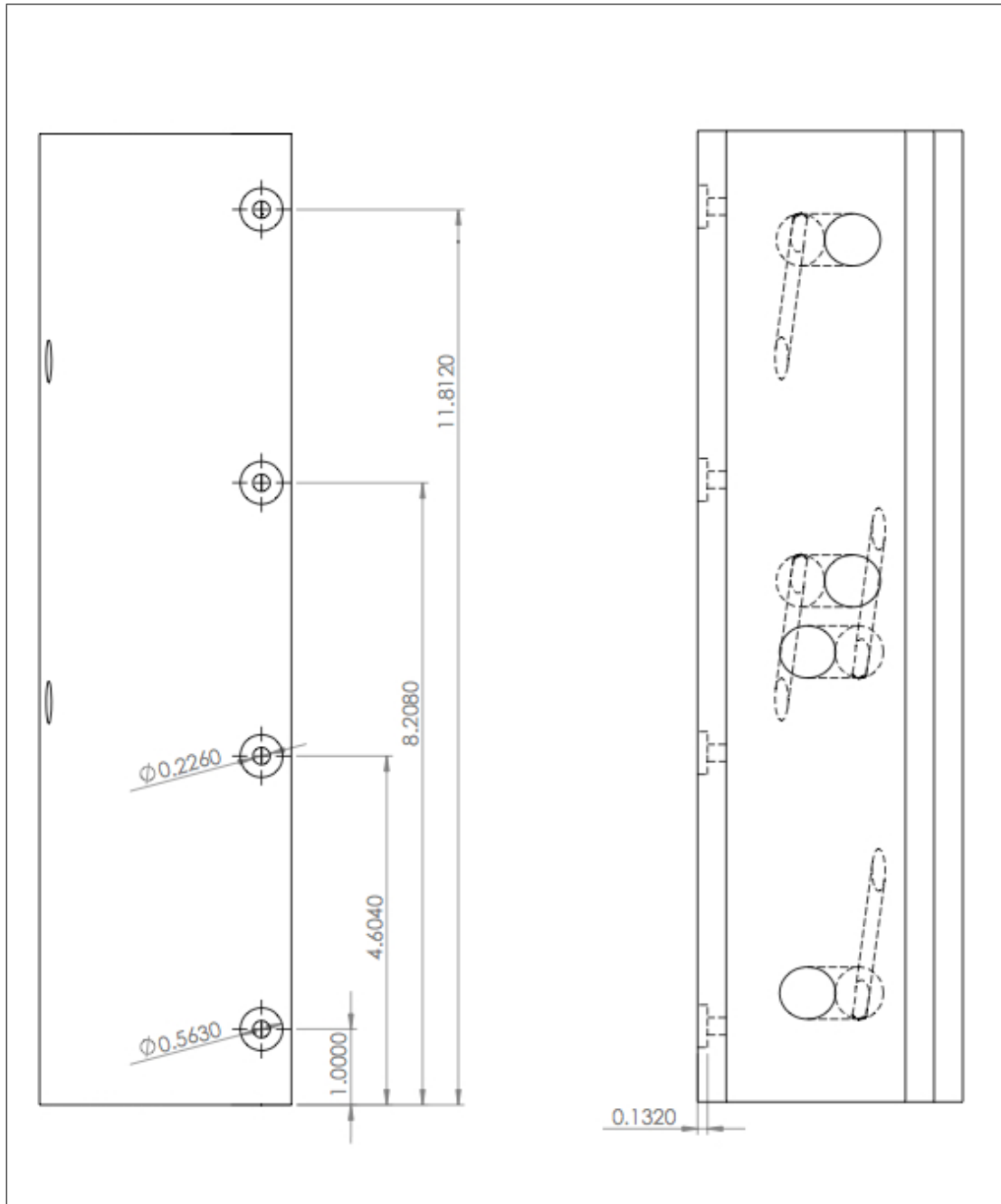
Figure 148   Dimensions shown for countersunk holes used to attach model to plexiglass flat afterbody. Dimensions are in inches. The view on the right shows the back of the model with the coolant holes terminating in their respective plenums.
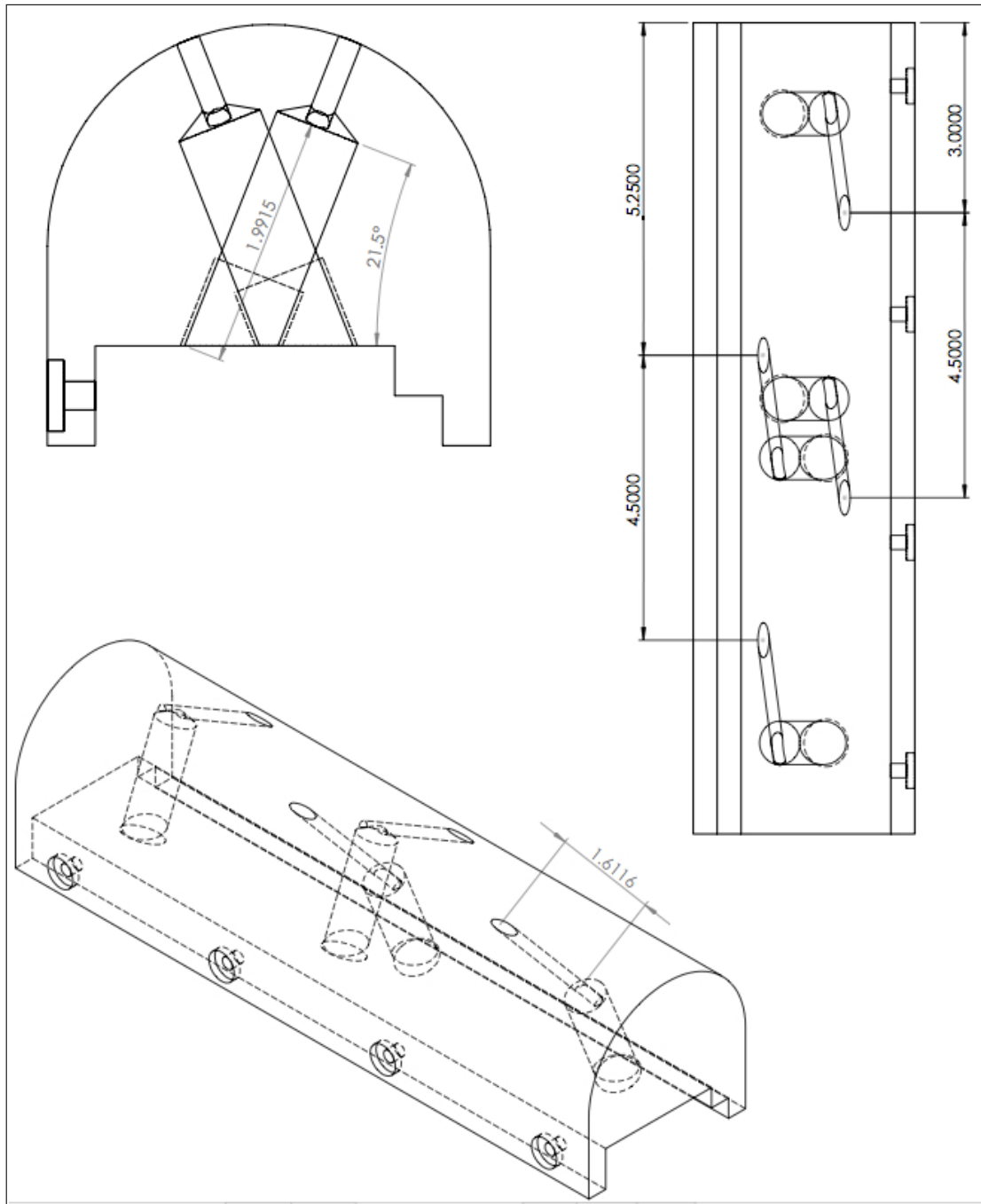
Figure 149   Dimensions shown for coolant holes and plenums. Dimensions are in inches. Upper left view looks down on the top of the model. The view on the right looks at the model from the front, showing the location of the coolant holes. The coolant holes were drilled on a compound angle. The upper left view shows their location at 21.5° off the model's centerline, and the bottom view illustrates their 20° angle to the surface.

105

Figure 150   Dimensions for small cylindrical dimples upstream. Dimple depth-to-diameter ratio is 0.2 and pattern was centered vertically on the coolant hole. This geometry was originally a single row of dimples and, after testing, the second staggered row was added and it was tested again.

Figure 151   Dimensions for small cylindrical dimples downstream. Dimple depth-to-diameter ratio is 0.2 and pattern was centered vertically on the coolant hole.

Figure 152   Dimensions for small spherical dimples upstream. Dimple depth-to-diameter ratio is 0.2 and pattern was centered vertically on the coolant hole. This geometry was originally a single row of dimples and, after testing, the second staggered row was added and it was tested again.
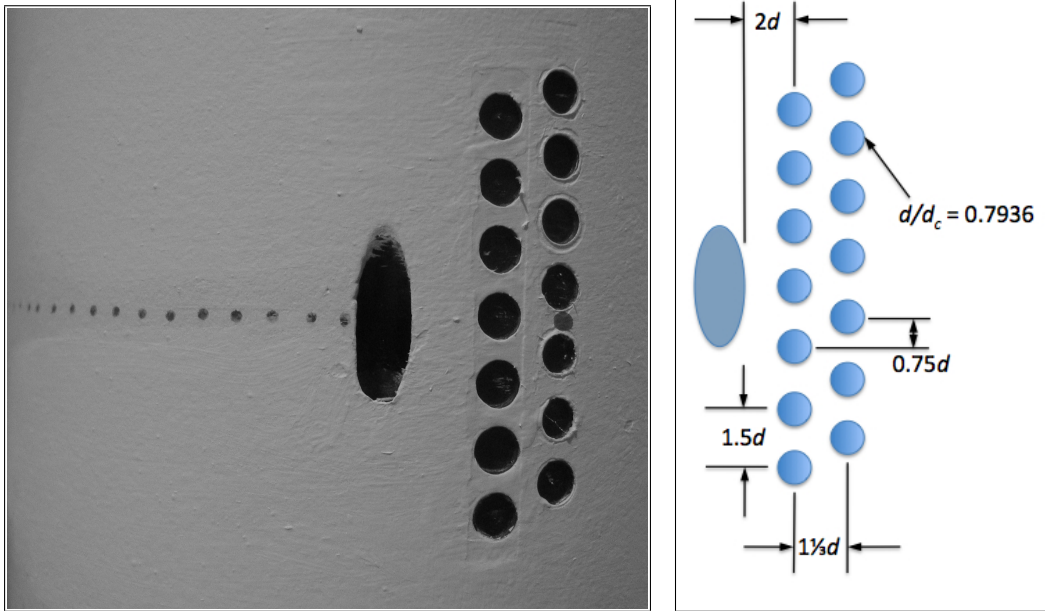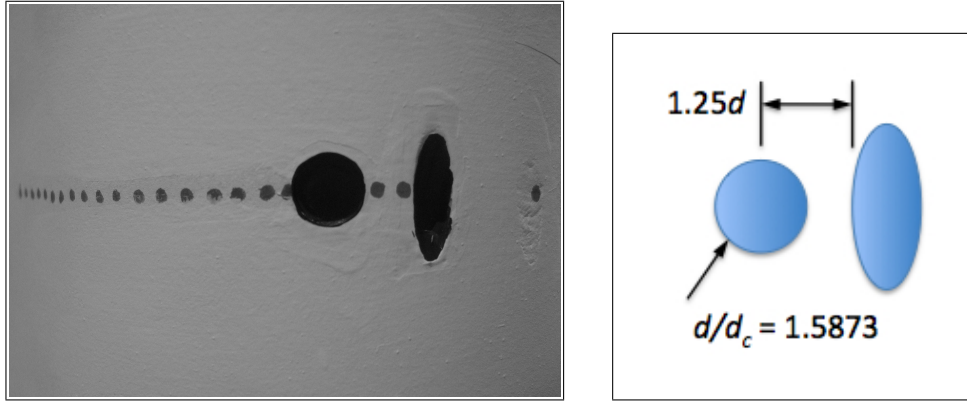
Figure 153   Dimensions for medium cylindrical dimple downstream of coolant hole. Dimple depth-to-diameter ratio is 0.2 and was centered vertically on the coolant hole.
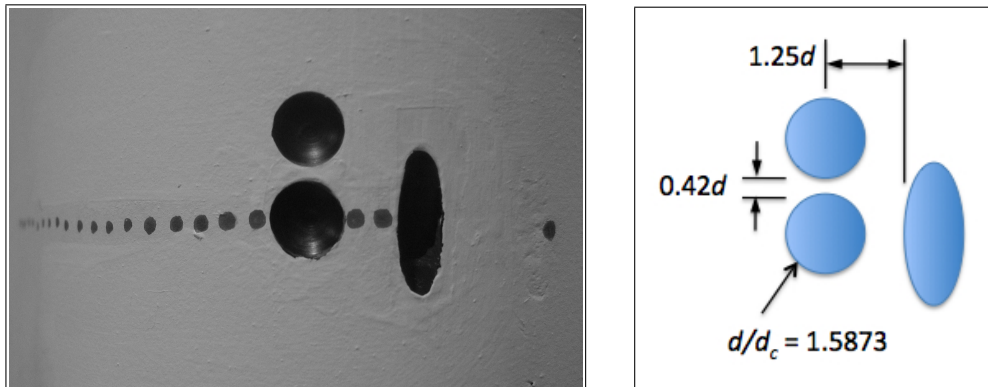
Figure 154   Dimensions for medium spherical dimples downstream of coolant hole. First, the single dimple centered on the coolant hole was tested, and then the second dimple above it was added and the geometry was retested. Dimple depth-to-diameter ratio is 0.2.
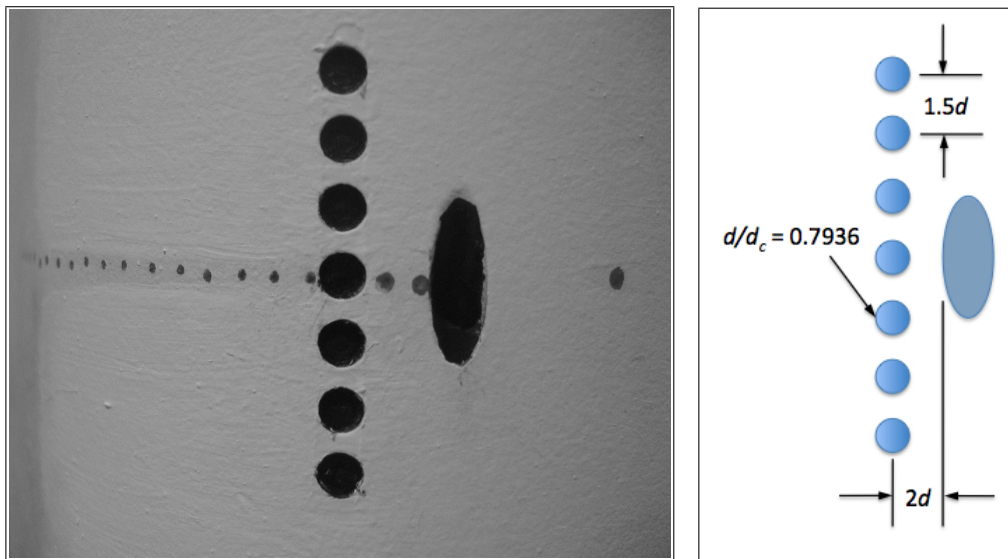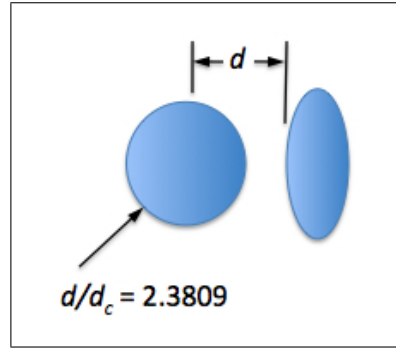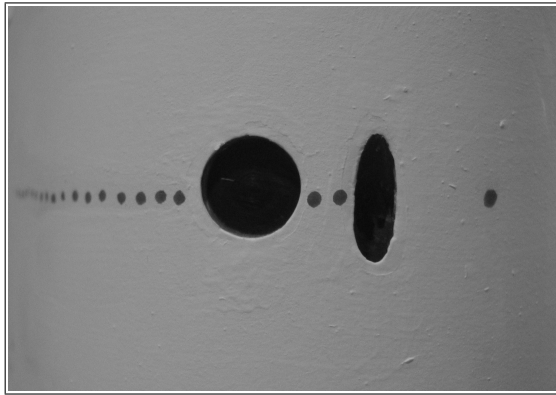
Figure 155   Dimensions for large cylindrical dimple downstream of coolant hole. Dimple depth-to-diameter ratio is 0.2 and was centered vertically on the coolant hole.
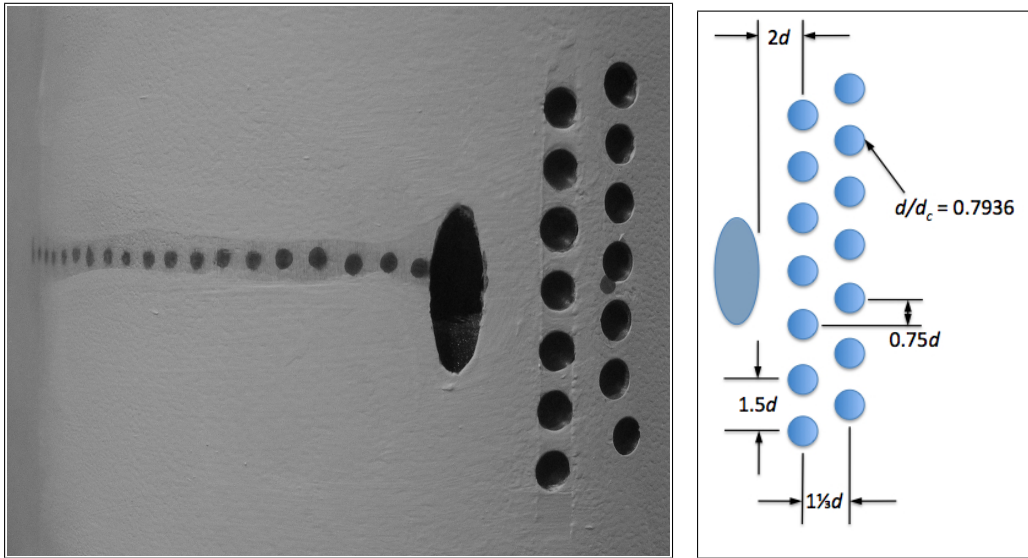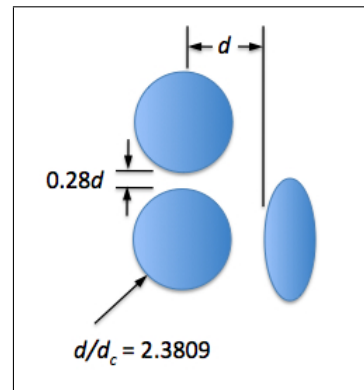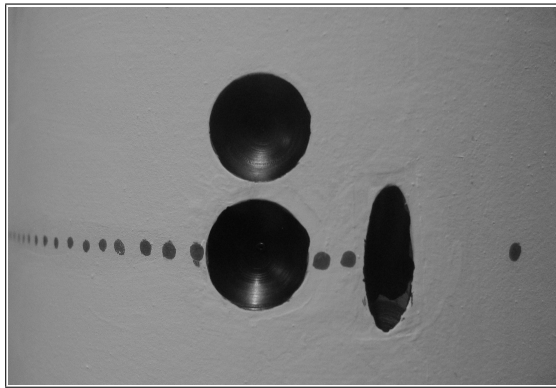

Figure 156   Dimensions for large spherical dimples downstream of coolant hole. First, the single dimple centered on the coolant hole was tested, and then the second dimple above it was added and the geometry was retested. Dimple depth-to-diameter ratio is 0.2.
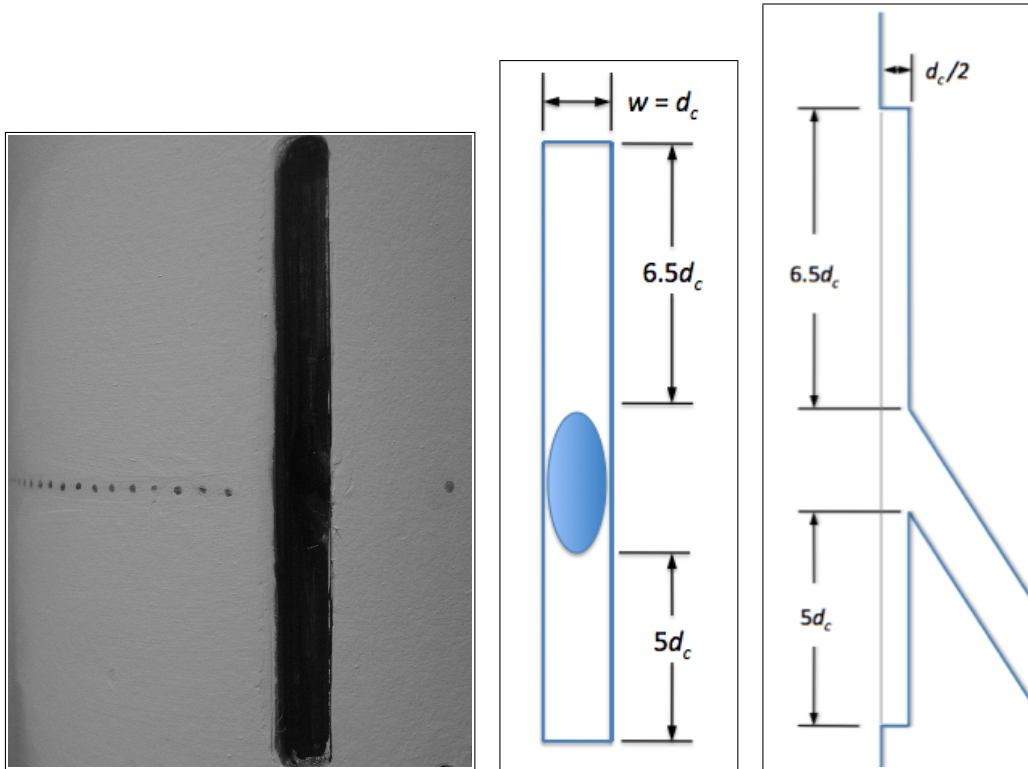
Figure 157   Dimensions for single-depth trench. This picture shows the trench after it was modified by placing a small fillet on the downstream lip. Image on right shows side view of trench illustrating the depth profile.
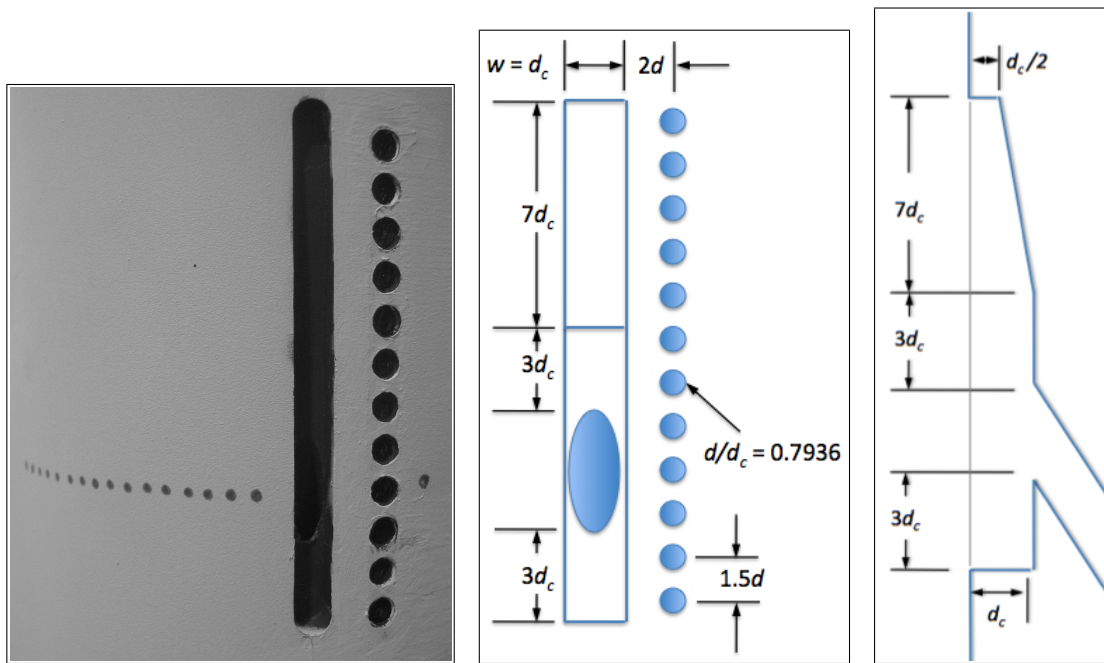
Figure 158   Dimensions for tapered-depth trench with small cylindrical dimples directly upstream. First the trench was tested without the dimples. When the dimples were added, the pattern was based off an initial dimple centered on the coolant hole. Image on right shows side view of trench illustrating the depth profile.

Figure 159   AFRL closed-loop water channel. Intake plenum on left, flow is from left to right. The test section is the straight, glass-walled section of the channel. Surface skimmer plates fore and aft of the test section (not visible) damp oscillations in the channel. Two honeycomb screens and three wire-mesh screens (not visible - located in the intake and return plenums) provide uniform flow throughout the test section.
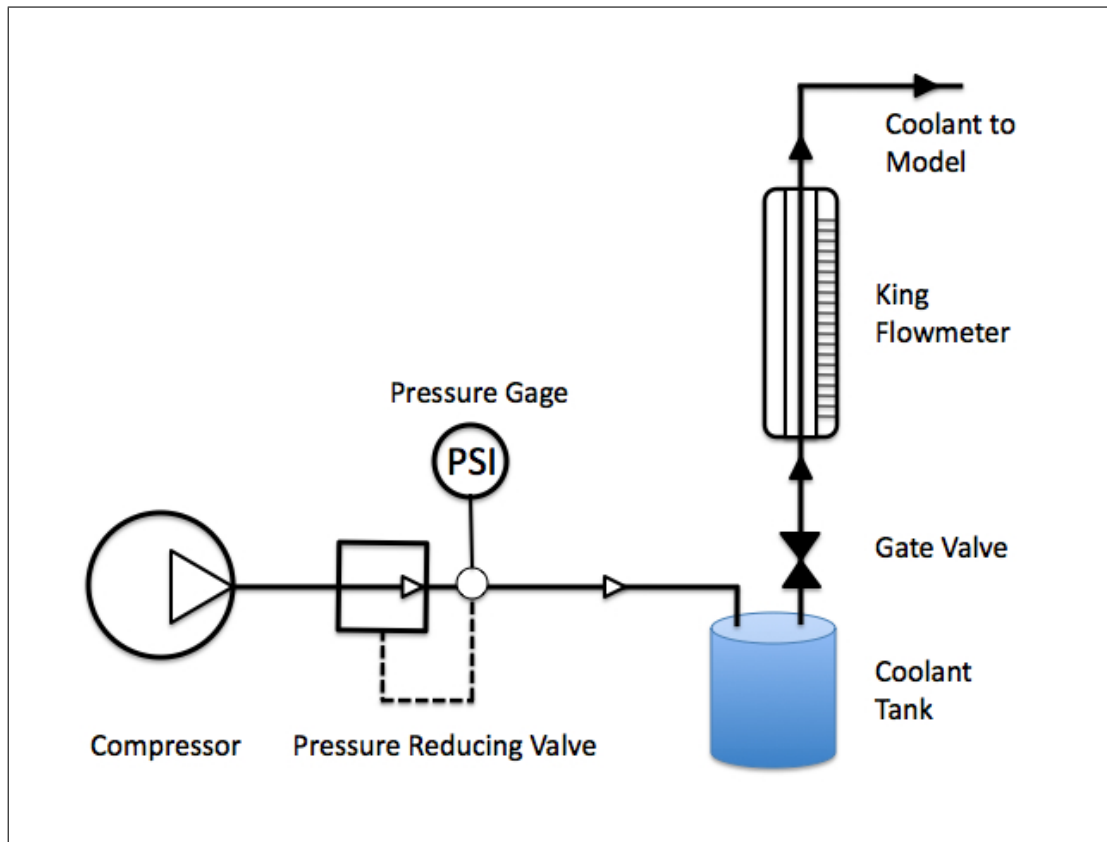
Figure 160   Schematic of the water channel setup. The coolant tank was pressurized by air at 206 kPa, and the float height in the flowmeter was manually controlled by a gate valve.
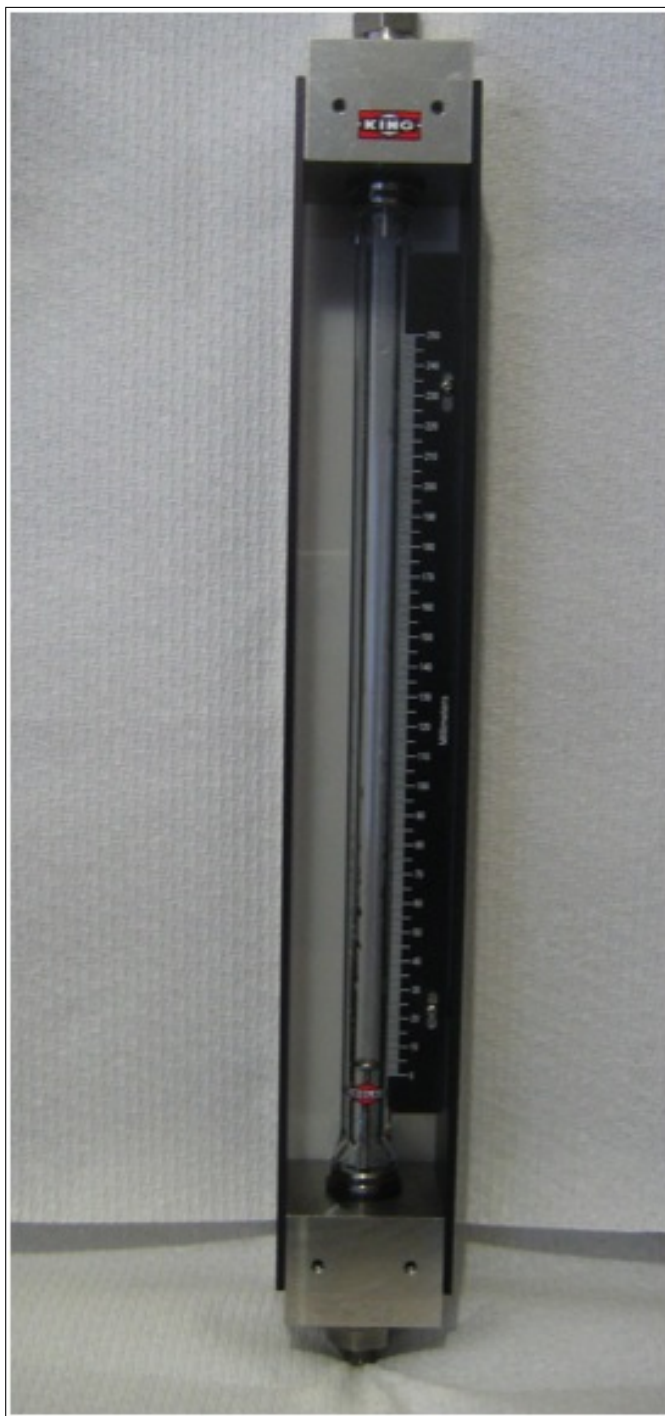
Figure 161   A King 7459-31W flowmeter was used with a 250 mm scale, maximum rated
flow rate of 0.83 Liters per minute.
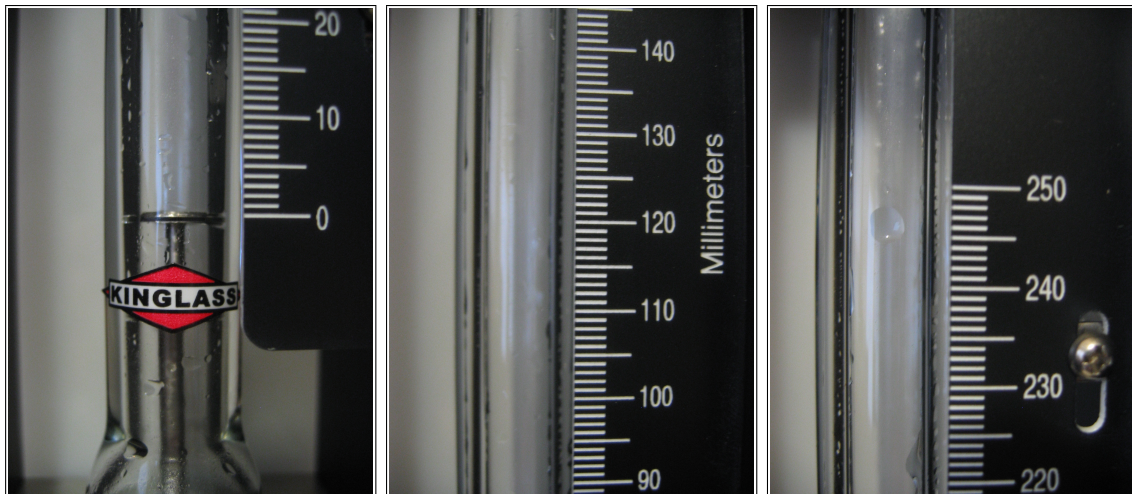
Figure 162   Close-up views of the King 7459-31W 250 mm scale.
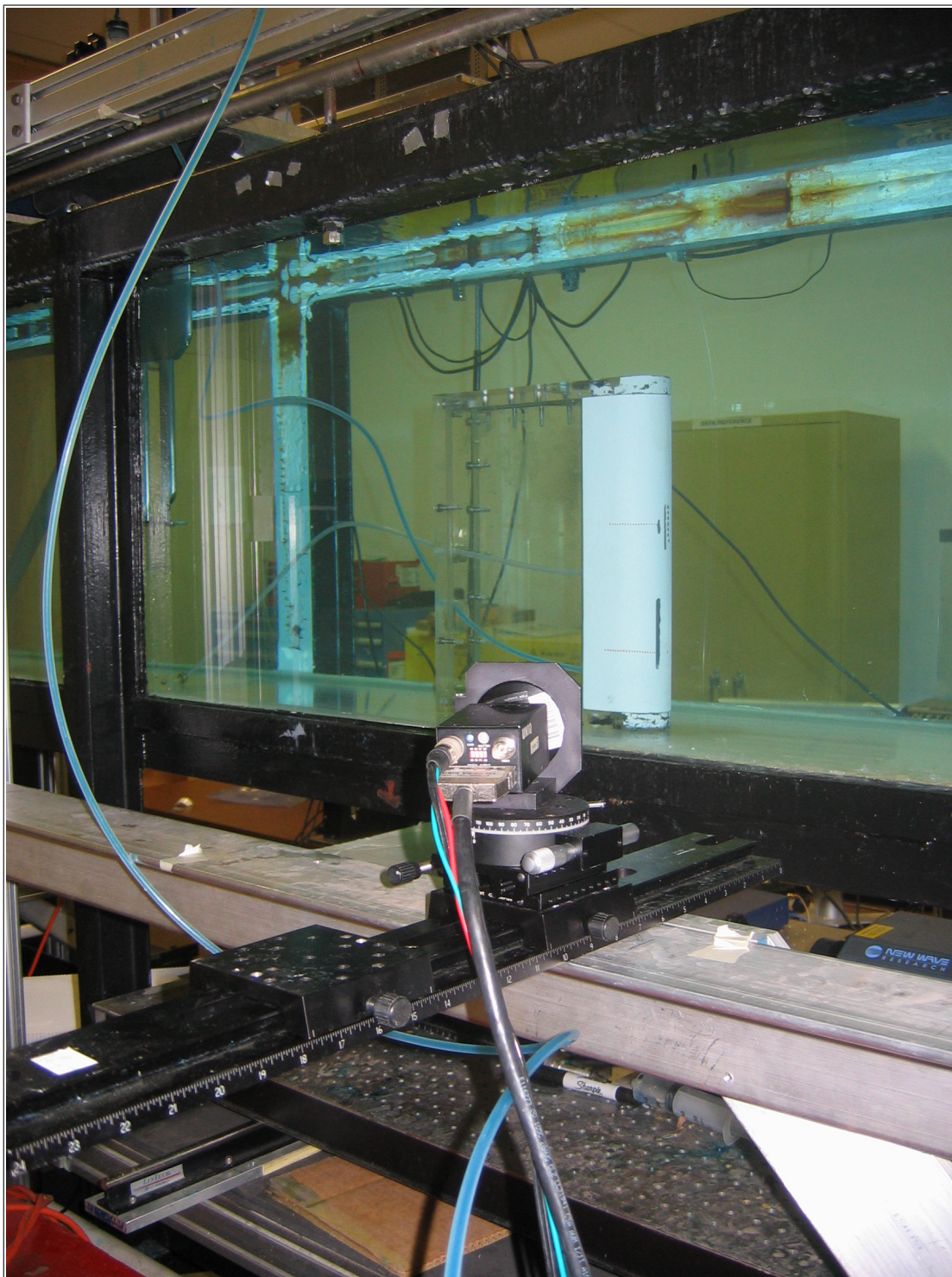
Figure 163   Picture of a leading edge model in the water channel showing the camera in place prior to taking side-view data. Coolant line is shown running behind camera and into water channel.
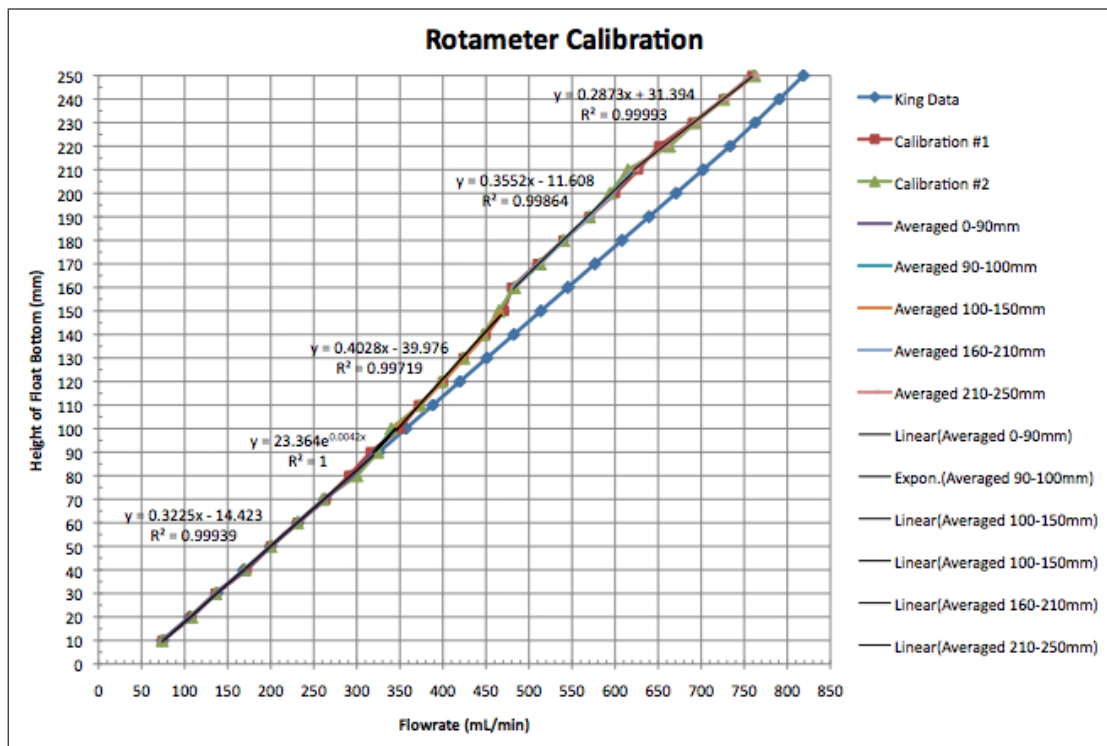
Figure 164   King 7459-31W calibration data.

Bibliography

1. Wilson, D., and Korakianitis, T., 1984. *The Design of High-Efficiency Turbomachinery and Gas Turbines*, Second ed. Prentice Hall, Inc., Upper Saddle River, NJ.

2. Martini, P., Schulz, A., and Bauer, H.-J., 2006. "Film Cooling Effectiveness and Heat Transfer on the Trailing Edge Cutback of Gas Turbine Airfoils with Various Internal Cooling Designs." *Journal of Turbomachinery,* **128**(1), pp. 196–205.

3. Han, J.-C., and Ekkad, S., 2001. "Recent Developments in Turbine Blade Film Cooling." *International Journal of Rotating Turbomachinery,* **7**, pp. 21–40.

4. Ko, S.-Y., Yao, Y.-Q., Xia, B., and Tsou, F.-K., 1986. "Discrete-Hole Film Cooling Characteristics over Concave and Convex Surfaces." In Heat Transfer: Proceedings of the Eighth International Heat Transfer Conference, Vol. **3**, ASME, Hemisphere Publishing Corporation, pp. 1297–1301.

5. Mick, W., and Mayle, R., 1988. "Stagnation Film Cooling and Heat Transfer, Including Its Effect Within the Hole Pattern." *Journal of Turbomachinery,* **110**, pp. 66–72.

6. Salcudean, M., Gartshore, I., Zhang, K., and McLean, I., 1994. "An Experimental Study of Film Cooling Effectiveness Near the Leading Edge of a Turbine Blade." *Journal of Turbomachinery,* **116**(1), pp. 71–79.

7. Goldstein, R., Eckert, E., and Ramsey, J., 1968. "Film Cooling with Injection Through a Circular Hole (NASA CR-54604)." *NASA Scientific and Technical Information Facility.* NASA Contract NAS 3-7904.

8. Luckey, D., Winstanley, D., Hanus, G., and L'Ecuyer, M., 1997. "Stagnation Region Gas Film Cooling for Turbine Blade Leading-Edge Applications." *Journal of Aircraft,* **14**(5), pp. 494–501.

9. Teng, S., Han, J.-C., and Poinsatte, P., 2001. "Effect of Film-Hole Shape on Turbine-Blade Film-Cooling Performance." *Journal of Thermophysics and Heat Transfer,* **15**(3), pp. 257–265.

10. Kim, H.-C., Kim, H.-J., Nakahashi, K., Kato, T., and Tsunoda, M., 2006. "Flow Analysis around Golf Balls without and with Spinning." In Collection of Technical Papers - 24th AIAA Applied Aerodynamics Conference, Vol. **1**, pp. 637–651.

11. Lake, J., 1999. "Flow Separation Prevention on a Turbine Blade in Cascade at Low Reynolds Number." PhD Thesis, Air Force Institute of Technology Graduate School of Engineering, Wright-Patterson AFB, OH 45431. AFIT/DS/ENY/99-01.

12. Roland, I., 2008. "An Experimental Investigation of the Effect of Dimples on Turbine Adiabatic Film Cooling." MS Thesis, Air Force Institute of Technology Graduate School of Engineering and Management, Wright-Patterson AFB, OH 45431. AFIT/GAE/ENY/08-M24.

13. Frisinger, P., 2009. "An Experimental Investigation Studying the Influence of Dimples on a Film Cooled Turbine Blade Leading Edge." MS Thesis, Air Force Institute of Technology Graduate School of Engineering and Management, Wright-Patterson AFB, OH 45431. AFIT/GAE/ENY/09-M10.

14. Khalatov, A., Byerley, A., and Vincent, R., 2005. "Flow Characteristics Within and Downstream of a Single Shallow Cylindrical Dimple and Spherical Dimple: Effect of Pre-Dimple Boundary Layer Thickness." In Proceedings of the ASME Turbo Expo, Vol. **3A**, pp. 61–77.

15. Bunker, R., 2002. "Film Cooling Effectiveness Due to Discrete Holes Within a Transverse Surface Slot." In Proceedings of the ASME Turbo Expo, Vol. **3A**, pp. 129–138.

16. Lu, Y., Dhungel, A., Ekkad, S., and Bunker, R., 2007. "Effect of Trench Width and Depth on Film Cooling from Cylindrical Holes Embedded in Trenches." In Proceedings of the ASME Turbo Expo, Vol. **4A**, pp. 339–349.

17. Waye, S., and Bogard, D., 2007. "High-Resolution Film Cooling Effectiveness Measurements of Axial Holes Embedded in a Transverse Trench With Various Trench Configurations." *Journal of Turbomachinery,* **128**(3), pp. 294–302.

18. Khalatov, A., 2005. *Heat Transfer and Fluid Mechanics over Surface Indentations (Dimples).* National Academy of Sciences of Ukraine, Kiev.

19. Kaplan, S., Altman, A., and Ol, M., 2007. "Wake Vorticity Measurements for Low Aspect Ratio Wings at Low Reynolds Number." *Journal of Aircraft,* **44**, pp. 241–251.

20. Rutledge, J., 2009. "Pulsed Film Cooling On a Turbine Blade Leading Edge." PhD Thesis, Air Force Institute of Technology Graduate School of Engineering, Wright-Patterson AFB, OH 45431. AFIT/DS/ENY/09-S03.

21. ASTM, 1978. *Manual on Water*, Fourth ed. The American Society for Testing and Materials, Philadelphia.

22. Barlow, J., Rae, W., and Pope, A., 1999. *Low-Speed Wind Tunnel Testing.* John Wiley & Sons, Inc., New York.

23. Dorrington, J., Bogard, D., and Bunker, R., 2007. "Film Effectiveness Performance for Coolant Holes Embedded in Various Shallow Trench and Crater Depressions." In Proceedings of the ASME Turbo Expo, Vol. **4A**, pp. 749–758.

24. White, F. M., 1991. *Viscous Fluid Flow*, Second ed. McGraw-Hill, Inc., New York.

25. Ekkad, S., Han, J., and Du, H., 1998. "Detailed Film Cooling Measurements on a Cylindrical Leading Edge Model: Effect of Free-Stream Turbulence and Coolant Density." *Journal of Turbomachinery,* **120**(4), pp. 799–807.

1. REPORT DATE December 2009	2. REPORT TYPE Master's Thesis	3. DATES COVERED *(From – To)* Sept 2008 – Dec 2009

4. TITLE AND SUBTITLE Flow Visualization Study of Passive Flow Control Features on a Film-Cooled Turbine Blade Leading Edge	5a. CONTRACT NUMBER
	5b. GRANT NUMBER
	5c. PROGRAM ELEMENT NUMBER
6. AUTHOR(S) Carroll, Daniel R., Captain, USAF	5d. PROJECT NUMBER
	5e. TASK NUMBER
	5f. WORK UNIT NUMBER

7. PERFORMING ORGANIZATION NAMES(S) AND ADDRESS(S) Air Force Institute of Technology Graduate School of Engineering and Management (AFIT/ENY) 2950 Hobson Way, Building 640 WPAFB OH 45433-8865	8. PERFORMING ORGANIZATION REPORT NUMBER AFIT/GAE/ENY/09-D01
9. SPONSORING/MONITORING AGENCY NAME(S) AND ADDRESS(ES) Intentionally left blank	10. SPONSOR/MONITOR'S ACRONYM(S)
	11. SPONSOR/MONITOR'S REPORT NUMBER(S)

12. DISTRIBUTION/AVAILABILITY STATEMENT

APPROVED FOR PUBLIC RELEASE; DISTRIBUTION UNLIMITED.

13. SUPPLEMENTARY NOTES

14. ABSTRACT

A flow visualization study was conducted on a model of a film-cooled turbine blade leading edge in a closed-loop water channel at $Re_D = 30$k. The model consisted of an 8.89 cm diameter half-cylinder with flat afterbody joined at the ninety-degree point. A single radial coolant hole drilled $21.5°$ from the stagnation line, angled $20°$ to the surface generated a coolant jet transverse to the freestream. Water channel testing assessed the hydrodynamic effects of 16 surface modifications, to include a variety of dimples adjacent to the coolant hole and transverse trenches milled over the coolant hole. Compared to an unmodified coolant hole, a single row of small cylindrical or spherical dimples upstream of the coolant hole steadies the coolant at low blowing ratios. Medium and large spherical dimples downstream of the coolant hole have a similar effect. None of the dimple geometries studied affect the coolant jet at $M \geq 0.75$. A single-depth, square-edged transverse trench spreads the coolant, increasing spanwise coverage of a single coolant hole more than two times. This trench suffers from coolant blow-out above $M = 0.50$, but a deeper, tapered-depth trench provides very effective film cooling at blowing ratios above $M = 0.50$. It spreads the coolant in the spanwise direction, prevents coolant jet liftoff, and was the only geometry studied that holds the coolant tighter to the surface than an unmodified coolant hole.

15. SUBJECT TERMS
film cooling; gas turbine blades; flow visualization; visualization of flow; dimples; trenches;

16. SECURITY CLASSIFICATION OF:			17. LIMITATION OF ABSTRACT	18. NUMBER OF PAGES	19a. NAME OF RESPONSIBLE PERSON Dr. Paul I. King, AFIT/ENY
a. REPORT	b. ABSTRACT	c. THIS PAGE	UU	137	19b. TELEPHONE NUMBER *(Include area code)* (937) 255-3355 ext 3422
U	U	U			